# DOCTORAATSPROEFSCHRIFT

2007 | Faculteit Wetenschappen

## Study of the Dithiocarbamate Route as a viable synthetic route towards Poly(Thienylene Vinylene) Derivatives

Proefschrift voorgelegd tot het behalen van de graad van
Doctor in de Wetenschappen, richting scheikunde, te verdedigen door:

Fateme BANISHOEIB

Promotor: prof. dr. Dirk Vanderzande
Copromotor: dr. Laurence Lutsen

D/2007/2451/46

universiteit hasselt

*Alla mia piccola Nonnina*
*con affetto da "Roma Nord"*

*Partire è un po' morire*
*rispetto a ciò che si ama*
*poiché lasciamo un po' di noi stessi*
*in ogni luogo ad ogni istante.*
*E' un dolore sottile e definitivo*
*come l'ultimo verso di un poema...*
*Partire è un po' morire*
*rispetto a ciò che si ama.*
*Si parte come per gioco prima del viaggio estremo*
*e in ogni addio seminiamo un po' della nostra anima.*
**Edmond Haracourt**

# Table of contents

# Chapter One

# Introduction

## *1.1 Polymers a unique class of materials*

### 1.1.1 What polymers are and why are they interesting?

Polymer is a term used to describe large molecules consisting of repeating structural units, or monomers, connected by covalent chemical bonds. The term is derived from the Greek words: *polys* meaning *many*, and *meros* meaning *parts*. Thus, a key feature that distinguishes polymers from other molecules is the repetition of many identical, similar, or complementary molecular subunits in these chains. The development of polymer science is quite recent and, it has occurred over the last 80 years. Polymer science is driven by the desire to produce new materials for new applications. There is still a massive drive to understand these materials and improve their properties in order to meet material requirements. Polymers are used in a wide range of applications, as coatings, as adhesives, as engineering and structural materials, for packaging, and for clothing to name a few. A key feature of the success and versatility of these materials is that it is possible to build in properties by careful design of the (largely) organic molecules from which the chains are built up. For example, rigid aromatic molecules can be used to make high-strength fibres, the most high profile example of this being Kevlar®. There is now an increasing demand for highly specialised materials for use in for example optical and electronic applications.

### 1.1.2 The conducting polymers: a special class of polymers.

Polymers are normally used in electrical and electronic applications as insulators due mainly to the intrinsic property of the covalent bonds present in most commodity plastics. These polymers with localised electrons are

incapable of providing electrons as charge carriers or a path for other charge carriers to move along the chain. However, polymers are also widely exploited because of their special characteristics such as low densities, mechanical strength, ease of fabrication, flexibility in design, stability, resistance to corrosion and low cost. The promise of combining these properties with the electrical properties has prompted great interest in conducting polymers over the last 30 years.

The search for conducting polymers began at the end of 1970s, since the discovery in 1977, by Alan J. Heeger, Alan G. MacDiarmid and Hideki Shirakawa, for which they were, rewarded the Nobel Prize in chemistry in 2000 (**Figure 1.1**).

***Figure 1.1*** *MacDiarmid, Shirakawa and Heeger.*

An increase in conductivity of 12 orders of magnitude was observed in polyacetylene upon charge transfer doping[1]. This was followed by the fabrication of a free standing polypyrrole film by the oxidative electro-polymerisation of pyrrole. Despite that progress, the field languished because few practical applications were developed beyond electrostatic coatings[1] and because of the intractability and insolubility of these conjugated systems, especially in the doped state. Within the last fifteen years, however, a number of potentially lucrative applications, such as flat-panel displays[2] and photovoltaic devices[3, 4], have emerged. These applications take advantage of the semi-conducting properties of conjugated polymers relative to their

ability to be coated into thin films over large areas in the ambient using simple techniques, such as screen and inkjet printing. This provides practical advantages for displays and photovoltaic cells, both of which are cost-driven applications[5-7]. In addition, polymeric materials have the promise of enabling mechanically flexible electronics.

## *1.2 Conjugated polymers: semi-conducting materials*

### 1.2.1 Electronic structure of conjugated polymers

Conjugated polymers are a special class of polymers because of their extended π-electron delocalisation along the backbone. They are in general constructed from a combination of aromatic units and/or multiple bonds alternating with single bonds. The interaction of adjacent $p_z$-orbitals, leading to the delocalisation of electrons is the distinguishing feature of this class of polymers (**Figure 1.2**).

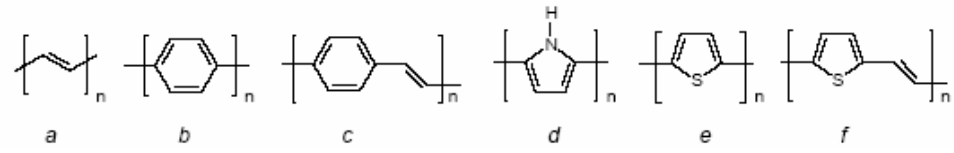


***Figure 1.2*** *Examples of conjugated polymers: polyacetylene, PA (a), poly(p-phenylene) PPP (b), poly(p-phenylenevinylene) PPV (c), polypyrrole PPy (d), polythiophene PT (e) and polythienylenevinylene PTV (f).*

In conjugated polymers, each CH unit is linked by σ-bonds formed by three equivalent, triangular $sp^2$ hybrid orbitals, thus leaving free a fourth-orbital the $2p_z$ orbital. These $p_z$ orbitals, out-of-plane, overlap with neighbouring $p_z$ orbitals to give π-bonds. According to the molecular orbital theory the overlap of the $p_z$ orbitals yields lower energy bonding (π) and higher energy anti-bonding (π*) of molecular orbitals. This is exemplified in **Figure 1.3** where the energy levels of PT with n ranging from 1 to infinity are shown as a

function of the polymer length[8]. The $\pi$-orbitals form the occupied valence band (VB) and the $\pi^*$-orbitals generate the conduction band (CB).

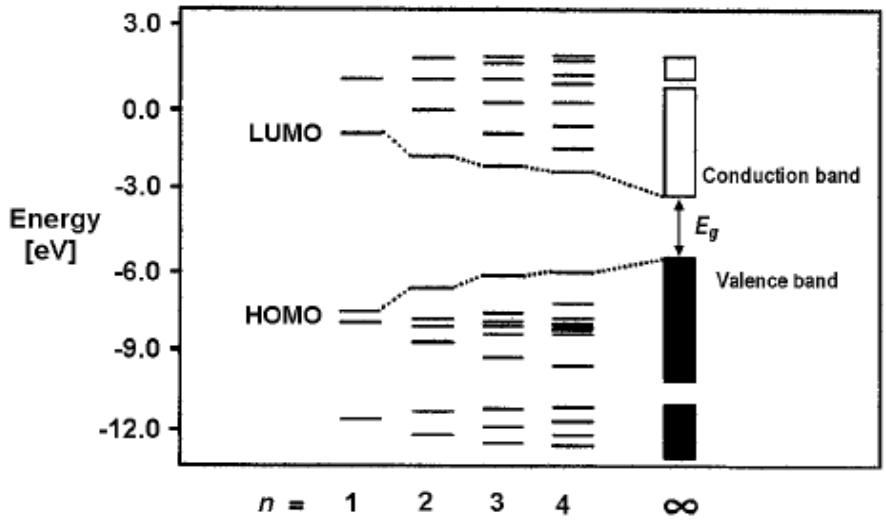


***Figure 1.3*** *Band model for polythiophene, where $E_g$ is the band gap.*

The difference in energy between the highest occupied molecular orbital (HOMO) of the repeating units and the lowest unoccupied molecular orbital (LUMO) is called band gap $E_g$, which lies in general between 1.0 eV and 4 eV for conjugated polymers. If the carbon-carbon bond lengths were equal, the polymer would behave as a metal ($E_g$ = 0 eV) (**Figure 1.4** top) In this case no energy difference between the "bonding" valence band and the "anti-bonding" conduction band can occur due to the equivalency of both geometries. However, already in the year 1956, Rudolf Peierls predicted the instability of the 1-dimensional atomic system of the conjugated polymers the so called Peierls distortion[9]. In his theorem he predicts the lifting of the bond length degeneracy, leading to significant bond length alternation. As a result, one dimensional system shows a significant difference between the HOMO and the LUMO energy levels.

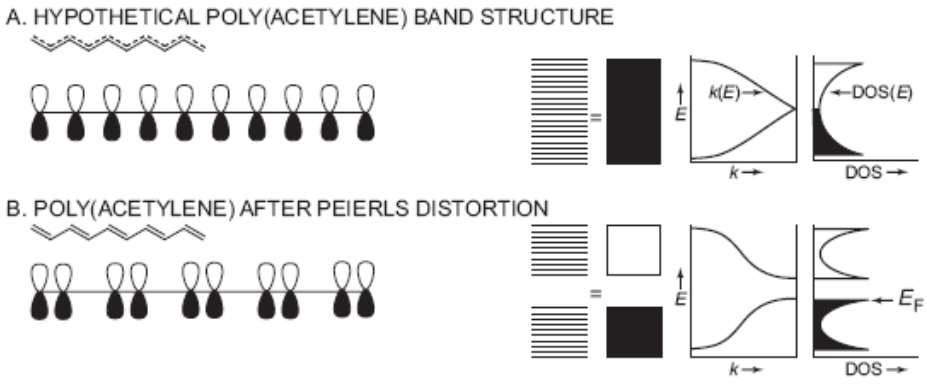


***Figure 1.4*** *Band gap formation by localisation of double bonds in PA*[10]

### 1.2.2 Low band gap materials

Quite early in the history of conjugated polymers, was set the goal to develop new materials with a reduced $E_g$ so, that, the absorption of the doped polymer shifts from the visible towards the near infrared region of the electromagnetic spectrum. A low band gap (LBG) polymer can be defined as a conjugated polymer with an $E_g$ < 2 eV. A smaller band gap would facilitate the ease of doping with the possibility of achieving intrinsic metallic conductivity. Furthermore, these LBG materials would possess improved photo-conductivities.

### 1.2.3 Optical absorption properties of conjugated polymers

Optical properties are usually related to the interaction of a material with electromagnetic radiation in the frequency range from IR to UV[11]. Since conjugated polymers are semiconductors with a band gap ranging from 0.5 eV till 4 eV most of them interact with visible light. When light with sufficient energy is absorbed by the material an electron is promoted or excited from the valence band into the conduction band creating an exciton (electron-hole pair) as shown in **Figure 1.5** (left). The lowest energy (light with the highest wavelength) necessary to excite an electron is equal to the $E_g$. A decrease of the $E_g$ results in a red shift of the absorption spectrum. The exciton can

eventually decay to the ground state radiatively (*i.e.* photoluminescence) or non-radiatively.

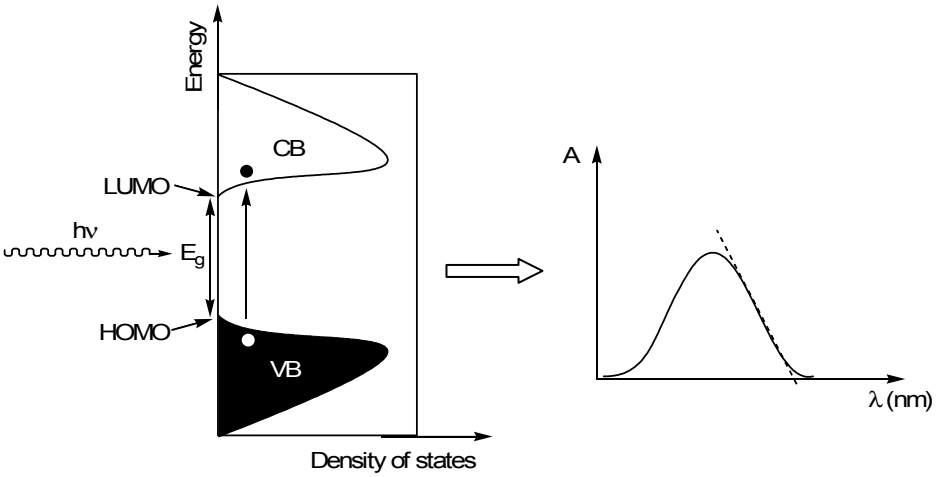


***Figure 1.5*** *Density of States band structure (left) and corresponding absorption spectrum (right).*

The $E_g$ can be derived from a UV-Vis spectrum, taking the tangent on the low energetic side of the absorption spectrum (**Figure 1.5**, right). The intersection of this tangent with the abscissa gives a value for the band gap (optical band gap). Since in a UV-Vis spectrum, the absorbance is plotted as a function of the wavelength, it is necessary to convert the nanometre scale into electron-volt using the equation of Planck.

$$E = h\upsilon = \frac{hc}{\lambda}$$

In this equation, E is the energy (in J), h is the Planck constant (6.626 $10^{-34}$ Js), c is the speed of light (3 $10^{8}$ $ms^{-1}$), $\nu$ is the frequency (in $s^{-1}$ or Hz) and $\lambda$ is the wavelength (in m). Knowing that 1 eV equals 1.602 $10^{-19}$ J, calculations can be made for the conversion leading to the simple conversion equation.

$$E(eV) = \frac{1240.8}{\lambda\,(nm)}$$

It is clear now that the band gap of a conjugated polymer not only influences the electronic properties but also determines the optical properties such as absorbance (colour), photoluminescence and electroluminescence (conversion of electrical energy into light).

## *1.3 Band gap engineering*

Synthetic chemists have demonstrated their ability to construct molecules and materials capable of fulfilling a huge variety of requirements in terms of mechanical, physical, and chemical properties. However the synthesis of LBG polymers or of a true organic metal poses specific problems that concern both the conception of the proper target compounds and the definition of the relevant synthetic strategies. The ambition to obtain conjugated polymers with desired electrical and optical properties implies the capability of "band gap engineering". The "band gap engineering" may give the polymer its desired electrical and optical properties.

Roncali[12] did a thorough investigation on the relationships between the chemical structure of conjugated polymers and the relative band gap of these materials. According to him, the band gap of polyaromatic conjugated polymers can be viewed as the result of five different contributions i.e. the energy related to the bond length alternation ($E^{\Delta r}$), the mean deviation from planarity ($E^{\theta}$), the aromatic resonance energy ($E^{res}$), the inductive or mesomeric electronic effects of substituents ($E^{sub}$), and the intermolecular or inter-chain coupling in the solid state ($E^{int}$). These parameters can be visualised in **Figure 1.6** in which polythiophene (PT) is taken as a representative molecule. All the afore mentioned parameters, will be discussed into details.

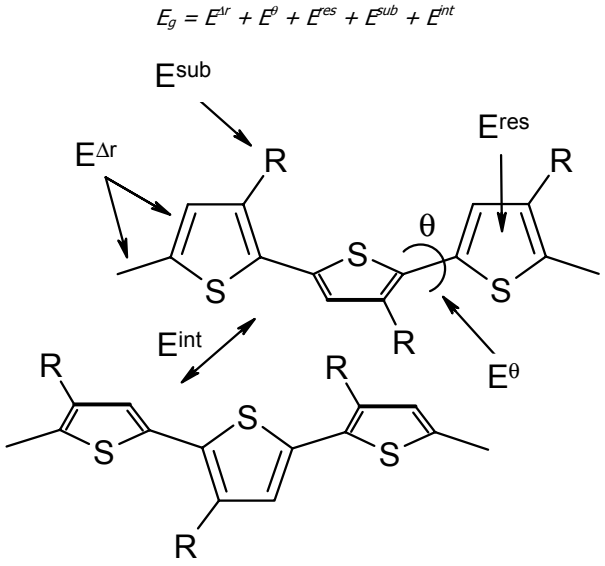


***Figure 1.6*** *Parameters determining the band gap of conjugated polymers.*

### 1.3.1 Bond length alternation, $E^{\Delta r}$

Due to the Peierls instability, the band gap mainly depends on the degree of bond length alternation ($\Delta r$). This contribution is related to the difference between single and double bond lengths. $\Delta r$ is defined by Brédas[13, 14] as the maximum difference between the length of a C-C bond inclined relative to the chain axis and a C-C bond parallel to the chain axis. An aromatic and a quinoid geometry can be distinguished for all polyaromatics. The larger $\Delta r$, the larger $E_g$. In **Figure 1.7** the potential energy as a function of bond length alternation is shown. The upper picture represents a conjugated polymer with degenerate ground state, the trans-polyacetylene. In the lower picture is shown the potential energy for PT system with non-degenerate ground state.

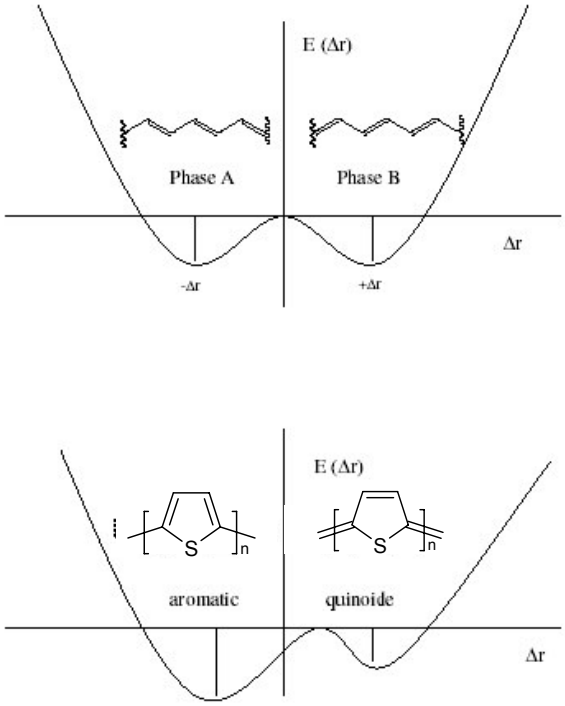


***Figure 1.7*** *Potential energy diagram of PA (upper diagram) and of PT (lower diagram).*

Brédas calculated the evolution of the band gap of PT as a function of the two possible geometries, the aromatic and the quinoid structures. For each geometry, the degree of bond length alternation, $\Delta r$, was calculated. The band gap was found to decrease with increasing the quinoid character of the backbone.

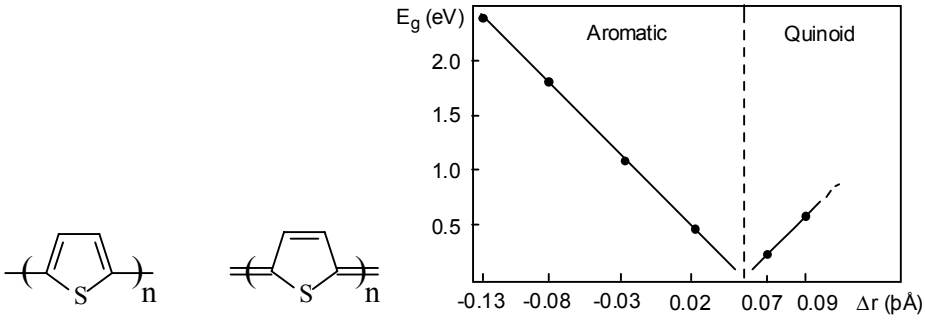


***Figure 1.8*** *The band gap of PT as a function of* $\Delta r$

In the case of PT (**Figure 1.8**), the quinoid structure is energetically unfavourable. That is why the experimental $E_g$ value ($\cong$ 2eV) is closer to the calculated $E_g$ for the aromatic structure than to the calculated $E_g$ for the quinoid PT ($\cong$ 0.47 eV).

### 1.3.2 The mean deviation from planarity, $E^{\theta}$

The deviation from planarity $E^{\theta}$, has a strong influence on the value of $E_g$. It is related to rotational disorder occurring around the single bonds between the monomeric units. Single bonds allow rotations between them, thus the rings twist away from planarity. The orbital overlap varies with the cosine of the twist angle ($\theta$),[15] so that any departure from coplanarity will result in an increase of $E_g$ **Figure 1.9**.

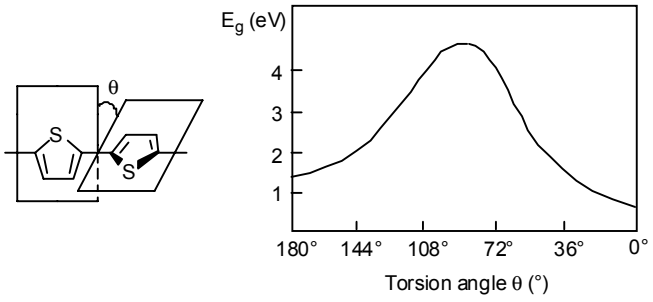


***Figure 1.9*** *The band gap of PT as a function of the torsion angle* $\theta$

Essentially the deviation from coplanarity reduces the $p_z$-orbital overlap and hence reduces the double bond character, and this reduction of the double bond character implies an increase in bond length alternation.

### 1.3.3 Aromatic resonance energy, $E^{res}$

A third factor influencing the band gap is the aromatic resonance energy, $E^{res}$. The aromaticity results in a competition between $\pi$-electron confinement within the ring and delocalization along the polymer backbone[16]. Molecules with a large resonance energy i.e. highly aromatic compounds, will have a higher band gap since this high $E^{res}$ prevents the delocalization. This can be noticed when comparing the resonance energy per electron (REPE) values of the monomer with the $E_g$ values of the polymer[17]. A high REPE results in a high $E_g$. For example consider: REPE (benzene) = 0.065 and $E_g$ (PPP) = 3 eV, REPE (pyrrole) = 0.039 and $E_g$ (PPy) = 2.5 eV, REPE (thiophene) = 0.032 and $E_g$ (PT) = 2 eV, etc. In terms of bond length alternation, it is clear that a molecule with high resonance energy has a low quinoid contribution and thus a large bond length alternation i.e. a low double bond character between the monomeric units.

### 1.3.4 Electronic effects of substitution, $E^{sub}$

The parameters discussed so far are primary factors to minimize the band gap but, there are also others ways to modify the HOMO and LUMO energy levels causing then a minimization of $E_g$. The introduction of substituents represents the most direct and straightforward approach towards reducing the band gap of conjugated backbone. On the basis of electronic effects alone, the energy of absorption decreases with alkyl substitution and is further diminished with alkoxy functionalisation. The presence of electron donating substituents primarily raises the HOMO with a consequent narrowing of the energy gap. Electron acceptor substituents instead lower the LUMO leading again to a narrowing of the band gap. The change of the energy levels is proportional to the electron donating or acceptor strength of the substituents.

### 1.3.5 Interchain coupling in the solid state $E^{int}$

These electronic effects are in contrast to increased steric effects upon functionalisation with pendant groups that raise the band gap by reducing coplanarity and therefore the extent of conjugation in the polymer backbone. The interactions between individual molecules can represent an important contribution to the band gap. The ordering of molecules, i.e. the $\pi$–$\pi$ interactions between the chains will force the molecules into a more planar structure and as a consequence a decrease of $E_g$ is seen due to a better delocalisation of the electrons **Figure 1.10**.

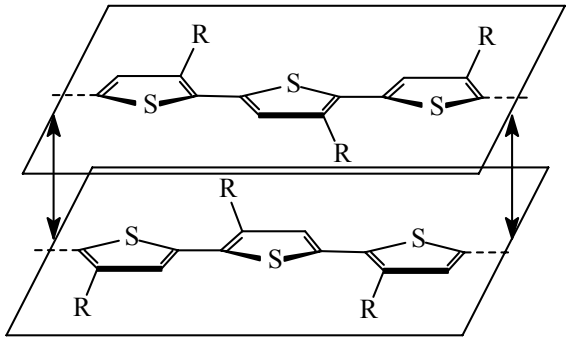


***Figure 1.10*** *$\pi$–$\pi$ interactions in P3RTh*

Also the introduction of conjugated spacer groups between the rings aims at minimizing steric effects between arylene rings. This is the case of poly(2,5-thienylenevinylene). By alternating thiophene rings and vinylene groups in the polymer backbone, a significant lowering of the band gap was observed.
To draw some conclusions we can say that all the five parameters analysed are interconnected to each other. In order to reduce the $E_g$ it is of crucial importance to tune the double bond character between the monomeric units. Moreover, the introduction of appropriate substituents reduces also the energy levels.

## *1.4 Approaches towards LBG thiophene based polymers*

Basically, two major approaches towards conjugated polymers can be distinguished. The first one is the direct synthesis towards the conjugated polymer via oxidative or reductive coupling. In this case the polymer consists out of a chain of aromatic molecules. The second approach, often referred to as precursor route, is an indirect way to obtain conjugated polymers.
In this approach a non conjugated precursor polymer is converted into its conjugated form in such a way that the aromatic cores are connected via an ethylene linkage. Since in the thesis only the second approach will be presented we will focus just on the indirect synthesis in this introduction.

### 1.4.1 Poly(thienylenevinylene)s

The importance of reducing the band gap is related to the opportunity of enhancing the thermal population of the conduction band and thus increase the number of intrinsic charge carriers. The red shift of the absorption and emission spectra resulting from a decrease of $E_g$ will make conjugated polymers excellent candidates for the absorption of light in organic solar cells and potentially useful for the fabrication of LED's operating in the IR.
Ever since the first low band gap material, poly(isothianaphthene) (PITN), was synthesised in 1984 by Wudl *et al.*, scientists were eager to synthesise more of these small band gap polymers. A problem however in the synthesis of conjugated polymers is the insolubility of conjugated polymers due to their rigid backbone. In order to obtain processable polymers, we have to make them soluble. Two possible solutions are within reach. First, we can make the polymer soluble by introducing long and flexible side chains on the conjugated structure. Secondly, one can use precursor routes[18-20] to circumvent the problem of insolubility. Here, first a soluble, non-conjugated precursor polymer is synthesised that can easily be processed. After processing this polymer, the precursor can be converted to the fully conjugated polymer by a simple (e.g. thermal) elimination of a small molecule. The main difference between polymers synthesised *via* either the

side chain approach or the precursor approach is their solubility in the conjugated form.

The discovery of electroluminescence in poly(*p*-phenylene vinylene)s[21] boosted the development of these routes. In the course of time this type of chemistry was also developed for the synthesis of poly(heteroarylene vinylene)s. The different precursor routes are represented in **Figure 1.11**.

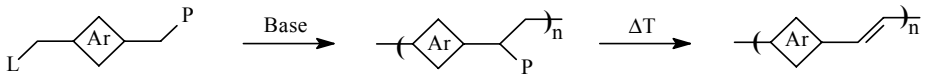


***Figure 1.11*** *Precursor routes towards poly(arylene vinylene)s: Wessling-Zimmerman: L = P = $\oplus$ $SR_2$; Gilch: L = P = Cl; Xanthate: L = P = SC(S)OR; Sulphinyl: L = Cl, P = S(O)R*

These four routes differ by their polymerisation conditions (base, solvent, reaction temperature and reaction time), leaving group (L) and polarizer group (P). Two of these precursor routes were developed in our group, namely the sulphinyl[22] and the dithiocarbamate[23] precursor route.

A more detailed review of the precursor routes will be given in the following chapter.

## *1.5 Applications of conjugated polymers*

### 1.5.1 Organic materials for electronics

Conjugated polymers are being considered as the active materials in several types of electronic devices e.g. thin-film transistors (TFTs)[24-27], light emitting diodes (LEDs)[2, 21, 24, 28], biosensors[29-31], smart windows[32, 33], lasers[34, 35] and photovoltaics (PVs)[3, 4, 7, 36-41]. In all these devices the polymer is used in a thin film of solid material.

Thin-film transistors based on conjugated polymers are being studied for applications in plastic electronics. In principle this could lead to low-cost, flexible electronic devices such as displays[42] and potentially for low-

performance radio-frequency identification tags that can be read from a distance[43].

The second application of conjugated polymers is as the emissive layer in light-emitting diodes. Two of the most challenging performance requirements for these applications are full coverage of the colour spectrum and stable electrical performance. A reasonable value for the lifetime of a display is ~10000 hours of use over five years; this target has been achieved in prototype displays[44]. The synthesis and development of new, in particular blue, light-emitting polymers will help address the requirements in performance in tandem with the development of optimised device structures to achieve the desired level of performance for both of these applications.

Conjugated polymers can also be applied as the absorbing layer in photovoltaic devices, in which the processes occurring in LEDs are reversed.

### 1.5.2 Organic solar cells

Today, three different types of solar cells using organic molecules are existing: dye sensitized nonocrystalline $TiO_2$ solar cells, molecular organic solar cells and polymer solar cells. In 1954, Chapin, Fuller, and Pearson developed the first photovoltaic cell based on a silicon p-n junction with an efficiency of 6 %[45]. Since then, solar cells have been made from many other semiconductors, using various device configurations and employing single-crystal, poly-crystalline, and amorphous thin-film structures[46]. Molecular organic solar cells use organic dyes. The active layers are cast by vacuum evaporation techniques. The organic dyes show high absorption coefficients and a good match of the solar spectrum. But their efficiencies are limited by the low exciton diffusion length and the low charge mobility of the materials. The third type of organic solar cells, the polymer solar cells will be discussed in more details because the materials presented in the thesis are mainly intended for these applications.

### 1.5.3 The photovoltaic principle in organic solar cells

The simplest device structure consists of an organic light-absorbing layer sandwiched between two different electrodes with unequal work functions. One side of the substrate is covered with a typically 100-200 nm thick uniform layer of a transparent indium-tin-oxide (ITO) electrode, which is covered by an approximately 100 nm thick conductive layer of poly(3,4-ethylene-dioxythiophene):polystyrenesulfonic acid (PEDOT:PSS) blend. On top of the cathode, the photoactive layer is applied either by spin-coating or by thermal evaporation. The other electrode is very often aluminium but can be either calcium or golden. It is normally deposited in vacuo. To guarantee a good ohmic contact between the metal and the organic layer the deposition of an interfacial layer of lithium fluoride (LiF) has been found to be advantageous. The schematic representation of the device is given in **Figure 1.12**.

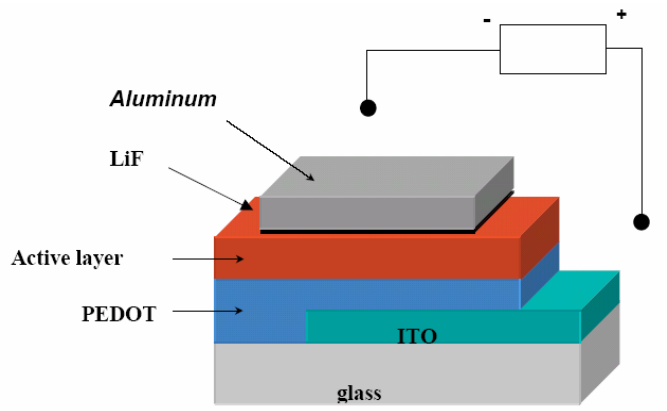


***Figure 1.12*** *Device architecture of a photovoltaic device*

In general, in an organic photovoltaic cell three processes occur in the conversion of solar energy into electrical energy[41]:

1. Absorption of light;
2. Charge transfer and separation of the opposite charges;
3. Charge transport and collection at the electrodes.

When light is absorbed an electron is promoted from the highest occupied molecular orbital (HOMO) to the lowest unoccupied molecular orbital (LUMO) forming an exciton (see **Figure 1.13**). In bulk heterojunction solar cell device this process must be followed by exciton dissociation upon which the charges are created.

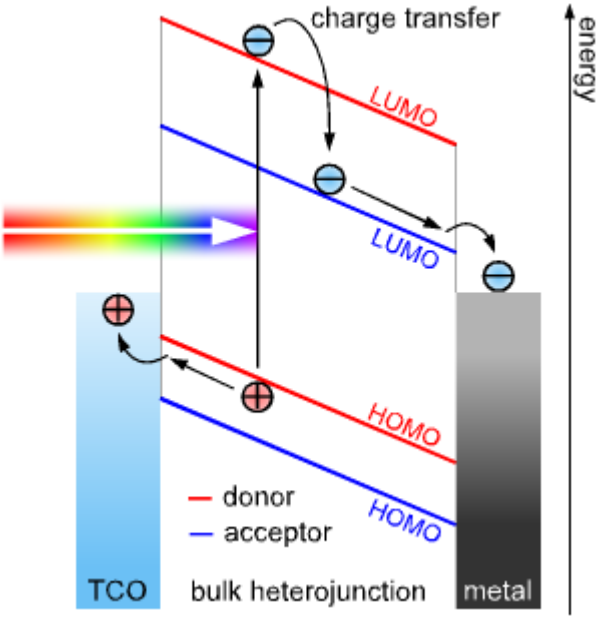


***Figure 1.13*** *Schematic drawing of the working principle of an organic solar cell*

This is one of the key steps in photovoltaic devices in the conversion of solar light into electrical energy. In most organic solar cells, charges are created by photoinduced electron transfer. In this reaction an electron is transferred from an electron donor, a p-type semiconductor, to an electron acceptor, an n-type semiconductor. It is important that the energy of the absorbed photon is used for generation of the charge-separated state and is not lost *via* competitive processes like fluorescence, non-radiative decay, internal conversion or intersystem crossing. In addition, it is of importance that the charge-separated state is stabilised, so that the photogenerated charges can migrate to one of the electrodes.

### 1.5.4 Characterisation of solar cells

Before discussing the characteristics of a solar cell, many definitions have to be clarified. So, a schematic representation of them will be given in this paragraph.

**Air Mass (AM)** – Is a measure of the relative distance sunlight must travel through the atmosphere to reach the earth's surface. This is denoted as "AM(x)", where x is the inverse of the cosine of the zenith angle of the sun. A typical value for solar cell measurements is AM 1.5, which means that the sun is at an angle of about 48°. Air mass describes the spectrum of radiation, but not its intensity. For solar cell purposes, the intensity is commonly fixed at 100 W/cm$^2$.

**Standard test conditions**

In order to reproducibly characterise photovoltaic devices standard test conditions had to be defined. This task has already been accomplished in the case of conventional inorganic solar cells and consequently was adapted for the organic counterparts. These test conditions are based on a spectral distribution, reflecting the emission spectrum of the sun measured on a clear sunny day with a radiant intensity of 1000 W/m$^2$ that is received on a tilted plane surface with an angle of incidence of 48.2°. This spectrum that also counts for a model atmosphere containing specified concentrations of, e.g., water vapour, carbon dioxide, and aerosol is referred to as an "Air Mass 1.5 Global" (AM1.5G, IEC 904-3) spectrum (**Figure 1.14**). These standard test conditions also include a measuring temperature of 25 °C.

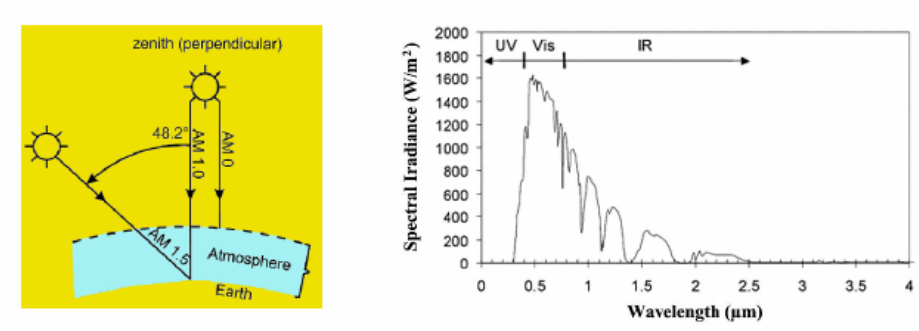


***Figure 1.14*** *Definition of AM0, AM1.0 and AM1.5 solar spectra (left) and the corresponding AM 1.5 spectrum (right).*

**Open-Circuit Voltage ($V_{oc}$)** – The maximum possible voltage across a photovoltaic cell; the voltage across the cell in sunlight when no current is flowing.

**Short-Circuit Current ($J_{sc}$)** – Under short-circuit conditions an appliance is prevented from receiving charges. If the path has no resistance, there is no voltage change, and thus, no work is done even though a current is flowing.

The short-circuit current $J_{SC}$ is heavily dependent on the number of absorbed photons which originates from two different facts. Firstly, $J_{SC}$ shows a linear dependence on the incident light intensity as long as no saturation effects occur within the active layer. Secondly, the short-circuit can be maximized by enlarging the absorption spectrum of the photoactive layer to harvest more photons within the terrestrial sun spectrum. This can either be accomplished by carefully designing the thickness of the distinct layers as optical modelling of the organic solar cells revealed that the light distribution varies considerably throughout the whole photovoltaic devices, or by the use of low-band gap materials which can also contribute to improved photon harvesting. The short-circuit current also depends on the charge carrier mobilities of the active layer as the photocurrent increases with temperature due to a thermally active hopping transport. Therefore, the syntheses of organic materials which are characterized by high charge carrier mobilities and a low band gap at the same time are highly desired (**Figure 1.15**).

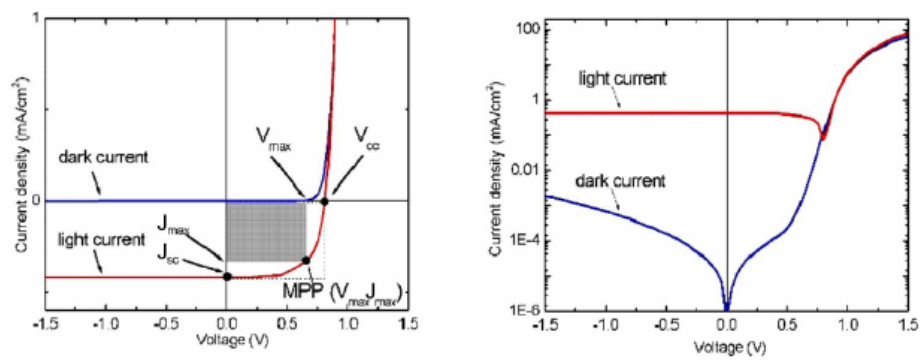


***Figure 1.15*** *Linear (left) and logarithmic (right) current-voltage (I-U) curves of a photovoltaic device. The short-circuit current $J_{SC}$ corresponds to the ordinate while the open-circuit voltage $V_{OC}$ is determined at the point where the I-U curve crosses the abscissa.*

**Maximum Power Point ($P_{mp}$)** – The point ($I_{mp}$, $V_{mp}$) on the I-V curve where the maximum power is produced. Power (P) is the product of current and voltage (P = I•V) and is illustrated in the **Figure 1.15** as the area of the rectangle formed between a point on the I-V curve and the axes. The maximum power point is the point on the I-V curve where the area of the resulting rectangle is largest.

**Fill Factor (FF)** – The fill factor FF which describes the quality of the solar cell is determined by the fraction of photo-generated charge carriers that reach the electrodes when the built-in field is lowered towards the open-circuit voltage to the total number of photoexcitons generated. It gives information about the degree to which $V_{max}$ and $J_{max}$ match $V_{OC}$ and $J_{SC}$, respectively. The largest power output $P_{max}$ is determined by the point where the product of voltage $V_{max}$ and current $J_{max}$ is largest (**Figure 1.15**). The fill factor is defined as the division of $P_{max}$ by the product of $V_{OC}$ and $J_{SC}$. The formula for FF in terms of the above quantities is:

$$FF = \frac{V_{max} \cdot J_{max}}{V_{OC} \cdot J_{SC}} = \frac{P_{max}}{V_{OC} \cdot J_{SC}}$$

In order to determine the power conversion efficiency η of a photovoltaic device, the maximum power $P_{max}$ that can be extracted from the solar cell has to be compared to the incident radiation intensity:

$$\eta = \frac{P_{out}}{P_{in}} = \frac{V_{\max} \cdot I_{\max}}{P_{in}} = \frac{V_{OC} \cdot J_{SC} \cdot FF}{P_{in}}$$

In order to obtain a high fill factor FF the shunt resistance of a photovoltaic device has to be very large in order to prevent leakage currents. This resistance is reflected in the horizontal part of the U-I curve at a negative applied bias. Another inherent resistance sums up all contributions of series resistances in the device. Among them are transport through the contact, interface transfer, and bulk transport. For a good fill factor, this series resistance has to be very low, which then is reflected by a sharp rise in the forward current. For polymer-fullerene solar cells fill factors as high as 0.6 have been determined.

**Power Conversion Efficiency (PCE or $\eta_e$)** – The ratio of power output to power input. In other words, PCE measures the amount of power produced by a solar cell relative to the power available in the incident solar radiation ($P_{in}$). $P_{in}$ here is the sum over all wavelengths and is generally fixed at 100 W/cm$^2$ when solar simulators are used. This is the most general way to define efficiency. The formula for PCE, in terms of quantities defined above, is:

$$\eta_e = \frac{I_{mp} \cdot V_{mp}}{P_{in}} = \frac{I_{sc} \cdot V_{oc} \cdot FF}{P_{in}}$$

### 1.5.4.1 Single layer devices

The first generation of organic photovoltaic cells was based on single organic layers sandwiched between two metal electrodes of different work functions[47, 48]. The difference in work function provides an electric field that drives separated charge carriers towards the respective contacts. This electric field is seldom sufficient to break up the photogenerated exciton.

Instead the exciton diffuses within the organic layer until it reaches a contact, where it may be broken up to supply separate charges, or recombine. Since exciton diffusion lengths are short, typically 1-10 nm for organic materials[49], only those excitons generated in a small region within <10 nm from the contacts contribute to the photocurrent. The exciton diffusion limits the charge carrier generation in such a device. Single layer solar cells of this type made with PPV delivered power conversion efficiencies of less than 0.1 % under white light illumination[50].

### 1.5.4.2 Bilayer heterojunction devices

The next breakthrough was achieved in 1986 by introducing the bilayer heterojunction concept[51]. At the interface between a *p*-type and an *n*-type semiconductor, electrostatic forces occur because of the differences in electron affinity and ionisation potential (**Figure 1.16**). Both of these properties are much more pronounced in the acceptor moiety rather than in the donor material which results in a strong electric field at the interface between the *p*- and the *n*-type semiconductor, providing a strong driving force for charge separation.

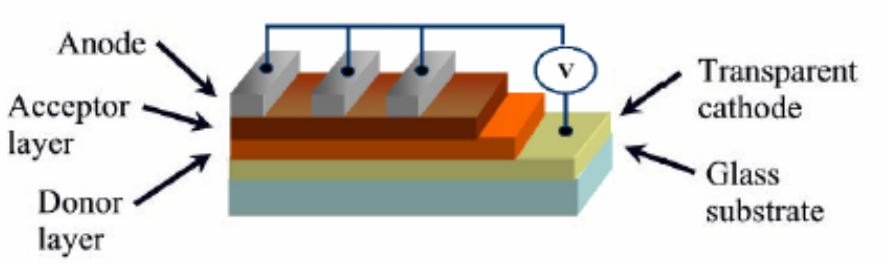


***Figure 1.16*** *Bilayer heterojunction device.*

In this device a copper phthalocyanine and a tetracarboxylic derivative were sandwiched between the electrodes and yielded a power conversion efficiency of 0.95 %. Following this discovery, conjugated polymers were also investigated in such devices and in 1993, Sariciftci *et al.*, triggered by their discovery of the ultra fast photoinduced charge transfer from conjugated polymers onto fullerenes[52], first applied this two-layer technique to a

conjugated polymer solar cell by evaporating $C_{60}$ on top of a spin-cast poly(2-methoxy-5-(-2'-ethyl-hexyloxy)-1,4-phenylene vinylene) (MEH-PPV)[53]. In this cell the MEH-PPV was used to absorb visible light and transport holes to the ITO electrode following exciton dissociation at the interface. The $C_{60}$, with an electron affinity about 0.7 eV larger than the conjugated polymer was used to accept electrons and transport them to the aluminium electrode. The first devices based on these materials yielded efficiencies of 0.1 %[49]. However after optimization, efficiencies of 1.9 % were reached[54].

#### 1.5.4.3 Bulk heterojunction devices

The main intrinsic problem of bilayer heterojunction devices is the exciton diffusion length which is typically in the range of 1-10 nm[49]. Therefore, only exciton created within this distance of the heterojunction interface can be separated into free charge carriers and extracted out of the photoactive layer. Hence, a significant loss of absorbed photons is immanent and the quantum efficiencies of these photovoltaic devices are usually low. This issue has been addressed by substituting the separated bilayers by microphase-separated blends of the corresponding donor and acceptor moieties, resulting in a tremendously increased interfacial area. If the length scale of the microphase separation is similar to the exciton diffusion length, all the photo-generated excitons will immediately diffuse to the nearby interface where they can be separated into free charge carriers. The existence of percolation paths throughout the photoactive layer allows the free charge to travel independently towards the opposite electrodes and consequently a photocurrent can be extracted from the device (**Figure 1.17**).

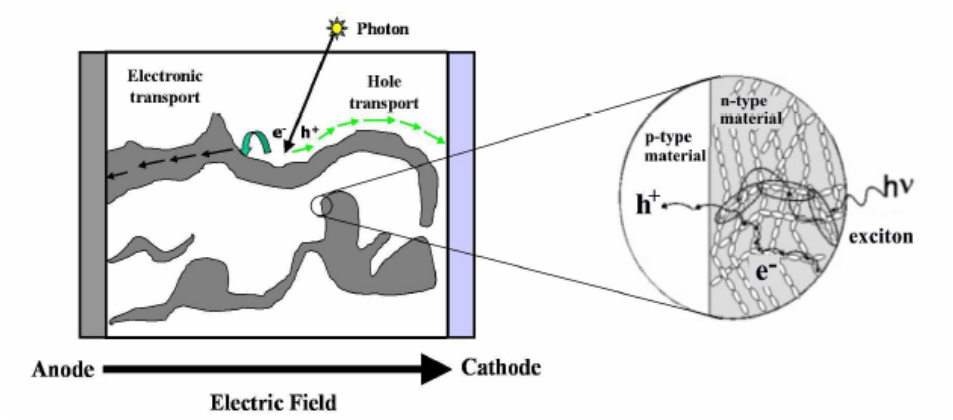


***Figure 1.17*** *Continuous paths for the transport of the free charge carriers in bulk heterojunction solar cells.*

Research towards suitable acceptor polymers is still necessary in order to make a truly all-polymer solar cell. The control of morphology in dispersed heterojunction devices is a critical point[55, 56]. The degree of phase separation and domain size depend on solvent choice, speed of evaporation, solubility, miscibility of the donor and acceptor etc.

### 1.5.5 Improving light harvesting of the photovoltaic layer

The optical band gap of PPV and polythiophene derivatives that are currently used in the manufacturing of polymer-fullerene solar cells are in the range between 2.2 and 1.9 eV, which is not optimal with respect to the solar spectrum. Hence there is a clear mismatch between the absorption spectrum of these materials and the terrestrial solar spectrum, which extends into the near infrared. One promising strategy is to use materials with enhanced light absorption properties. This can be either achieved by applying a low-band gap polymer with an optical band gap below 1.8 eV or by using a different acceptor moiety which absorbs light beyond 600 nm (**Figure 1.18**).

The first approach to an improved light harvesting of the photoactive layer has been studied by employing suitable low-band gap polymers. In order to obtain an enhanced overlap of the polymer absorption spectrum with the solar emission, the band gap of the corresponding polymers has to be pushed

below 1.8 eV. In the case of a conventional homojunction solar cell the overall absorption of the photoactive layer and the simultaneous lowering of the open-circuit voltage $V_{OC}$ have to be balanced. This, however, is more complex in the case of polymer-fullerene solar cells where the HOMOs and LUMOs of both, the donor polymer and the acceptor moiety, have to be matched. The decrease of the polymer band gap can either be achieved by raising the polymer HOMO in energy and/or energetically lowering the polymer LUMO. The first case in which the polymer HOMO is raised while the LUMO remains unaffected, results in a reduced open-circuit voltage, whereas the second possibility of altering the polymer band gap is more favourable because it would not change the open-circuit voltage. Nevertheless, it has to be considered that both the polymer HOMO and the LUMO have to be higher in energy than the corresponding acceptor frontier orbitals to maintain electron transfer. Another, non-trivial issue in the case of low-band gap polymers is the frequently observed efficient non-radiative decay, which limits the lifetime of the excited state and hence the exciton diffusion length.

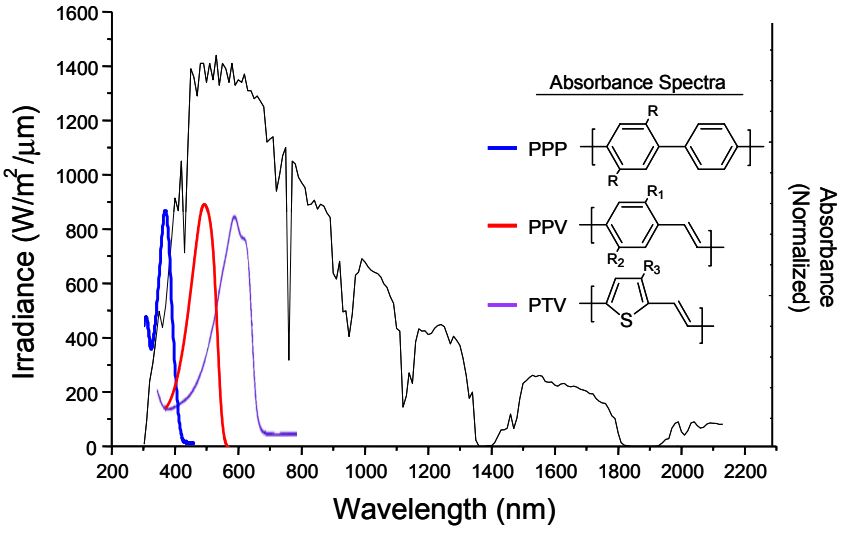


***Figure 1.18*** *Standard AM1.5 terrestrial solar spectrum (black line) compared to the absorption spectrum of PPV (red line), PPP (blue line) and a low band gap polymer PTV (violet line).*

The other challenge is to have a large enough driving force for electron transfer from the polymer to the electron acceptor. This means that the LUMO of the electron donor must be closer in energy to vacuum than the LUMO of the electron acceptor in order to have enough driving force for exciton dissociation at the interface of the electron donor and acceptor. When decreasing the band gap of a polymer, both the LUMO level and the HOMO level are affected. The LUMO position of the polymers might be shifted away from the vacuum level so much that the use of new electron acceptors with lower LUMO levels than the commonly used PCBM is needed for preparing an efficient solar cell. In a recent publication[57] Scharber et al. describe some design rules for electron donor materials. Based on his model the ideal material parameters for a conjugated polymer-PCBM device were determined. He claims that the efficiency of a solar cell can be predicted solely as a function of the band gap and the LUMO level of the donor. So besides a reduction of the band gap, new donor materials must be designed to optimize the LUMO as this parameter dominantly drives the solar cell efficiency.

## *1.6 Aim and outline of the thesis*

Mankind is still searching for reliable, cheap and environmentally friendly energy sources. The classical energy sources cannot provide these requirements for the future any more. The fossil energy sources coal, oil and gas cause air pollution and climate problems. Carbon dioxide, the final product of the combustion of all organic materials, is known to influence earth climate significantly. Also, the stock of these carbon-based fuels is limited and taught to run out in roughly 50 years. The use of nuclear power as energy source is not accepted by a wide section of the population because of security and health risks. Further, the disposal of nuclear waste is still an unsolved problem, worldwide. Over the last decades, there have been big efforts for developing new, alternative energy sources. The sun, on the other hand, matches all requirements of an ideal energy source. It is reliable,

ubiquitous and for free. The nature uses the sun as its nearly only energy source in photosynthesis since billions of years. The direct conversion of sunlight into electricity by photovoltaic cells is known for many years. Monocrystalline silicon and gallium-arsenide devices exceed efficiencies of 24 % energy conversion of the terrestrial sunlight, but the production costs are too high for economic use in widespread energy production. Thin film technique should reduce material consumption and production costs. Typical materials, which are used in thin film photovoltaic devices, are inorganic semiconductors like amorphous and polycrystalline silicon, cadmium telluride and copper indium diselenide. Generally, all these inorganic semiconductors need high temperature operations in their production, which causes high cost, and are difficult to handle. Scientists and engineers are looking for new materials and systems. Organic semiconductors, including conjugated polymers, are promising materials for solar cells. Organic molecular and polymeric materials with an extended $\pi$-conjugated system gain interest as alternative semiconductors materials in the last decade. Several applications were demonstrated for these materials. Devices like light emitting diodes, field effect transistors and also photovoltaic devices have got industrial interest. Organic materials show several advantages for the application in solar cells. Their synthesis can be much cheaper as compared to conventional inorganic materials. Processing from solution is possible and offers an easy way for device fabrication. Spin coating, printing techniques and roll to roll processing are possible and realized. Further, the properties of organic materials can be tuned for the desired application. A wide range of possible materials is accessible.

Solar cells from polymeric materials show several advantages. The devices can be made flexible and semi-transparent. Plastic solar cells can be easily integrated into other devices. Materials are light weight and different colours can be selected. For the application in solar cells, material properties like good environmental stability, broad and intense absorption spectra and high charge carrier mobility are needed.

More specifically **chapter two** focuses on the synthesis of the plain PTV via the precursor approach. Different precursor routes will be compared. It will

be demonstrated that the dithiocarbamate precursor route allows for the synthesis of the low band gap PTVs. The production of photovoltaic device will be also discussed.

In **chapter three** a family of three alkyl substituted derivatives of PTV is synthesised also via a precursor approach. By changing the alkyl side chain of the polymer we are able to tune the chemical, electronic and solubility properties of the polymers.

In **chapter four** are presented the polar derivatives of PTV. Different polar side chains were introduced on the thienylene vinylene units. The problems related to the polymerisation of such polar precursor polymers via the dithiocarbamate precursor route are also analysed and discussed.

An alternative way to convert the precursor polymer is presented in **chapter five**. An easy way of modifying the precursor polymer is also shown.

Finally some ideas for future work are presented in **chapter six**, and a general conclusion on the study carried out for the development of the dithiocarbamate route will be given as well.

The dissertation is then completed with a list of abbreviations and publications followed by a summary and the acknowledgements.

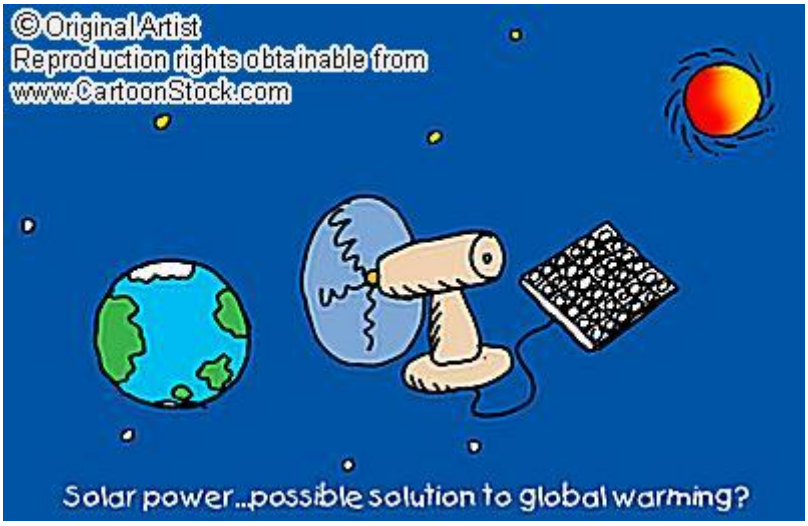

## 1.7 References


1. Groenendaal B. L., Jonas F., Freitag D., Pielartzik H. and Reynolds J. R., *Adv. Mater.* 12, (7), **2000**, 481.
2. Geffroy B., Le Roy P. and Prat C., *Polym. Int.* 55, (6), **2006**, 572.
3. Hoppe H. and Sariciftci N. S., *J. Mater. Res.* 19, (7), **2004**, 1924.
4. Spanggaard H. and Krebs F. C., *Sol. Energy Mater. Sol. Cells* 83, (2-3), **2004**, 125.
5. de Gans B. J., Duineveld P. C. and Schubert U. S., *Adv. Mater.* 16, (3), **2004**, 203.
6. Sheats J. R., *J. Mater. Res.* 19, (7), **2004**, 1974.
7. Brabec C. J., *Sol. Energy Mater. Sol. Cells* 83, (2-3), **2004**, 273.
8. Salzner U., Lagowski J. B., Pickup P. G. and Poirier R. A., *Synth. Met.* 96, (3), **1998**, 177.
9. Peierls R.E., *Quantum Theory of Solids,* **1955**.
10. van Mullekom H. A. M., Vekemans J. A. J. M., Havinga E. E. and Meijer E. W., *Mater. Sci. Eng. R-Rep.* 32, (1), **2001**, 1.
11. Rohatgi M., *Fundamentals of Photochemistry,* **1978**.
12. Roncali J., *Chem. Rev.* 97, (1), **1997**, 173.
13. Bredas J. L., *J. Chem. Phys.* 82, (8), **1985**, 3808.
14. Bredas J. L., *Synth. Met.* 17, (1-3), **1987**, 115.
15. Bredas J. L., Street G. B., Themans B. and Andre J. M., *J. Chem. Phys.* 83, (3), **1985**, 1323.

16. Hernandez V., Castiglioni C., Delzoppo M. and Zerbi G., *Phys. Rev. B* 50, (14), **1994**, 9815.

17. Conwell E.M., *Transport in Conducting Polymers,* **1997**.

18. Gilch H.G. and Wheelwright W.L., *J. Polymer Science* (4), **1966**, 1337.

19. Wessling R. A., *J. Polymer Science* (72), **1985**, 55.

20. Son S., Dodabalapur A., Lovinger A.J. and Galvin M.E., *Science* 269, (5222), **1995**, 376.

21. Burroughes J. H., Bradley D. D. C., Brown A. R., Marks R. N., Mackay K., Friend R. H., Burns P. L. and Holmes A. B., *Nature* 347, (6293), **1990**, 539.

22. Vanderzande D. J., Issaris A. C., VanderBorght M. J., van Breemen A. J., de Kok M. M. and Gelan J. M., *Macromol. Symp.* 125, **1998**, 189.

23. Henckens A., Lutsen L., Vanderzande D., Knipper M., Manca J., Aernouts T. and Poortmans J., *Proc. SPIE Int. Soc. Opt. Eng.* 5464, **2004**, 52.

24. Burroughes J. H., Jones C. A. and Friend R. H., *Nature* 335, (6186), **1988**, 137.

25. Chua L. L., Zaumseil J., Chang J. F., Ou E. C. W., Ho P. K. H., Sirringhaus H. and Friend R. H., *Nature* 434, (7030), **2005**, 194.

26. Horowitz G., *Adv. Mater.* 10, (5), **1998**, 365.

27. Newman C. R., Frisbie C. D., da Silva D. A., Bredas J. L., Ewbank P. C. and Mann K. R., *Chem. Mat.* 16, (23), **2004**, 4436.

28. Bradley D. D. C., *Synth. Met.* 54, (1-3), **1993**, 401.

29. Davis J., Vaughan D. H. and Cardosi M. F., *Enzyme Microb. Technol.* 17, (12), **1995**, 1030.

30. Gerard M., Chaubey A. and Malhotra B. D., *Biosens. Bioelectron.* 17, (5), **2002**, 345.

31. Heeger P. S. and Heeger A. J., *Proc. Natl. Acad. Sci. U. S. A.* 96, (22), **1999**, 12219.

32. Argun A. A., Aubert P. H., Thompson B. C., Schwendeman I., Gaupp C. L., Hwang J., Pinto N. J., Tanner D. B., MacDiarmid A. G. and Reynolds J. R., *Chem. Mat.* 16, (23), **2004**, 4401.

33. Gustafsson-Carlberg J. C., Inganas O., Andersson M. R., Booth C., Azens A. and Granqvist C. G., *Electrochim. Acta* 40, (13-14), **1995**, 2233.

34. McGehee M. D. and Heeger A. J., *Adv. Mater.* 12, (22), **2000**, 1655.

35. Hide F., DiazGarcia M. A., Schwartz B. J., Andersson M. R., Pei Q. B. and Heeger A. J., *Science* 273, (5283), **1996**, 1833.

36. Brabec C. J., Sariciftci N. S. and Hummelen J. C., *Adv. Funct. Mater.* 11, (1), **2001**, 15.

37. Nelson J., *Materials Today* 5, (5), **2002**, 20.

38. Meissner D., *Photon* **1999**,

39. Dennler G. and Sariciftci N. S., *Proc. IEEE* 93, (8), **2005**, 1429.

40. Coakley K. M. and McGehee M. D., *Chem. Mat.* 16, (23), **2004**, 4533.

41. Brabec C. J., Dyakonov V., Parisi J and Sariciftci N. S., *Organic Photovoltaics, concepts and realization,* **2003**.

42. Chabinyc M. L. and Salleo A., *Chem. Mat.* 16, (23), **2004**, 4509.

43. Clemens W., Fix I., Ficker J., Knobloch A. and Ullmann A., *J. Mater. Res.* 19, (7), **2004**, 1963.

44. Liu M. S., Niu Y. H., Luo J. D., Chen B. Q., Kim T. D., Bardecker J. and Jen A. K. Y., *Polym. Rev.* 46, (1), **2006**, 7.

45. Chapin D.M., Fuller C.S. and Pearson G.L., *J. Appl. Phys.* 25, **1954**, 676.

*46.* Miles R. W., Hynes K. M. and Forbes I., *Prog Cryst Growth Ch*

47. *Prog Cryst Growth Ch* 51, (1-3), **2005**, 1.

48. Weinberger B. R., Akhtar M. and Gau S. C., *Synth. Met.* 4, (3), **1982**, 187.

49. Glenis S., Tourillon G. and Garnier F., *Thin Solid Films* 139, (3), **1986**, 221.

50. Halls J. J. M., Pichler K., Friend R. H., Moratti S. C. and Holmes A. B., *Appl. Phys. Lett.* 68, (22), **1996**, 3120.

51. Karg S., Riess W., Meier M. and Schwoerer M., *Synth. Met.* 57, (1), **1993**, 4186.

52. Tang C. W., *Appl. Phys. Lett.* 48, (2), **1986**, 183.

53. Sariciftci N. S., Smilowitz L., Heeger A. J. and Wudl F., *Science* 258, (5087), **1992**, 1474.

54. Sariciftci N. S., Braun D., Zhang C., Srdanov V. I., Heeger A. J., Stucky G. and Wudl F., *Appl. Phys. Lett.* 62, (6), **1993**, 585.

55. Geens W., Aernouts T., Poortmans J. and Hadziioannou G., *Thin Solid Films* 403, **2002**, 438.

56. Hoppe H. and Sariciftci N. S., *J. Mater. Chem.* 16, (1), **2006**, 45.

57. Hoppe H., Niggemann M., Winder C., Kraut J., Hiesgen R., Hinsch A., Meissner D. and Sariciftci N. S., *Adv. Funct. Mater.* 14, (10), **2004**, 1005.

58. Scharber M. C., Mühlbacher D., Koppe M. , Denk P., Waldauf C. , Heeger A. J. and Brabec C. J., *Adv. Mat.* 18, (6), **2006**, 789

# Chapter Two

# Poly(2,5-thienylene vinylene)

## *2.1 Introduction*

Conjugated polymers are of a great interest for development of optical and electronic applications because of their extended $\pi$-electron delocalisation along the backbone. However, a problem in the synthesis of conjugated polymers is their insolubility due to their rigid backbone. Quite often this problem is circumvented using a soluble and easy processable non-conjugated precursor polymer. Nowadays, such precursor polymers can be synthesised via four different routes: the dehalogenation or Gilch route[1], the sulphonium or Wessling-Zimmerman precursor route[2,3], the xanthate precursor route[4] and the sulphinyl precursor route[5-7]. These four routes have in common that they make use of the polymerisation behaviour of p-quinodimethane systems. However, they differ in the choice of the leaving group (L) and of the polariser group (P) in the pre-monomer structure as well as of the polymerisation conditions used (base and solvents, reaction temperatures and reaction time). Initially these methods were developed for the synthesis of poly (*p*-phenylene vinylene) (PPV) derivatives and later they were adapted for the synthesis of other poly (heteroarylene vinylene)s, although leading to mixed results.

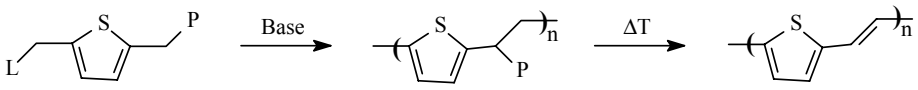


***Scheme 2.1*** *Synthesis routes towards poly (arylene vinylene)s: Wessling-Zimmerman: L = P = $^{\oplus}SR_2$; Gilch: L = P = Cl; Xanthate: L = P = SC(S)OR; Sulphinyl: L = Cl, P = S(O)R.*

In particular, the synthesis of electron rich conjugated polymers such as Poly (2,5-Thienylene Vinylene), *via* these precursor routes is problematic (**Scheme 2.1**). Despite the fact that *Harper and Watson*[8] patented the Wessling route towards PTV, it was when *Elsenbaumer*[9-11] polymerised 2, 5-bis (tetrahydrothiophenonium methyl) thiophene dichloride in water, that research towards PTV accelerated. The precursor polymer obtained was not stable, thus leading to spontaneous elimination to the unprocessable PTV. *Saito*[12-15] and *Murase*[16, 17], working independently, reported on the synthesis of a precursor polymer bearing methoxy leaving groups. This polymer, precipitated from the reaction mixture, when the water-soluble sulphonium precursor was treated with methanol. Moreover, this precursor was soluble in organic solvents, which was favourable for the characterisation and processability of the polymer.

Later, *Eevers*[18, 19] and *Xie*[20] reported on a preparation method for PTV from a methoxy precursor polymer. In 1989, *Iwatsuki*[21] described an alternative method to prepare a film of fully conjugated PTV by a dehydrogenation reaction in dioxane from a poly (2,5-thienylene ethylene) (PTE) film using 2,3-dichloro-5,6-dicyano-1,4-benzoquinone (DDQ) as an oxidising reagent and, more recently, *Herwig*[22] patented a method involving the polymerisation of 2,5-bisthioalkylmethylthiophenes.

Anyhow, all these routes suffer from one or more drawbacks, e.g. the need to use HCl gas to promote conversion or the use of an additional reagent for post-polymerisation modification. Furthermore until recently, the high reactivity of intermediates or even the monomer itself, preclude the development of a reproducible, versatile and high yield polymerisation process towards PTV derivatives. This feature is directly related to the electron rich nature of the thiophene ring.

For example, in our research group[23-25] the development of the synthesis of PTV via the sulphinyl precursor route was started, but instability of the intermediary products towards the corresponding sulphinyl monomer precluded good results. Consequently we started a study of another precursor route, which could hold the promise of a stable monomer structure: the xanthate precursor route. Both in our research group[24] and by *Burn* and co-

workers[26], it was found that the xanthate precursor route could be used to synthesise PTV. However, in the use of this method, some drawbacks as the rather low yield and the high polydispersity (PD > 15) of the obtained polymers were found. A shift to lower wavelengths of the maximum absorption $\lambda_{max}$ of the polymer so obtained ($\lambda_{max}$ < 540 nm compared to $\lambda_{max}$ = 600 nm found in literature[9]) was also observed. This was interpreted as an indication for the presence of structural chemical defects in the backbone of the conjugated polymer. Independently we[25] and Padmanaban[27] considered the use of a dithiocarbamate functional group as a potential precursor for a double bond. In the latter case a PPV-precursor was synthesised by competitive nucleophilic substitution of the Wessling polyelectrolyte with the respective nucleophile, sodium diethyl dithiocarbamate. Detailed studies of the thermal-elimination kinetics of the dithiocarbamate precursor, both in solution and in thin films, were carried out by an *in situ* monitoring of their ultraviolet-visible (UV-Vis) spectra. We could obtain a similar precursor polymer by base induced polymerisation of a bis-dithiocarbamate derivative of the corresponding monomer[28, 29].

## *2.2 Synthesis of PTV via the dithiocarbamate precursor route*

### 2.2.1 Monomer synthesis

The bis-dithiocarbamate thiophene monomer was synthesised starting from the commercially available di-methyl 2,5-thiophenedicarboxylate **1a**, which was firstly transformed into the diol **2a** using Lithium Aluminium Hydride ($LiAlH_4$) (**Scheme 2.2**) under $N_2$ atmosphere. The reduction step gave the diol in a yield of 90 %.

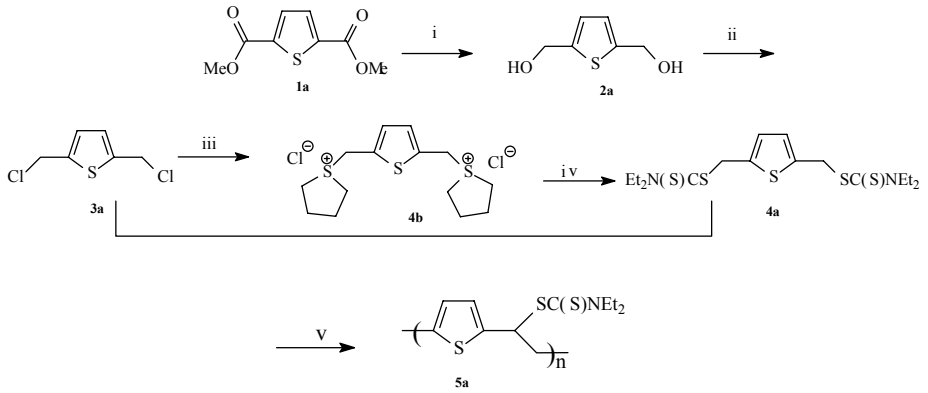


***Scheme 2.2*** *Synthesis of dithiocarbamate precursor polymer 5a: i) $LiAlH_4$, THF; ii) $SOCl_2$, THF; iii) THT; iv) $NaSC(S)NEt_2.3H_2O$; v) LDA (or LHMDS), THF*

It is well known that esters are less reactive towards nucleophilic substitution than aldehydes or ketones. Therefore, they can be reduced only by $LiAlH_4$ and not by the less reactive $NaBH_4$. Then 2,5-bischloromethylthiophene **3a** is obtained by the reaction of the formed alcohol with thionylchloride ($SOCl_2$) in dry THF. Since the dichloride proved to be highly unstable, an *in-situ* conversion towards the dithiocarbamate monomer was performed: the dichloride **3a** was dissolved in ethanol and sodium diethyl dithiocarbamate trihydrate was added to the reaction mixture as a solid to obtain the monomer **4a**. In alternative, the dichloride can be firstly converted into the relative bissulphonium salt **4b** by reaction with tetra-hydrothiophene. The bissulphonium salt is more stable, then it can be stored and used when necessary.

## 2.2.2 Polymerisation

The monomer **4a** was purified in a first instance *via* a recrystallisation from an ethanol/water (6/5) mixture. The polymerisation reactions from this batch led to precursor polymers with very low molecular weights ($M_w$) and yield. The presence of traces of water, not detectable in NMR, interfered with the polymerisation reactions. Therefore, it was then necessary to freeze dry the monomer in order to eliminate all the traces of water.

The polymerisation of the thiophene dithiocarbamate monomer, **4a**, was performed in a three-necked flask. The monomer was dissolved in dried THF

and degassed by passing through a continuous nitrogen stream. A solution of base (2 M LDA solution in THF/n-hexane or, 1 M LHMDS solution in THF) was added in one go through a septum. Then, the reaction was stirred at a given temperature for 90 minutes under nitrogen atmosphere. After this time, the mixture was poured out in ice water in order to stop the reaction. In case of a polymerisation temperature of -78 °C, the mixture was quenched first with ethanol instead of water. Afterwards an extraction with chloroform was performed. The combined organic layers were concentrated in vacuo. The crude product was dissolved again in chloroform, and afterwards precipitated in a 1/1 mixture of diethyl ether/n-hexane at 0 °C, then collected and dried in vacuo. The polymerisation results are presented in **Table 2.1.** Molecular weights were determined by size exclusion chromatography (SEC) with dimethylformamide (DMF) as eluent.

| Polymer | Entry | # eq. LDA | $\lambda_{max}$ (nm) | $M_w$ g/mol | PD | Temp. (°C) | Yield (%) |
|---|---|---|---|---|---|---|---|
| **5a** | 1 | 1.0 | 527 | 16900 | 1.8 | -78 | 45 |
| | 2 | 1.0 | 392 | 7400 | 1.3 | 0 | 45 |
| | 3 | 1.0 | 425 | 8700 | 1.4 | R.T. | 40 |
| | 4 | 1.2 | 546 | 10800 | 1.4 | -78 | 65 |
| | 5 | 1.5 | 527 | 13100 | 1.3 | -78 | 63 |
| | 6 | 2.0 | 500 | 209200[a]<br>5300[b] | 4.0<br>1.2 | -78 | 50 |
| | 7 | 3.0 | 525 | 77400[a]<br>4600[b] | 2.5<br>1.1 | -78 | 60 |

[a] *bimodal $M_w$ distribution,* [b] *low molecular weight peak*

***Table 2.1*** *Polymerisation results for 5a with the use of LDA*

The $M_w$ values reported in the table are average values between experiments done in duplo. The experiments done in the same conditions showed a very good reproducibility.

The maximum absorption values depicted in the table are derived from UV-Vis measurements *in situ* (further details on the measurements are given in the experimental section). They are values at high temperature and are of a

great importance for the evaluation of the conjugated system and consequently for the structural properties of the obtained polymers as they refer to the presence/absence of defects in the conjugated system.

The polymerisation of **4a** led only to low $M_w$ polymers when one equivalent of base is used whatever the polymerisation temperature ($M_w$ < 17000 g/mol). After $^1$H-NMR analysis, the residual fraction showed only the presence of unreacted monomer (**Figure 2.1**). The chemical shifts of the monomer are listed in **Table 2.2.**

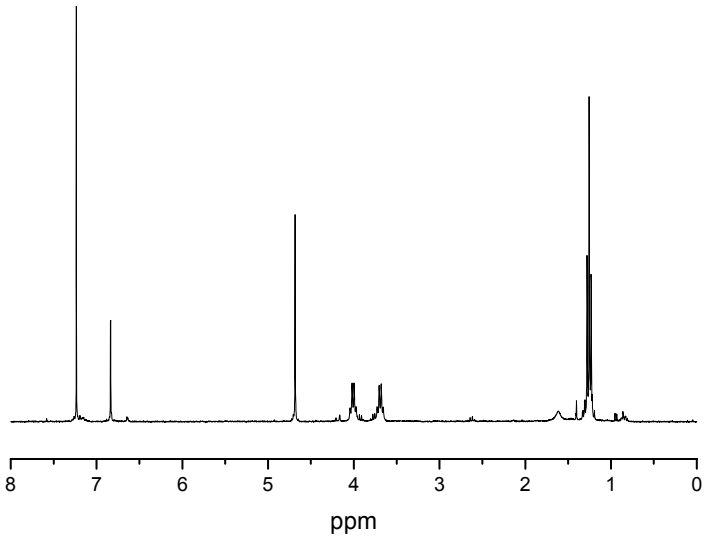


***Figure 2.1*** *$^1$H-NMR of the residual fraction after polymerisation of PTV with one equivalent of LDA*

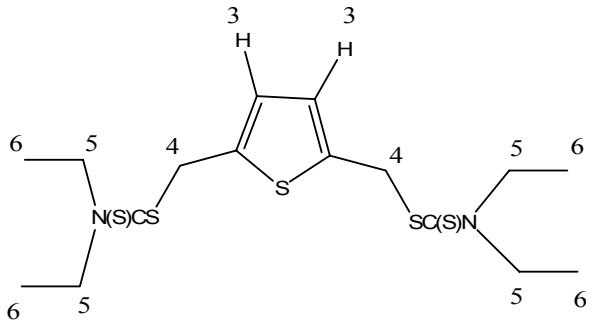


| Proton | 1H δ (ppm) |
|---|---|
| 3; 2H, s | 6.84 |
| 4; 4H, s | 4.69 |
| 5; 8H, dq | 4.01/3.69 |
| 6; 12H, t | 1.26 |

***Table 2.2*** *$^1$H-NMR chemical shifts values of 4a*

The observation that equimolar amounts of base led to the formation of oligomers, can be explained taking into account the actual kinetics of the formation of the real monomer, the quinodimethane system. In order to increase the velocity of its formation it is necessary to increase the concentration of base in the reaction mixture.

High $M_w$ PTV's are indeed obtained when 2.0 equivalents of base are used in the polymerisation reaction ($M_w \cong 200000$). The analysed residual fractions showed in this case the formation of side products besides some remaining monomer (**Figure 2.2**).

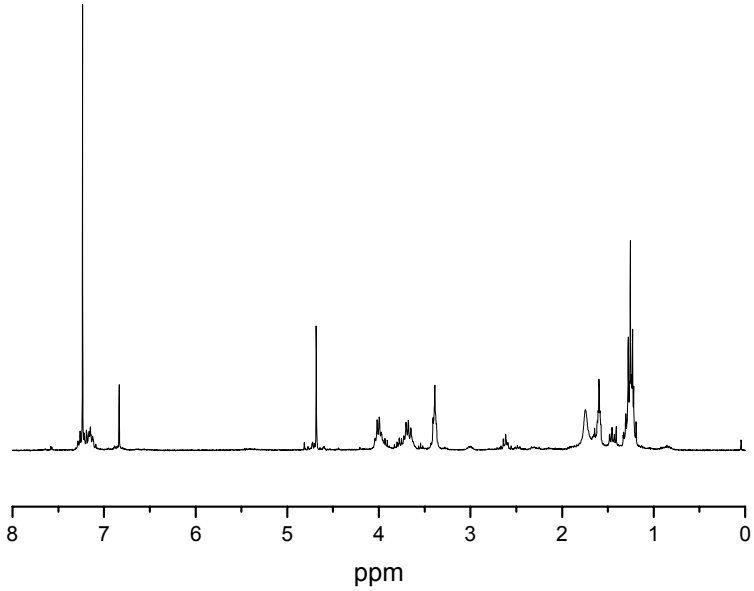


***Figure 2.2*** *$^{1}$H-NMR of the residual fraction after polymerisation of PTV with two equivalents of LDA*

This is clear from the appearance of extra peaks in the aromatic area around 7.2-7.1 ppm and in the aliphatic region between 1.0 and 3.5 ppm. The analysis of this complex mixture was quite difficult since the formation of many products was observed, and thus difficult to separate and isolate. Their presence was confirmed by thin layer chromatography (TLC) analysis on silica plate in different mixtures of solvents. Many products with very close relative retention factor ($R_f$) values, difficult to separate were observed.

The high $M_w$ precursor polymer produced in this way has a typical bimodal distribution, which could be explained by the presence of two mechanisms taking place simultaneously during the polymerisation process: anionic and radical polymerisation[30, 31].

Evidence for the existence of these two mechanisms was delivered earlier by our laboratory[30]. To our knowledge the high molecular weight fraction arises from a radical polymerisation mechanism and the low molecular weight fraction is due to an anionic mechanism.

In order to better characterise the polymers with bimodal distribution of $M_w$, and be able to handle homogeneous samples, purification by preparative gel permeation chromatography was carried out (**Figure 2.3**).

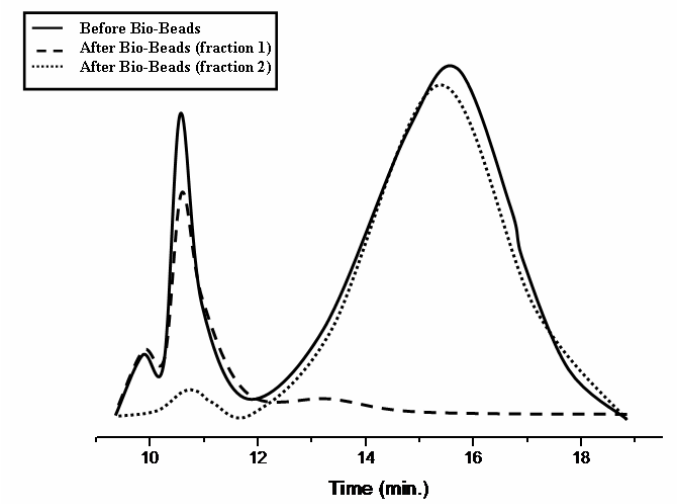


***Figure 2.3*** *GPC chromatogram before and after separation on Bio-Beads® of 5a*

With this aim, Bio-Beads® S-X were used, they are neutral porous styrene divinylbenzene copolymer beads. The beads chosen for the separation/purification of the polymers had an exclusion limit of 14000 Daltons (**Table 2.3**).

| **Before Preparative SEC $M_w$ (g/mol)** | **After Preparative SEC $M_w$ (g/mol)** | |
|---|---|---|
| **Polymer 5a** | **Fraction 1** | **Fraction 2** |
| 209209<br>5342 | 194321 | 4212 |

***Table 2.3*** *Results after purification with Bio-Beads® of 5a (entry 6)*

Going to higher concentration of base (3.0 equivalents), led again to a lower $M_w$, probably due to competing side reactions ($M_w \cong 70000$). However in this

case all the monomer is consumed and the analysis of the residual fraction shows a very complex mixture of compounds in accordance with the $^{1}H$ NMR spectrum (**Figure 2.4**).

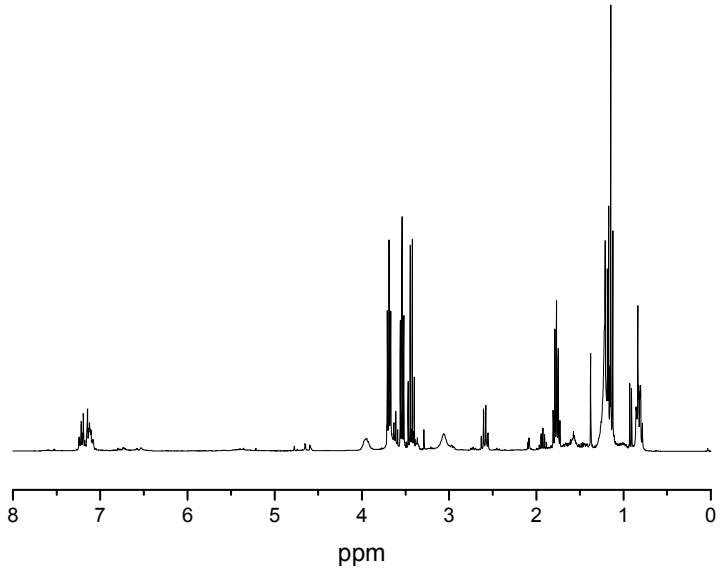


***Figure 2.4*** *$^{1}H$-NMR of the residual fraction after polymerisation of PTV with three equivalents of LDA*

The precise mechanism leading to such complex reactions is not yet completely clear, but it was assumed that is related to the use of LDA as a base[32]. LDA is a prominent reagent used in organic synthesis but a few drawbacks are related to its use. It shows a characteristic behaviour mainly caused by dominant solvatation and aggregations effects[33]. In THF solution, LDA exists primarily as a dimer (**Figure 2.5**) and, it is proposed to dissociate in order to afford the active base[34,35]. Furthermore, in hexane, LDA resides as a distribution of at least three as possibly as many as five cyclic oligomers[36-39].

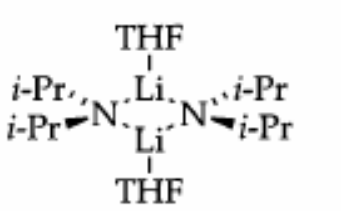


***Figure 2.5*** *Schematic representation of LDA dimer*

Seebach has alerted chemists on the possible consequence of aggregation and mixed aggregation in organolithium compounds[38]. It has to be noted that the dimers also act as base. Furthermore, LDA, promotes single electron transfer (SET) and deprotonation[40,41]. Recently, an LDA-mediated anionic Fries rearrangement of aryl carbamates was also reported. The choice of solvent and substrates dictates which intermediates can be observed as reaction proceeds[42]. The solvent is thus of extreme importance in order to understand the mechanism to optimise yields, rates, and selectivities of organolithium reactions. The presence of such complex mixture of side products after polymerisation has to be ascribed then to the properties of LDA besides being a base.

However, the use of an alternative base was suggested, *e.g.* Lithium Bis(trimethylsilyl)amide (LHMDS)[43]. Preliminary studies showed that the use of LHMDS (**Table 2.4**) instead of LDA yielded the precursor polymer **5a** into excellent yield and high molecular weight especially at 0 °C and room temperature[44]. The $\lambda_{max}$ values were derived from *in situ* UV-Vis measurements and give an indication on the quality of the materials made. The absorption value is directly correlated to the effective conjugation length of the polymer.

The $M_w$ values depicted in the table are average values between experiments done in duplo. The experiments done in the same conditions showed a very good reproducibility

| Polymer | Entry | # eq. LHMDS | $\lambda_{max}$ (nm) | $M_w$ g/mol | PD | Temp. (°C) | Yield (%) |
|---|---|---|---|---|---|---|---|
| **5a** | 8 | 1.0 | 480 | 5000 | 3.5 | -78 | 18 |
| | 9 | 2.0 | 476 | 19800 | 2.4 | -78 | 15 |
| | 10 | 3.0 | 523 | 146900 | 8.1 | -78 | 40 |
| | 11 | 1.0 | 476 | 4500 | 1.5 | 0 | 45 |
| | 12 | 2.0 | 555 | 225100 | 8.8 | 0 | 65 |
| | 13 | 3.0 | 549 | 153500 | 6.0 | 0 | 45 |
| | 14 | 1.0 | 498 | 7500 | 2.0 | R.T. | 25 |
| | 15 | 2.0 | 545 | 54900 | 5.2 | R.T. | 69 |
| | 16 | 3.0 | 530 | 43900 | 4.5 | R.T. | 45 |

***Table 2.4*** *Polymerisation results for 5a with the use of LHMDS*

These data demonstrate that: the type and concentration of the base, as well as the reaction temperature are significant parameters in the described polymerisation process.

The main advantages of using LHMDS instead of LDA relate to the opportunity to increase the reaction temperature from -78 °C to 0 °C, which is very important for a possible industrial application of this route. Another remarkable improvement is the absence of side reactions competing with the polymerisation process even when an excess of base was used (compare the NMR spectrum of **Figure 2.6** with that of **Figure 2.1**).

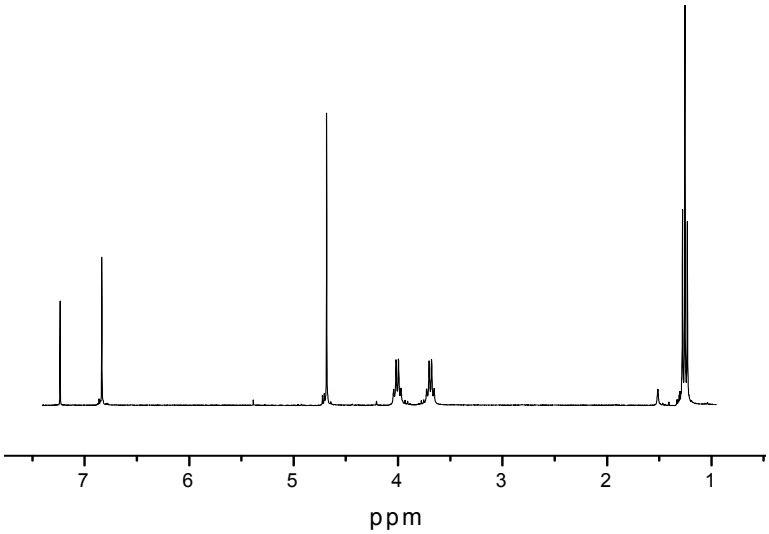


***Figure 2.6*** *$^1$H-NMR of residual fraction after polymerisation of PTV with three equivalent of LHMDS for 5a entry 13*

As a comparison also the NMR spectrum of the precursor polymer **5a** (**Figure 2.7**) is reported.

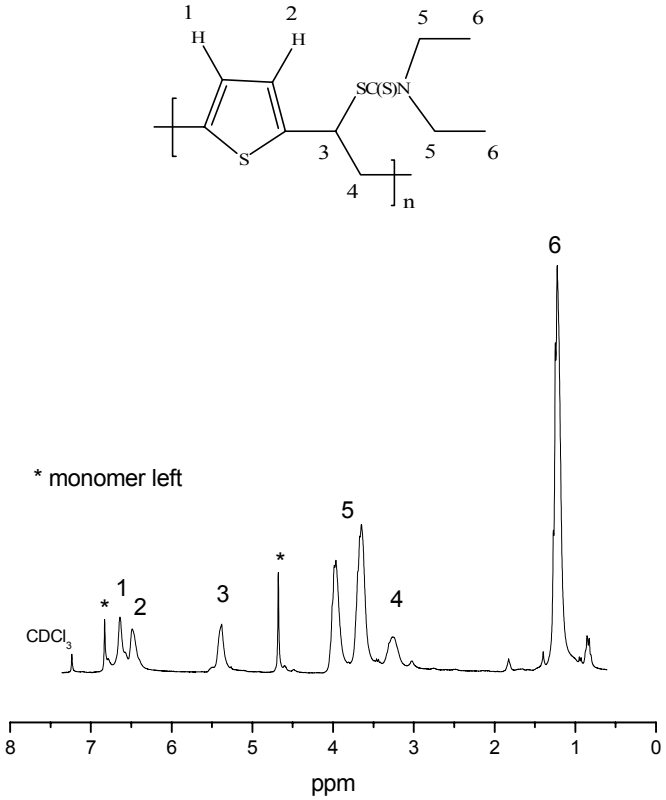


***Figure 2.7*** *$^1$H-NMR of 5a in $CDCl_3$*

Thirdly the $\lambda_{max}$ values of the obtained precursor polymer are higher than the one obtained with the use of LDA. This characteristic points to the presence of less structural defects in the conjugated system obtained using LHMDS.
Finally, the typical bimodal distribution observed with LDA (entry 6 and 7) is partially suppressed by using LHMDS and, even though, the apparently high values of polydispersity (PD) measured, are due to some tailing in the $M_w$ distribution as shown in **Figure 2.8**.

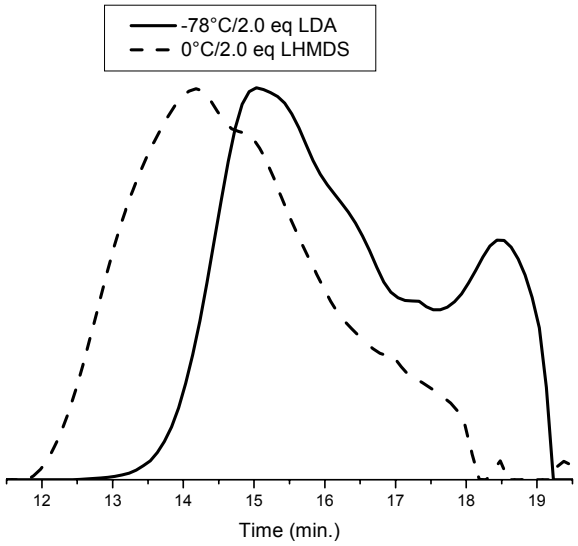


***Figure 2.8*** *GPC chromatogram for 5a: (solid line) when LDA was used; (dashed line) when LHMDS was used in the polymerisation reaction.*

This broad distribution finds an explanation in the fact that, one of the two mechanisms (presumably the anionic polymerisation) promoted by LDA is partially suppressed.

## *2.3 Characterisation*

### 2.3.1 Study of thermal conversion of the precursor polymers to the conjugated structure

The last step in the synthesis of the PTV polymers is the thermal elimination of the polarizer group, i.e. the dithiocarbamate group (**Scheme 2.3**).

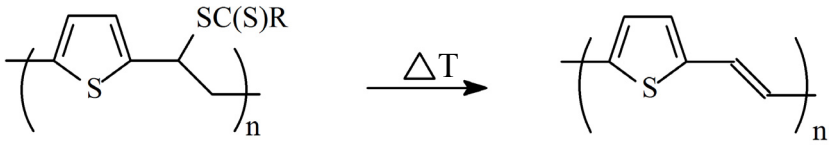


***Scheme 2.3*** *Conversion step towards the conjugated polymer*

The thermal elimination of the dithiocarbamate groups of the precursor polymer as well as the thermal stability of the conjugated polymer was studied by means of *in situ* techniques. Indeed, in order to deduct the conversion reaction protocol of the precursor polymers towards their conjugated forms, an *in-situ* UV-Vis and a complementary *in-situ* FT-IR studies were carried out. The reported UV-Vis and FT-IR spectra (**Figure 2.9** and **Figure 2.11**) are representative for both the low and the higher $M_w$ polymers, as they did not show significant differences in the conversion profiles but only in the $\lambda_{max}$ values.

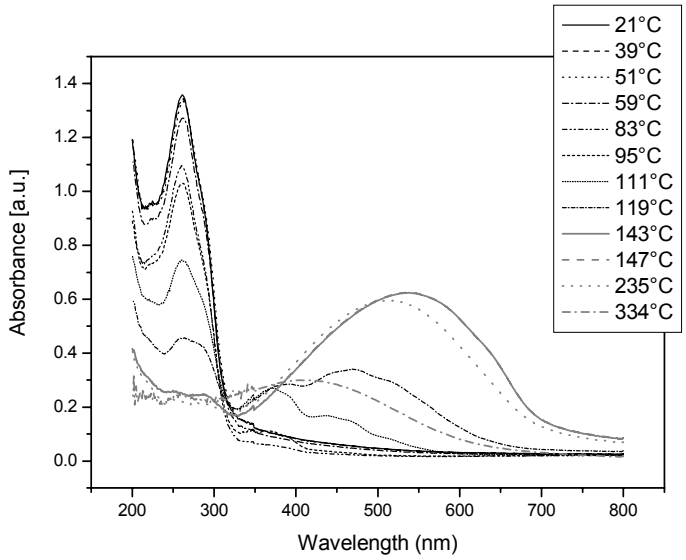


***Figure 2.9.*** *Uv-Vis in situ at different temperatures of 5a*

In general, when studying the thermal conversion to the conjugated structure from *in-situ* UV-Vis spectroscopy, it was observed that the absorption maxima at R.T. of the conjugated polymers are shifted to higher wavelengths (lower energy), compared to the polymers prepared *via* the xanthate route[25, 26]. This points out to an increased effective conjugation length of the π-electron system was achieved and thus it is an indication of less structural defects in the backbone of the obtained PTV.

More specifically, using LDA as the base, only the polymers obtained *via* the polymerisation reaction at -78 °C showed an acceptable $\lambda_{max}$ value > 500 nm (**Table 2.1**). At 0 °C and at room temperature, polymers with a $\lambda_{max}$ = 392 nm and 425 nm respectively were obtained. This may be an indication of the presence of structural defects and/or to very low effective average conjugation length of the polymer backbone due to a too low molecular weight.

The $\lambda_{max}$ values mentioned above were all measured at high temperature during conversion, so the absorption spectrum is shifted to lower wavelength as a consequence of a thermochromic effect[28] (a more detailed explanation is given in chapter 3).

In **Figure 2.10**, the absorbance at $\lambda_{max}$ of both the dithiocarbamate precursor polymer and the conjugated polymer are plotted as a function of temperature. From these profiles, it can be seen that the elimination of the dithiocarbamate groups of the thienyl precursor starts at around 100 °C.

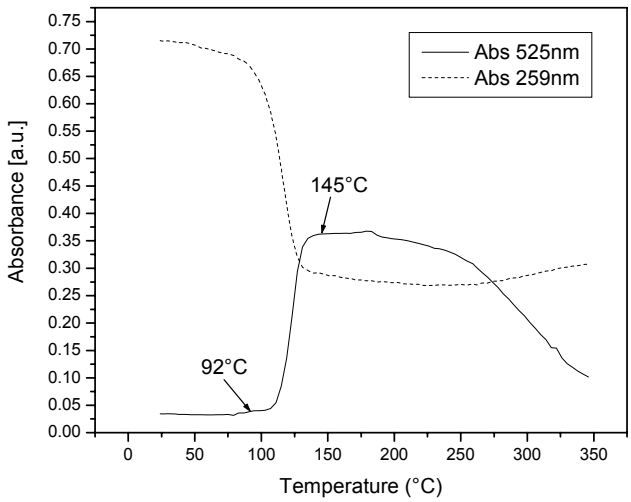


***Figure 2.10.*** *Absorbance profiles at 259 and 525 nm as a function of temperature on conversion of the precursor polymer 5a.*

*In-situ* FT-IR spectroscopy measurements were also carried out. **Figure 2.11** shows a part of the FT-IR spectra of the precursor polymer during the conversion reaction obtained at different temperatures.

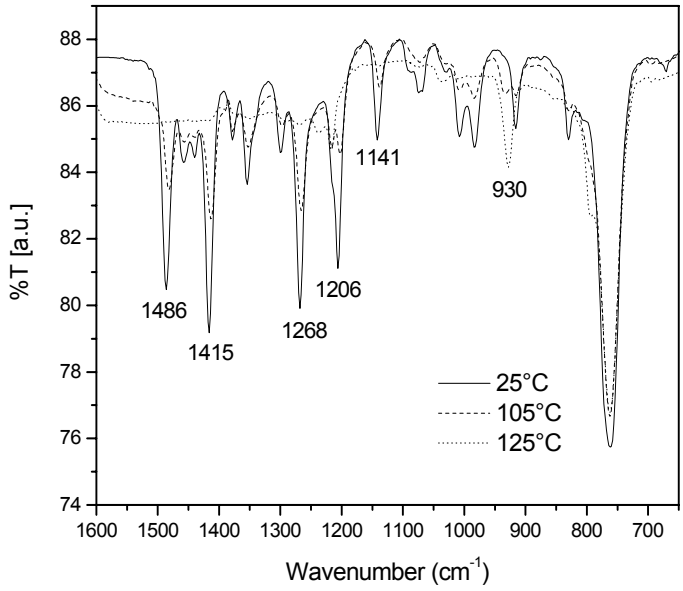


***Figure 2.11*** *FT-I.R. spectra at different temperature*

The dithiocarbamate precursor polymer shows strong transmission bands at 1486, 1415, 1268 and 1206 $cm^{-1}$ which all arise from the dithiocarbamate leaving group. By heating the precursor polymer at 2 °C/min from room temperature up to 350 °C, the conversion reaction is observed between 85 and 140 °C. This statement is corroborate by the decrease of the intensity of the typical dithiocarbamate groups absorption bands and the appearance of a absorption peak at 930 $cm^{-1}$ which is characteristic of the *trans*-vinylene double bonds as visualised in **Figure 2.12**.

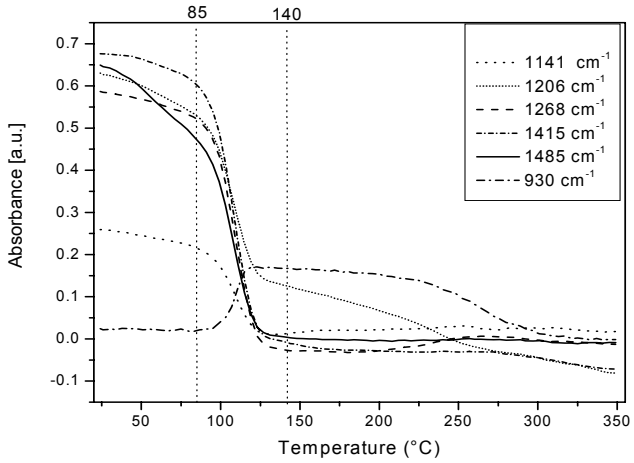


***Figure 2.12.*** *IR absorption profiles at 1415, 1268 and 930 cm-1 as a function of temperature*

In **Figure 2.13** and **Figure 2.14** the UV-Vis *in situ* and the absorbance profile in function of temperature for PTV obtained using LHMDS in the polymerisation process are presented. The high molecular weight polymers show typically higher $\lambda_{max}$ values ($\lambda_{max}$ = 555 nm) than the materials synthesised using LDA.

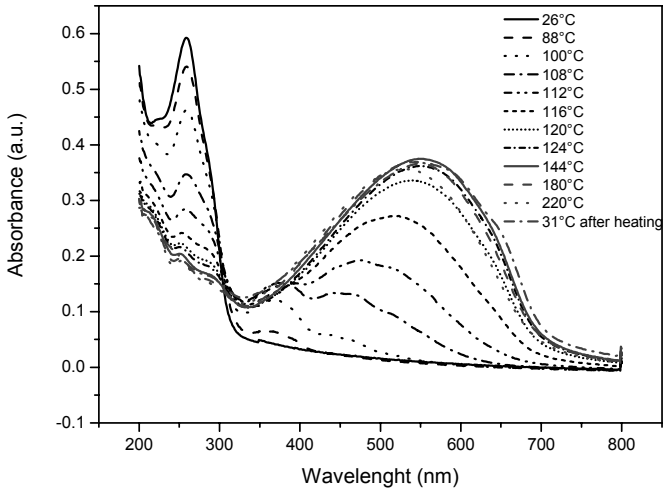


***Figure 2.13*** *Uv-Vis in situ of 5a entry 12*

It is noteworthy that no significant degradation of the conjugated system (**Figure 2.10** and **Figure 2.12**) was observed until 200-250 °C indicating a high stability of the conjugated system.

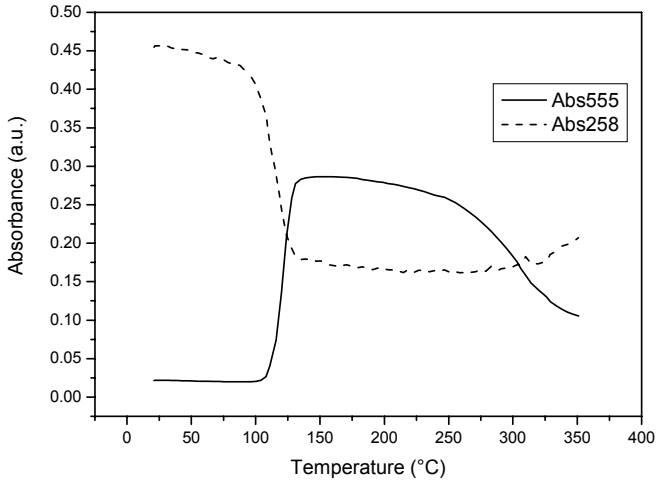


***Figure 2.14.*** *Absorbance profiles at 258 and 555 nm as a function of temperature for 5a entry 12*

## 2.3.2 Cyclic voltammetry (CV)

The measurements were performed by S. Fourier at Uhasselt.

Cyclic voltammetry measurement was applied on a PTV sample using 0.1 M $TBAPF_6$ as supporting electrolyte in anhydrous acetonitrile (ACN) was applied to investigate the redox behaviour of the different polymers and to estimate the highest occupied molecular orbital (HOMO) and the lowest unoccupied molecular orbital (LUMO) energy levels. The electrochemical experiments were carried out in a conventional three-electrode cell using 0.1 M tetrabutylammoniumhexafluorophosphate ($TBAPF_6$) in anhydrous acetonitrile as supporting electrolyte. The working electrode was a platinum disk electrode or an Indium-Tin-Oxide (ITO) coated glass substrate. The counter electrode was a platinum wire, which was placed in a separate compartment with a semi-porous frit. As a reference electrode, a silver wire in a 0.1 M

$AgNO_3$ containing electrolyte solution was used. After each measurement the reference electrode was calibrated with ferrocene (which under standard condition has an E° in the range 0.03 – 0.07 V *vs*. $Ag/AgNO_3$).

The oxidation process corresponds to the removal of electrons from the highest occupied molecular orbital (HOMO) and, it is associated with the ionisation potential (IP). Whereas, the reduction cycle corresponds to the filling by electrons of the lowest unoccupied molecular orbital (LUMO) (electron affinity EA). The onset oxidation and reduction potentials are closely related to the energies of the HOMO and LUMO levels of an organic molecule and thus can provide important information regarding the magnitude of the energy gap. The oxidation and reduction onset potentials are determined from a cyclic voltamogram. For the conversion from the oxidation and reduction potentials in Volt to an energy level in eV a large variety of calculation methods can be found in literature[45].

The energy parameters IP (HOMO) and EA (LUMO) are related to the measured redox potentials by the equations:

$$IP = E_{HOMO} = - (E_{OX} + 4.44)eV$$

$$EA = E_{LUMO} = - (E_{RED} + 4.44)eV$$

Where the $E_{OX}$ and $E_{RED}$ are the oxidation and reduction potentials in volt *versus* the NHE (Normal Hydrogen Electrode) potential. The reduction potential of the reference electrode SCE (Saturated Calomel Electrode) is 0.24 V *vs*. NHE.

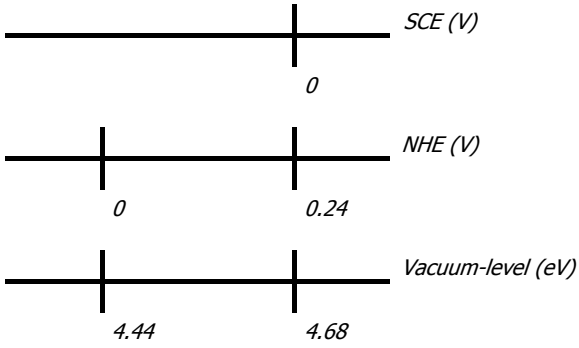


Based on the significant amount of theoretical work supporting this conversion method, this calculation procedure is deemed significantly more reliable than other methods. This leads to a general scheme (**Figure 2.15**) for the calculation of the HOMO and the LUMO values which has been used for the CV measurements done in this thesis.

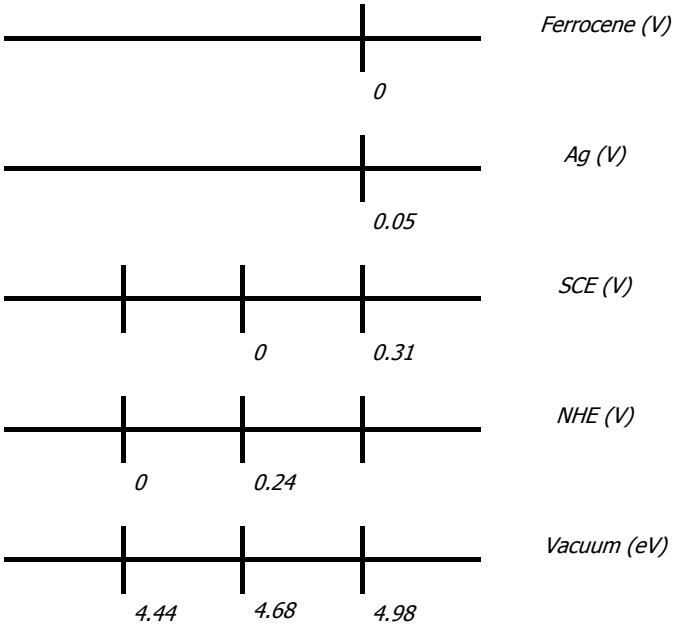


***Figure 2.15*** *Method of calculation for CV measurements*

The cyclic voltamograms for a typical PTV polymer (**Figure 2.16**) shows a reversible p- and n-doping behaviour. The electrochemical HOMO and LUMO

energy gap ($E_g$) was calculated from the oxidation and the reduction onset values.

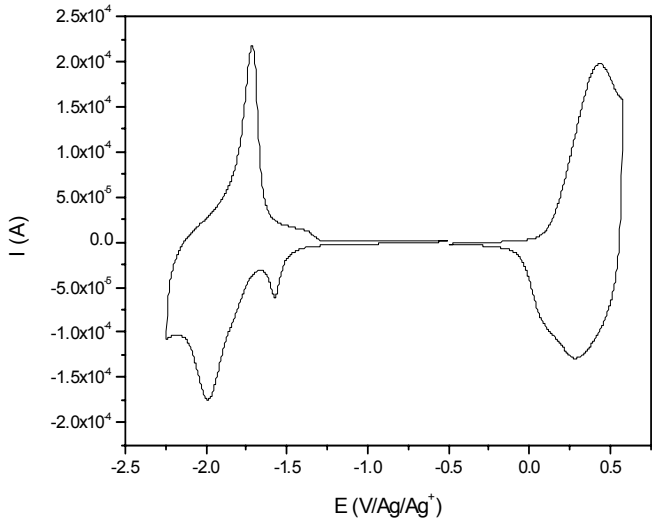


***Figure 2.16*** *CV Voltamogram for PTV*

The oxidation and reduction peak potentials are 0.44 V *vs.* $Ag/AgNO_3$ and -1.98 V *vs.* $Ag/AgNO_3$ respectively. The onset oxidation and reduction potentials are determined to be 0.15 V *vs.* $Ag/AgNO_3$ and -1.66 V *vs.* $Ag/AgNO_3$ from which the HOMO and the LUMO energy levels are estimated as -5.08 eV and -3.27 eV respectively. Hence, the electrochemical band gap energy is 1.81 eV. This band is comparable to the optical band gap, which has been determined from the absorption edge of a polymer thin film, *i.e.* 1.75 eV. These results indicate that PTV is a low band gap polymer[46].

At a potential of 1.5 V *vs.* $Ag/AgNO_3$, a shoulder is observed. During the synthesis of this polymer, a conversion step of a non-conjugated precursor polymer into its conjugated form is needed. This process takes place at high temperature. However, it is not uncommon that decomposition fragments of the leaving groups do not fully evaporate from the film. Since these leaving groups are electrochemically active, an additional peak may be observed in the cyclic voltammogram.

### 2.3.3 X-Ray Diffraction Spectroscopy (XRD)

The measurements were performed by G. Vanhooyland at IMO, Uhasselt.
The XRD profiles of PTV are given in **Figure 2.17**. This conjugated polymer was obtained by conversion in solution of the precursor polymer **5a** in 1, 2-dichlorobenzene under reflux for 3 hours. After precipitation of the solution in cold methanol, the conjugated polymer was filtered off and dried under vacuum in a desiccator.

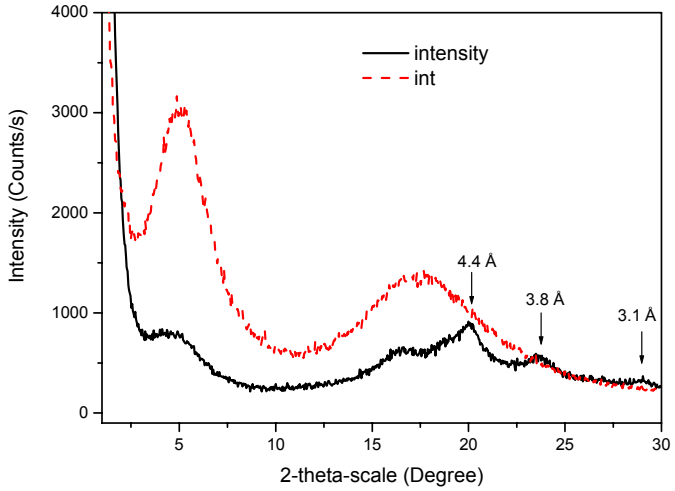


***Figure 2.17*** *XRD for PTV*

Looking at the XRD profiles a low radius order phenomenon can be observed as indicated by the presence of weak peaks near 2θ = 20°, 23.5° and 29° in the XRD profile. This corresponds to distances of 4.4 Å, 3.8 Å and 3.1 Å respectively.

### 2.3.4 Thermo Gravimetric analysis (TGA) and DIP-MS analysis

A TGA experiment on the precursor polymer with a molecular weight around 11000 (entry 4**, Table 2.1**) was performed at a heating rate of 10 °C per minute from room temperature up to 600 °C under a continuous flow of nitrogen (50 mL/min). In **Figure 2.18**, the weight loss of the sample (solid

line) and the derivative of the weight loss (dashed line) are plotted as a function of the temperature.

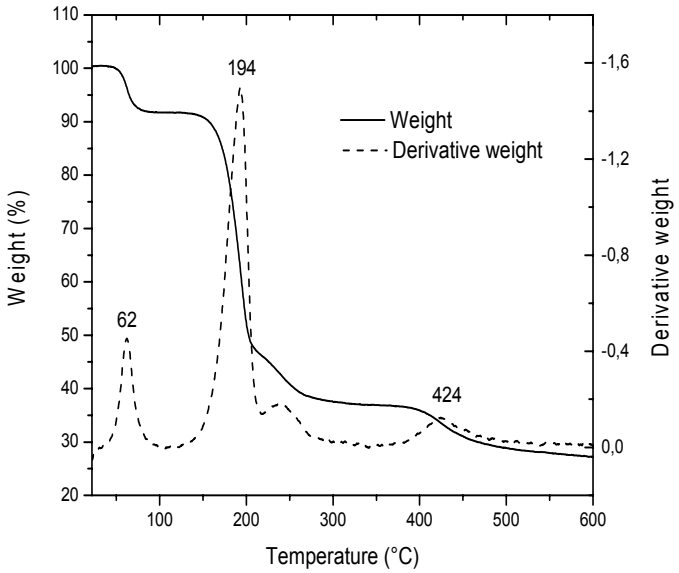


***Figure 2.18*** *TGA experiment for PTV 5a*

Two major steps of weight loss are visible: the first at 194 °C and the second at 424 °C. The first step is related to the conversion step (evaporation of the elimination products coming from the thermal cleavage of the dithiocarbamate groups). The second step of weight loss is assigned to a thermal degradation step (evaporation of the degradation products coming from a thermal degradation of the conjugated polymer backbone). The weight loss below 100 °C is assigned to the evaporation of residual solvents: chloroform (bp = 61 °C) and *n*-hexane (bp = 69 °C).

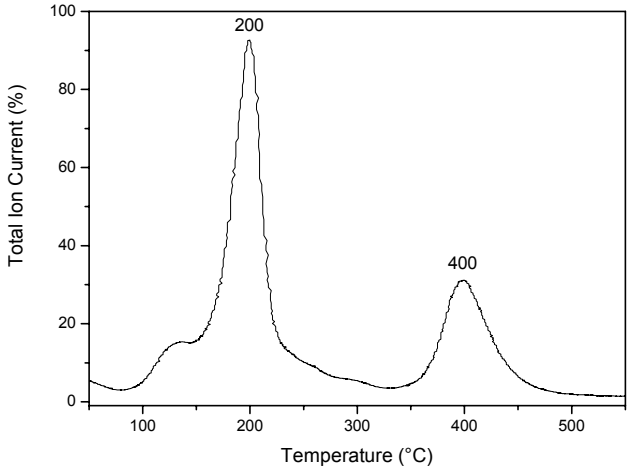


***Figure 2.19*** *DIP-MS analysis for PTV 5a*

The thermal behaviour of the same PTV dithiocarbamate precursor polymer (entry 4) was also evaluated by DIP-MS using a heating rate of 10 °C per minute (**Figure 2.19)**. It shows two distinct signals at a maximum temperature of 200 and 400 °C. The first signal, based on the detected fragments $Et_2N(S)CS$, $Et_2N(S)CS$ and $NEt_2$, was assigned to the elimination of the dithiocarbamate groups and the second one to the evaporation of the degradation products of the conjugated polymer. These observations are in accordance with those obtained with TGA analysis. The fact that a similar elimination temperature is observed in TGA (nitrogen atmosphere) and DIP-MS (vacuum) implies that the elimination products released are evaporated immediately at this temperature. Therefore, the elimination reaction and the evaporation process of the elimination products are not kinetically separated. The elimination temperature observed with these techniques (200 °C) is higher than that obtained from *in-situ* UV-Vis and *in-situ* FT-IR (90-140 °C). This difference is attributed to the difference in heating rate (10 °C/min and 2 °C/min respectively).

### 2.3.5 Determination of the glass transition temperature ($T_g$)

Differential Scanning Calorimetry (DSC) analyses of precursor polymer with low molecular weight were performed to determine the glass-transition temperature ($T_g$) of the polymer. From the thermogram (**Figure 2.20**) a $T_g$ of around 69 °C is deduced. A similar $T_g$ is also found for precursor polymer with higher $M_w$ ($T_g \cong 76$ °C).

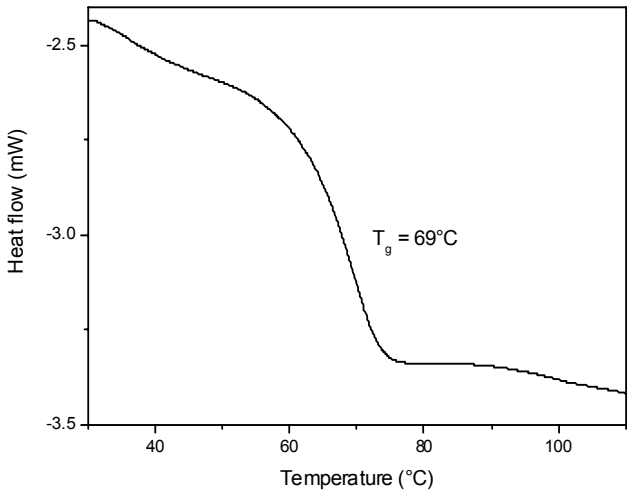


***Figure 2.20*** *Thermogram for PTV 5a*

These values are furthermore supported by a calculation based on the actual value of the absorption maximum of the π-π* transition plotted as a function of temperature. The intersection of the two obtained linear fits, with different slopes, gives a value of $T_g \cong 78$ °C[45].

Since the elimination does not start before 92 °C (**Figure 2.10**) we can conclude that the glass transition and the thermal conversion are two kinetically separated processes.

### 2.3.6 Charge Transfer processes

Charge transfer processes were studied in collaboration with the University of Antwerp, by Aranzazu Aguirre and Griet Janssen of the group of Etienne Goovaerts.

Light induced Electron Paramagnetic Resonance (Li-EPR) measurements were used to investigate the photoinduced charge transfer. EPR is a technique that focuses on unpaired electrons (paramagnetic species) and their close vicinity. It is not exclusively reserved for naturally occurring paramagnetic species but also applicable to materials that can after irradiation or any other physical or chemical treatment show a paramagnetic behaviour, like light induced radicals. In these experiments a static magnetic field is used in combination with a time dependent magnetic field, oscillating at high frequency. By the presence of the constant magnetic field and for species having one unpaired electron (S=1/2), the energy levels split in two due to the Zeeman interaction. The absorption/emission of microwaves (the time dependent magnetic field) with photon energy equal to this energy splitting allows the spin to flip from one level to the other. This resonant absorption/emission is what is detected in an EPR experiment. In practice, the resonance is measured at constant microwave frequency, by scanning of the static magnetic field. The importance of this technique is that the resulting spectrum is characteristic for the atomic/molecular system of interest, an identity card of the paramagnetic species.

Solutions of PTV in chlorobenzene (1 %) were prepared. Pristine PTV and blends with PCBM were prepared and a conversion *in situ* of the precursor polymer was performed under nitrogen at 175 °C for 13 minutes. The completeness of the conversion was monitored by UV-Vis measurements.

EPR experiments with PTV/PCBM blends (microwave power 70 μW, equivalent to 18 dB attenuation, 100 K and 10 scans) revealed an efficient electron transfer from the PTV polymer, identified by a significant increase of the polaron signal (positive radical, feature at lower magnetic field, at about 3.355 T) after laser light illumination, and the appearance of an intense

PCBM negative radical signal (feature at higher magnetic field at about 3.358 T **Figure 2.21**).

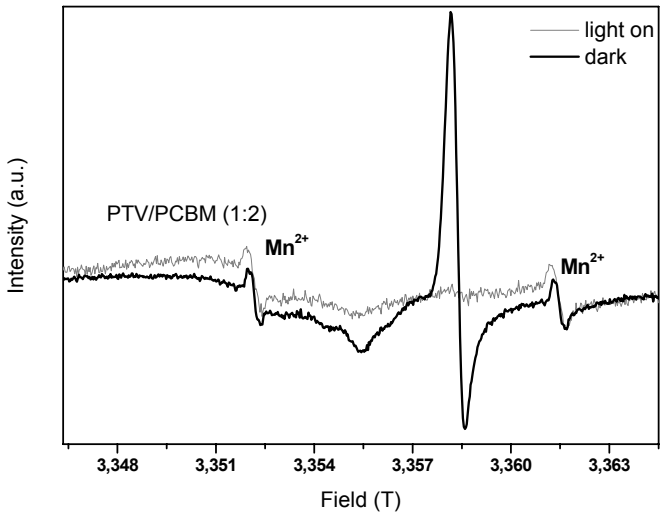


***Figure 2.21*** *W-band EPR (~95 GHz) spectrum of a PTV/PCBM blend obtained at 18 dB (microwave power 70μW), before and during illumination. The cavity originates a $Mn^{2+}$ signal.*

The EPR polaron signals are strongly saturated. Making an analysis of the g-values and of the geometry of the g tensor in the polaron is harder to achieve. The different microwave power saturation behaviour for the polarons and the PCBM radical is due to different spin-lattice relaxation times $T_1$.

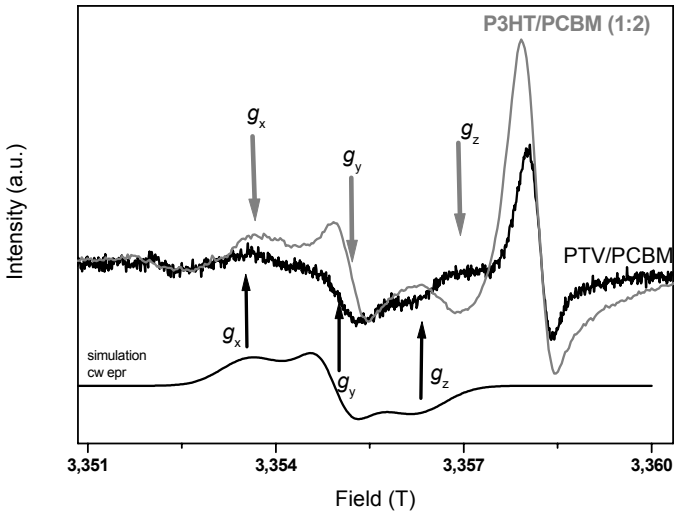


***Figure 2.22*** *W-band light induced EPR spectra under excitation at 488 nm of a PTV/PCBM blend (dark line) compared to that of a P3HT/PCBM blend (grey line), both measured at T = 100 K using low microwave powers, 42 dB (0.28 µW) and 48 dB (0.070 µW), respectively, to avoid saturation effects. Simulation of the EPR spectrum of the PTV/PCBM blend with g-values ($g_x$~2.0027, $g_y$~2.00185, $g_z$~2.00103)*

In continuous-wave (cw) EPR normally, the first derivative of the microwave absorption spectrum is measured (**Figure 2.22** the simulation and the spectra), while in saturation conditions (**Figure 2.21**) the signal resembles more the absorption spectrum. However, a light induced polaron with rhombic symmetry of the g-tensor ($g_x$~2.0027, $g_y$~2.00185, $g_z$~2.00103), could be confirmed in measurements at a lower microwave power of 0.28 µW (attenuation 42 dB) see **Figure 2.22**. This is similar to other observations in P3HT[47] and several other polythiophenes[48] which is indicative for the thiophene-like nature of the polaron state.

The saturation behaviour of the light-induced signal corresponds closely to that of the standard polymer blends like in P3HT/PCBM[47,49] and MDMO-PPV/PCBM[50,51], where the polaron signal is relatively more intense at lower microwave powers (while the PCBM radical signal would be more intense at higher power), due to the different relaxation properties.

## *2.4 Application in solar cells*

### 2.4.1 Mobility Measurements

The mobility of the polymers was studied in close collaboration with Martin Breselge from the group of Prof. Jean Manca at IMO-IMOMEC, University of Hasselt.

For the precursor polymers (entry 5 and entry 6 **Table 2.1**), the mobility was measured in an organic field effect transistor (OFET). From a 1 % dichlorobenzene solution a thin film was obtained and subsequently converted to PTV by heating the film from 25 °C up to 155 °C with a temperature ramp of 2 °C per minute. Then the sample was held at 155 °C for 20 min and than cooled down again at R.T. in argon atmosphere (cooling ramp of 2 °C / min). The hole mobility was measured in OFET geometry, standard polymer dielectric substrates. The mobility measurements were extracted from the transfer characteristics at $V_{sd}$ = -70V (saturation regime), using the following parabolic relationship between source-drain current $I_{sd}$ and gate voltage $V_{gate}$. The FET mobility can be calculated from the quadratic term of a least-square fit:

$$I_{sd} = ½ * W/L * c_i \mu_{FET} (V_{gate} - V_{thresh})^2$$

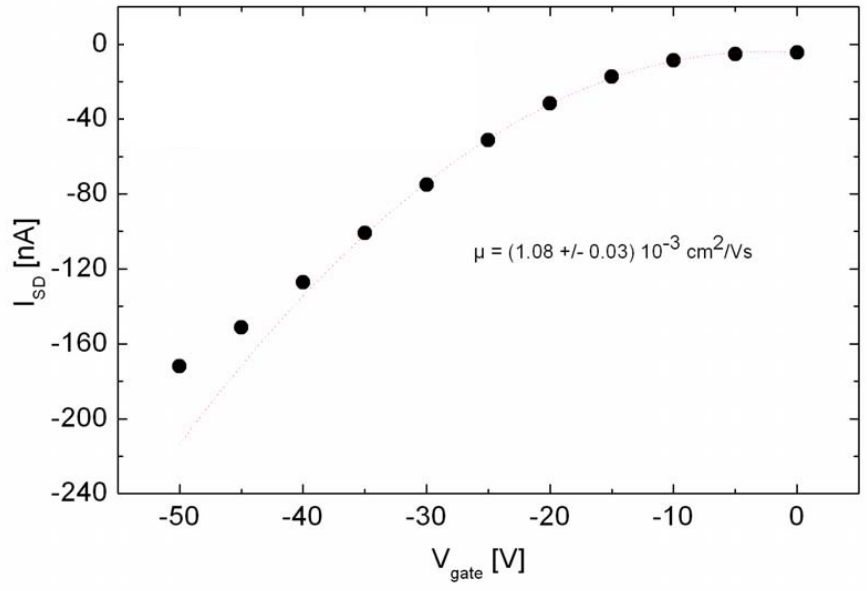


***Figure 2.23*** *Example of mobility measurement for high $M_w$ PTV 5a*

A typical curve is represented in **Figure 2.23**. All the curves produced showed to be regular and the calculated mobilities are: $\mu_{fe}$ ~ $5 \cdot 10^{-5} \div 1 \cdot 10^{-4}$ $cm^2$/Vs (entry 5); $\mu_{fe}$ ~ $1 \cdot 10^{-3} \div 5 \cdot 10^{-3}$ $cm^2$/Vs (entry 6). The mobility results show a correlation with the $M_w$, in the sense that, a high $M_w$ polymer shows crystallinity and this ordered structure induces higher μ values. The devices were measured in air without encapsulation.

## 2.4.2 Solar cell behaviour of PTV

Photovoltaic studies on solar cell devices were performed by Le Huong Nguyen and Helmut Neugebauer from the group of Serdar Sariciftci at Linz Institute for Organic Solar Cells (LIOS) in Austria[52].

PTV (**5a**) precursors with lowest (L: entry 5) and highest (H: entry 6) molecular weight were chosen for photovoltaic device (PV) testing. The best PV devices were obtained by preparing solutions of polymers L and H as donor component and the $C_{60}$-derivative 1-(3-methoxycarbonyl) propyl-1-phenyl [6,6] $C_{61}$ (PCBM) as acceptor in the bulk heterojunction concept at the optimized weight ratio of 1:2 and 1:1 respectively in chlorobenzene at a concentration of 10 mg polymer/ml.

Poly(3,4-ethylenedioxythiophene):poly(styrenesulfonate) (PEDOT:PSS) (Baytron P, Bayer Germany) was spin-coated on top of indium-tin oxide (ITO) (Merck, Germany) coated glass (~25 W/sq) which had been cleaned in an ultrasonic bath with acetone and isopropyl alcohol. The active layer (precursor polymer: PCBM blend) was spin-coated on the PEDOT: PSS layer and then converted to PTV under inert atmosphere (argon) in a dry glove box at optimised conditions which were preliminary studied *via* UV-vis measurements. Polymer L required 160 °C while polymer H needed a higher temperature of 190 °C for 10 min to obtain a sufficient conversion. 6 Å of lithium fluoride (LiF) and an 80 nm thick Al electrode was then deposited onto the blend film by thermal evaporation at ~5x $10^{-6}$ mbar. All current-voltage (I-V) characteristics of the photovoltaic devices were measured using a Keithley SMU 2400 unit under inert atmosphere (argon) in a dry glove box. A Steuernagel solar simulator was used as the excitation source with a power of 100 $mWcm^{-2}$ white light illumination (AM 1.5 conditions). A lock-in technique was used to measure the incident photon-to current efficiency (IPCE). With this technique the number of electrons produced from the cell under short-circuits conditions are related to the number of incident photons. Light intensity correction was performed using a calibrated Si photodiode.

I-V characteristics of ITO/PEDOT/PTV: PCBM/LiF/Al for the polymer L and H devices are shown in **Figure 2.24** both in dark and under AM 1.5 illumination.

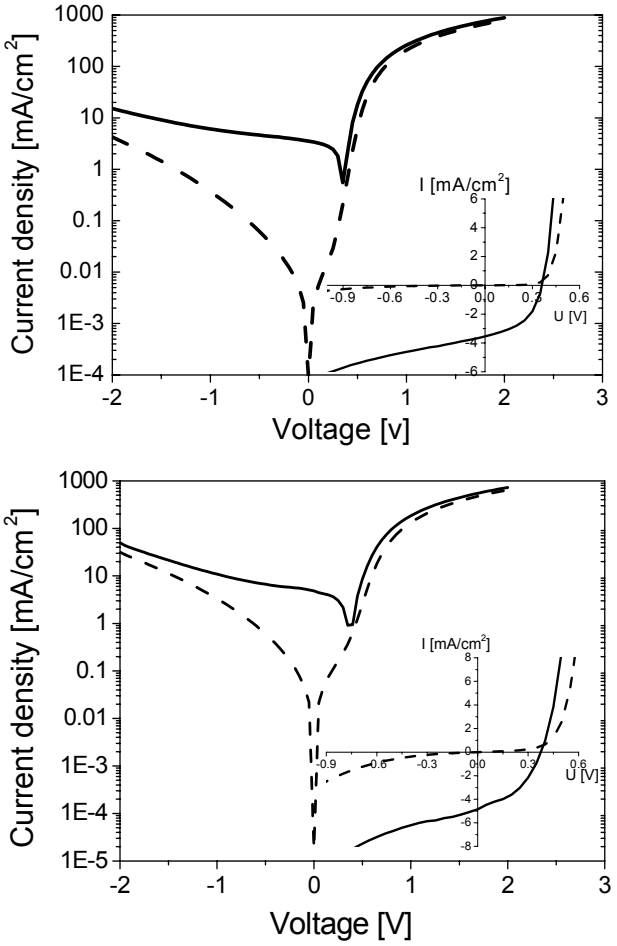


***Figure 2.24*** *I-V characteristics (AM 1.5, 100 mW/cm2) of the PTV: PCBM (upper figure) entry 5 and (below) entry 6*

**Table 2.5** compares the open-circuit voltage ($V_{OC}$), short-circuit current ($I_{SC}$), fill factor (FF) and conversion efficiency (h) for the different molecular weight PTVs. $V_{OC}$ and FF are comparable.

| Best Devices | $V_{oc}$ [mV] | $I_{sc}$ [mA/cm$^2$] | FF | Efficiency [%] |
|---|---|---|---|---|
| **L:PCBM (1:2)** | 350 | 3.5 | 0.49 | 0.61 |
| **H:PCBM (1:1)** | 350 | 4.85 | 0.45 | 0.76 |

***Table 2.5*** *Listed open-circuit voltage ($V_{OC}$), short-circuit current ($I_{SC}$), fill factor (FF) and conversion efficiency (h) for polymer 5a (entry 5 and 6)*

The polymer with higher molecular weight (H) shows a significant enhanced photocurrent. This may be contributed to the higher molecular weight having higher mobility[53]. This because charge carriers can travel further along longer chains before they have to hop to another chain, and longer chains give charge carriers more opportunities for hoping to neighbouring chains. Another explanation, may relate to the presence of crystallinity in high molecular weight polymers as anticipated earlier.

**Figure 2.25** reports the spectrally resolved photocurrent (IPCE) of the polymer L (black line) and polymer H (grey line) devices together with the corresponding absorption spectra of the pristine PTV (dashed lines). The IPCE spectrum of both devices shows an onset of the photocurrent at about 750 nm (1.65 eV) close to the optical band gap and exhibits a maximum of 17 % and 20 % at 550 nm for entries 5 and 6. The IPCE increases ~ 3 % for the highest molecular weight PTV.

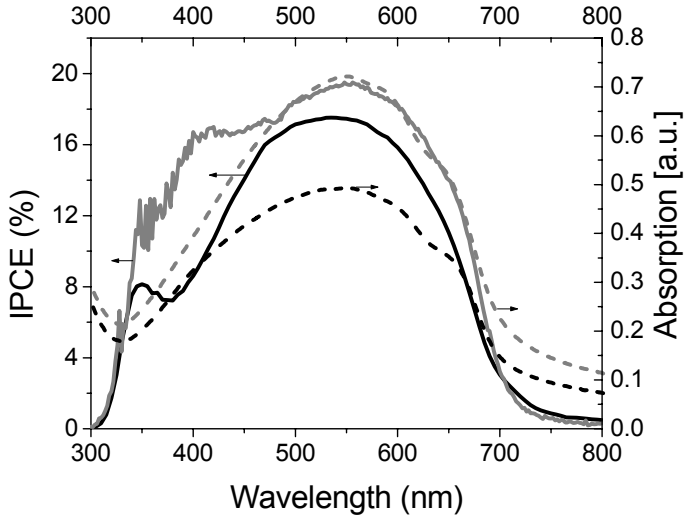


***Figure 2.25*** *IPCE % spectra of entry 5 (black solid line) and Entry 6 (grey solid line) devices and the corresponding optical absorption for the pristine PTV (dashed lines)*

In comparison to other low band gap polymer/PCBM systems such as polyfluorene/PCBM[54] and poly[5,7-bis-(3-octylthiophene-2-yl)thieno{3,4-b}pyrazine]/PCBM[55] the short circuit currents achieved in this study with the PTV/PCBM blend is significantly higher, up to about 5 mA/cm$^2$, leading to the final power efficiency of 0.76 %.

The low band gap polymer PTV can lead to a better matching of the absorption spectrum of the donor material to the solar emission spectrum. However, high performance devices require significant higher external quantum efficiencies. Molecular weight seems to have an effect on the performance of bulk heterojunction solar cells. Therefore, the further optimization of molecular weight of PTV could lead to significant improvements in device performance.

## *2.5 Synthesis of other thiocarbonyl-thio PTV derivatives*

In the previous section the use of the dithiocarbamate (DTC) precursor route was presented as a new pathway towards poly(arylene vinylene)s. The advantages inherent to the use of this route, as the good yield and the relative low polydispersity of the obtained precursor polymers, were also illustrated. However there were still some doubts regarding the possibility of polymerising thiocarbonyl thio compounds of a general formula S=C(Z)S, such as, trithiocarbonates (TTC) or xanthates (XTC).
To have a better understanding of the reactivity of these thio-compounds, we have synthesised different thiophene monomers, namely the xanthate and the trithiocarbonate monomers; the results are presented in the following paragraphs.

### 2.5.1 Substitution of halides with a dithiocarboxylic acid salt

The first step was the synthesis of the appropriate dithiocarboxylic salt necessary for the synthesis of the two new monomers. This process involves the nucleophilic substitution of a dithiocarboxylic acid salt with an alkyl or aryl halide to give dithioesters. Generally, the dithiocarboxylic acid salt is obtained by addition of carbon disulfide ($CS_2$) to an alcohol (ROH) and an alkali metal hydroxide (KOH)[56] as illustrated by the following reaction:

$$ROH + KOH + CS_2 \rightarrow KSC(S)OR + H_2O$$

After refluxing the corresponding alcohol (ethanol for **5b**, octanethiol for **5c**) in the presence of potassium hydroxide, carbon disulphide was added under constant stirring. The precipitated salt was filtered off and reacted with the bissulphonium salt yielding the appropriate monomer.

## 2.5.2 Variation of the dithiocarbamate group

By adding the dithiocarboxylic salt to the bissulphonium salt, the corresponding monomers were obtained. The procedure is described in **Scheme 2.4**.

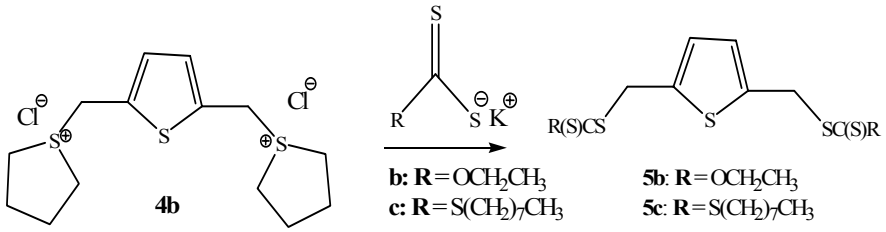


***Scheme 2.4*** *Synthesis of the xanthate and trithiocarbonate monomers*

The synthetic procedure used for the polymerisation of the dithiocarbamate monomers was also applied for the polymerisation of the xanthate and trithiocarbonate monomers (**Scheme 2.5**).

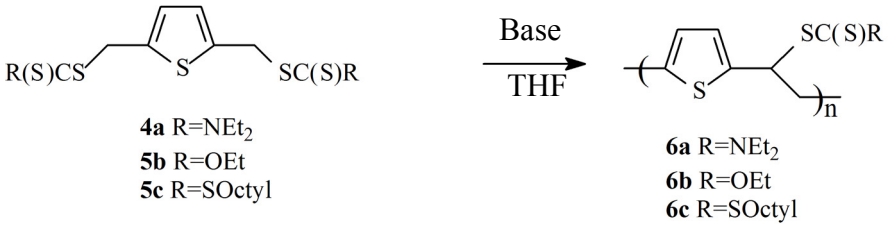


***Scheme 2.5*** *Polymerisation process*

The results are listed in **Table 2.6.** The molecular weights were determined by SEC in DMF relative to PS standards. As already said, the $\lambda_{max}$ values depicted in the table are values at high temperature (130 °C < T < 170 °C) and the $M_w$ are average results. All the experiments were done in duplo and they showed good reproducibility.

| Polymer | Entry | # eq. LHMDS | $\lambda_{max}$ (nm) | $M_w$ g/mol | PD | Temp. (°C) | Yield (%) |
|---|---|---|---|---|---|---|---|
| **5b** | 1 | 1.0 | 520 | 957200 | 8.6 | -78 | 15 |
| | 2 | 2.0 | 537 | 459600 | 64.8 | -78 | 22 |
| | 3 | 3.0 | 482 | 210000 | 11.7 | -78 | 55 |
| | 4 | 1.0 | /* | 37300 | 11.6 | 0 | 12 |
| **5c** | 5 | 1.0 | | 3400 | 1.7 | -78 | |
| | 6 | 2.0 | | 2400 | 1.5 | -78 | |
| | 7 | 3.0 | | 2500 | 1.3 | -78 | |
| | 8 | 1.0 | | 800 | 1.5 | 0 | |
| | 9 | 2.0 | | 700 | 1.4 | 0 | |
| | 10 | 3.0 | | 1800 | 2.8 | 0 | |
| | 11 | 1.0 | | 700 | 1.3 | R.T. | |
| | 12 | 2.0 | | 1400 | 1.3 | R.T. | |
| | 13 | 3.0 | | 1500 | 1.3 | R.T. | |

** The λmax was not measured*

***Table 2.6*** *Polymerisation results for 5b and 5c with the use of LHMDS*

The polymerisation data relative to the use of LDA (**Table 2.7**) in the polymerisation process are also reported for comparison.

| Polymer | Entry | # eq. LDA | $M_w$ g/mol | PD | Temp. (°C) |
|---|---|---|---|---|---|
| **5b** | 14 | 1.0 | 360600 | 19.7 | -78 |
| **5c** | 15 | 1.0 | 1000 | 1.3 | -78 |
| | 16 | 2.0 | 1400 | 1.4 | -78 |
| | 17 | 3.0 | 1500 | 1.4 | -78 |

***Table 2.7.*** *Polymerisation results for 5b and 5c with LDA*

The trithiocarbonate monomer can not be converted into polymers using either LDA or LHMDS as base. It shows indeed a poor reactivity towards conversion into polymers. Indeed TLC analysis run in different solvents showed the presence of the unreacted monomer as main component of the reaction mixture.

In the case of xanthate monomer, the ideal reaction temperature was -78 °C. The need to use a sufficiently low polymerisation temperature in this route was already reported earlier[57,58].

For all the xanthate precursor polymers very broad molecular weight distributions were observed. This could be an indication for the occurrence of different polymerisation mechanisms in competition with each other. The data obtained with the use of LHMDS are in good agreement with the earlier results using LDA[25]. Both show a broad PD and a low yield pointing to intrinsic polymerisation behaviour of the xanthate monomer.

### 2.5.3 Comparative study of the elimination of the dithiocarbamate and xanthate groups

The thermal elimination of the xanthate groups from the precursor polymer as well as the thermal stability of the conjugated polymer were studied using the same techniques used for the elimination of the dithiocarbamate group. An *in-situ* UV-Vis study was carried out in order to deduct the conversion reaction protocol of the precursor polymers towards their conjugated forms.

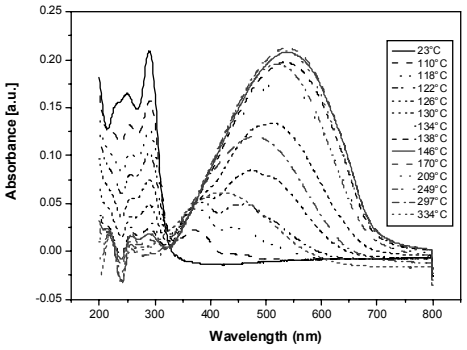


***Figure 2.26*** *Uv-Vis in situ of 5b entry 2*

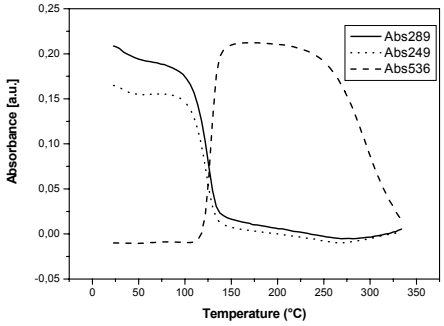


***Figure 2.27*** *Absorbance profiles at 289 and 537 nm as a function of temperature for 5b entry 2*

In **Figure 2.26** the UV-Vis spectrum of the precursor polymer **5b** with a $\lambda_{max}$ value of 537 nm is presented. For the ethyl xanthate precursor polymer (**5b Figure 2.27**), the formation of the first conjugated segment begins at about

115 °C and the elimination is completed at about 150 °C. The obtained conjugated polymer is stable till ~ 235 °C. Thus, it is clear that even in this case the effective conjugation length is smaller compared to the PTVs synthesised via the dithiocarbamate precursor route, using LHMDS as a base.
Strictly speaking, *in-situ* FT-IR measurements are expected to yield a confirmation of the conclusions derived from the *in-situ* UV-Vis measurements. Indeed, in the precursor polymer, most of the IR absorptions arise from stretching within the xanthate group. From the ethyl xanthate group, strong transmission bands at 1216 $cm^{-1}$, 1109 $cm^{-1}$ and 1044 $cm^{-1}$ are visible. When the precursor is heated, a new absorption band at 930 $cm^{-1}$ is formed. This band was assigned to the trans-vinylene C-H out-of-plane bending band. At the same time as this band is formed, the bands from the xanthate group decrease in intensity which is an indication that the xanthate group is being eliminated. The changes in intensity for the different peaks are shown in **Figure 2.28** where an overlay of IR spectra at different temperatures is plotted.

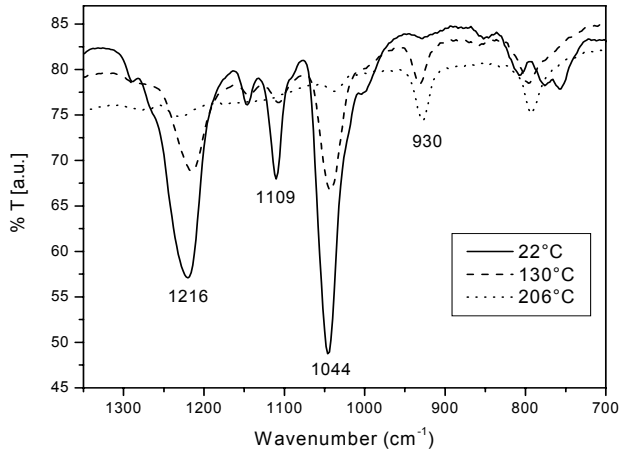


***Figure 2.28*** *IR spectra of 5b at 22, 130 and 206°C*

By plotting these signals as a function of temperature, the same trends seen before in the elimination behaviour can be recognised (**Figure 2.29**).

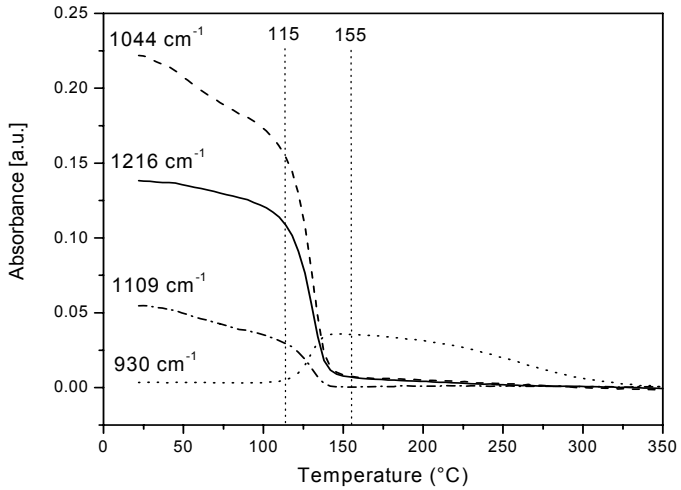


***Figure 2.29*** *IR absorption profiles at 1216, 1109, 1044 and 930 cm-1 as a function of temperature for 5b*

The slight decrease in intensity of the signal at 930 $cm^{-1}$ at increasing temperature in the region between 115 and 250 °C, is difficult to interpret because of the very small signal amplitude in that region.

## *2.6 Conclusions*

The dithiocarbamate precursor route was used for the synthesis of a precursor polymer towards Poly(2,5-Thienylene Vinylene) (PTV). Synthesis of the corresponding thiophene bis-methylene N,N-diethyl dithiocarbamate monomer was easily achieved. The polymerisation step was optimized and the best conditions were found at a temperature of 0 °C using an excess of base when LHMDS was used in the polymerisation reactions. This use of the dithiocarbamate precursor route for the synthesis of PTV shows some distinct advantages compared to the xanthate precursor route such as:

- Higher molecular weight;
- Lower values of polydispersity;
- Higher value for $\lambda_{max}$ of the conjugated PTV polymers and therefore higher effective conjugation lengths;

- Promising value for the field effect mobility and the energy conversion efficiency in organic solar cells.

All these observations indicate that the dithiocarbamate precursor route may provide a solution for the problem associated with the synthesis of electron rich Poly (p-Arylene Vinylene)s precursor routes.

Furthermore, the use of LHMDS allows to increase the reaction temperature from -78 °C (used with LDA) to 0 °C and this is very interesting for a possible industrial application of this route. Moreover, no side reactions were observed when LHMDS was used and the polymers so obtained showed better characteristics compare to the ones obtained with LDA.

When comparing the three different thiocarbonylthio compounds: dithiocarbamate, xanthate and trithiocarbonate derivatives it seems that only the dithiocarbamate route gives promising perspective as a polymerisation route.

## *2.7 Experimental part*

**Materials:** All solvents used in the synthesis were distilled before use. Tetrahydrofuran (THF) was refluxed under nitrogen with sodium metal and benzophenone until a blue colour persisted and was then distilled. All the commercially available products were purchased from Acros or Aldrich.

**Characterisation:** Nuclear magnetic resonance (NMR) spectra were recorded on a Varian Inova 300 spectrometer at 300 MHz for $^{1}H$ NMR and at 75 MHz for $^{13}C$ NMR using a 5 mm probe. Gas chromatography/mass spectrometry (GC/MS) analyses were carried out with TSQ – 70 or Voyager mass spectrometers (Thermoquest); the capillary column was a Chrompack Cpsil5CB or Cpsil8CB.

Average molecular weights and molecular weight distributions were determined relative to polystyrene standards (Polymer Labs) by Size Exclusion Chromatography (SEC). Chromatograms were recorded on a Spectra series P100 (Spectra Physics) equipped with two MIXED-B columns (10 μm, 2 x 30 cm, Polymer Labs) and a relative index (RI) detector (Shodex) at 70°C. A DMF solution of oxalic acid ($1.1\ 10^{-3}$ M) was used as the eluent at a flow rate of 1.0 ml/min. Toluene was used as flow rate marker.

GC/MS analyses were carried out at the TSQ – 70 and Voyager mass – spectrometers (Thermoquest), capillary column: Chrompack Cpsil5CB or Cpsil8CB.

Direct insertion probe mass spectroscopy (DIP-MS) was performed on a FINNIGAN TSQ 70, in electron impact mode, mass range of 35-650 and scan rate of 2 s. The electron energy was 70 eV. A chloroform solution of the precursor polymer was placed directly on the heating element of the probe and measurements were performed under high vacuum ($4.10^{-4}$ Pa). The polymer was heated from ambient temperatures till 650 °C at heating rate of 10 °C/min.

Fourier Transform Infra Red spectroscopy (FT-IR) was performed on a Perkin Elmer Spectrum One FT-IR spectrometer (nominal resolution 4 $cm^{-1}$, summation of 16 scans). Samples for the FT-IR characterisation were prepared by spin-coating the precursor polymer from a chloroform solution (6 mg/ml) onto NaCl disks (diameter 25 mm and thickness 1 mm) at 500 rpm. The NaCl disks were heated in a Harrick oven high temperature cell (purchased from Safir), which was positioned in the beam of the FT-IR to allow *in situ* measurements. The temperature of the sample and the heating source were controlled by a Watlow temperature controller. The heating source was in direct contact with the NaCl disk. Spectra were taken continuously and the heating rate was 2 °C/min from room temperature up to 350 °C. The atmosphere in the temperature cell could be varied from a continuous flow of nitrogen to vacuum (15 mmHg). Timebase software was used to investigate regions of interest.

Ultraviolet visible spectroscopy (UV-VIS) was performed on a VARIAN CARY 500 UV-VIS-NIR spectrophotometer (interval: 1 nm, scan rate: 600 nm/min, continuous run from 200 to 700 nm). The precursor polymer was spin-coated from a chloroform solution (6 mg/ml) onto quartz glass (diameter 25 mm and thickness 3 mm) at 700 rpm. The quartz glass was heated in the same Harrick oven high temperature cell as was used in the FT-IR measurements. The cell was placed in the beam of the UV-Vis spectrophotometer and spectra were taken continuously. The heating rate was 2 °C/min up to 350 °C. All measurements were performed under a continuous flow of nitrogen. Scanning kinetics software was used to investigate the regions of interest.

TLC analyses were made on Merck aluminium sheets, 20 x 20 cm, covered with silica gel 60 $F_{254}$.

Thin film electrochemical properties were measured with an Eco Chemie Autolab PGSTAT 20 Potentiostat/Galvanostat using a conventional three-electrode cell (electrolyte: 0.1 mol/L $TBAPF_6$ in anhydrous $CH_3CN$) with an $Ag/Ag^+$ reference electrode (0.01 mol/L $AgNO_3$, 0.1 mol/L $LiClO_4$ and $CH_3CN$), a platinum counter electrode and an Indium-Tin Oxide (ITO) coated glass substrate as working electrode. Cyclic voltamograms were recorded at 50 mV/s under $N_2$ atmosphere. All electrochemical potentials have been

referenced to a known standard, ferrocene/ferrocinium, which in acetonitrile solution is estimated to have an oxidation potential of -4.98 eV vs. vacuum-level.

The glass transition temperature ($T_g$), was measured by Differential Scanning Calorimetry (DSC) on a DSC 2920 of TA instruments. The heating rate was 20°C per minute and the $N_2$ flow was 40 mL per minute. $T_g$ was taken as the midpoint of the inflection tangent.

Thermo Gravimetric Analysis (TGA) was carried out on a TA Instrument 951 thermogravimetric analyser with a continuous flow of nitrogen (50 ml/min) and heating rate of 10 °C/min. The sample was inserted in the solid state.

A Bruker D8 Discover diffractometer equipped with a Göbel mirror (copper target $K_{\alpha 1}$and $K_{\alpha 2}$ lines) and centric cradle was used to obtain 1-D X-ray diffraction (XRD) profiles. The spectra were taken under a step-scan rate of 0.04° per 40 s in the scattering angle range of $2\theta = 2°\text{-}50°$.

A Bruker ELEXSYS E680 spectrometer in conjunction with a split-coil 6-T superconducting magnet was used for W-band (95 GHz) light-induced Electron Paramagnetic Resonance (Li-EPR). These measurements were performed at 100 K using an Oxford flow cryostat and with a Bruker cylindrical cavity which allows optical access to the sample *via* an optical fibre. Optical excitation was performed with the 488 nm line of an $Ar^+$ laser. The results presented here are recorded with a modulation frequency and amplitude of 100 kHz and 3 G respectively and a microwave frequency and microwave power of 94.0795 GHz and $7x10^{-2}$ mW. The samples were prepared from dried drop cast films of the 1:1 ratio polymer/PCBM solution.

**Synthesis of 2,5-bis(hydroxymethyl)-thiophene (2a).**

In a 100 mL round-bottom flask to dry THF (50 ml, dried over sodium) $LiAlH_4$ (0.38 g, 10 mmol) was added under argon atmosphere. This slurry was cooled to 0 °C and the diester **1a** (1 g, 5 mmol) was slowly added portion wise. When the addition was completed a reflux condenser was fitted and the slurry was heated at reflux temperature for 2 hours. During this time a grey, concrete-like substance was formed that was hard to stir. After cooling down, air was allowed to get in the system and the reaction mixture was placed in

an ice bath. Then, it was quenched by cautious sequential addition of water, aqueous 15 % NaOH solution, and again water until no more gas development could be detected. This solution was filtered and the residue was extracted with ether. The combined organic layers were dried over $MgSO_4$ and the solvent was evaporated under reduced pressure. The diol **2a** was obtained as yellowish oil (0.65 g, 91 %). $^1$H-NMR ($CDCl_3$): δ (ppm) 6.73 (2H), 4.62 (4H), 3.57 (2H). MS (EI, m/z, rel. int. (%)): 144 ($[M]^+$, 78), 113 ($[M- CH_2OH]^+$, 100), 82 ($[M- 2x\ CH_2OH]^+$, 74).

**Synthesis of 2,5-bis(chloromethyl)-thiophene (3a).**
To a cooled (0 °C), stirred solution of diol **2a** (0.9 g, 6.2 mmol) in THF (20 ml) was slowly added a solution of $SOCl_2$ (0.9 ml, 1.49 g, 12.5 mmol) in THF (5 ml). The temperature of the reaction mixture was allowed to increase to room temperature under continuous stirring for 1 hour. Then, the mixture was cooled down again at 0 °C and a saturated sodium carbonate solution was added dropwise until neutral. The mixture was extracted with ether and dried over $MgSO_4$. The solvent was evaporated and the highly reactive dichloride **3a** was obtained as yellow oil used as it was in the following step.

**Synthesis of 2,5-bis(tetrahydrothiopheniomethyl)thiophene dichloride (4b).** To a stirred solution of bischloromethyl **3a** (11 mmol) in MeOH (25 ml) was added THT (49.3 mmol). The reaction mixture was stirred under $N_2$ for three days. Then the reaction mixture was precipitated in cold acetone (-10 °C) and the bissulphonium salt was obtained as a white solid in a yield of 60 %. $^1$H-NMR ($CDCl_3$): δ (ppm) 7.22 (2H); 4.72 (4H); 3.52-3.35 (8H); 2.16 (8H).

**Thiophene-2,5-diylbismethylene N,N-diethyl dithiocarbamate (4a)**
To a solution of bischloromethyl (0.7g, 4 mmol) **3a** in ethanol (10 ml), sodium diethyldithiocarbamate trihydrate (or diethyldithiocarbamic acid sodium salt trihydrate) (5g, 12mmol) was added as a solid. The mixture was stirred at ambient temperature for two hours. Then, water was added and the desired monomer was extracted with ether (3 x 100 mL) and dried over $MgSO_4$. Evaporation of the solvent yielded (81 %) the pure product as a white solid.

$^1$H NMR ($CDCl_3$): 6.84 (s, 2H), 4.69 (s, 4H), 4.01 (q, J = 7.2 Hz, 4H), 3.69 (q, J = 7.2 Hz, 4H), 1.26 (t, J = 7.2 Hz, 12H); $^{13}$C NMR ($CDCl_3$): 194.29, 138.76, 126.77, 49.46, 46.70, 36.72, 12.46, 11.53; MS (EI, m/e): 258 ($M^+$ – $SC(S)NEt_2$), 148 ($SC(S)NEt_2$).

**Ethylxanthic acid potassium salt (b)**

In a flask, potassium hydroxide (KOH) pellets (14 g, 0.25 mol) and ethanol (50 mL, 0.25 mol) were refluxed for 1 hour. Then, $CS_2$ (16.7 mL, 0.25 mol) was slowly added under constant stirring. After cooling the reaction mixture in an ice-bath, the resulting solid was filtered off and washed with ether (3 x 10 mL). After drying the salt in an essicator, 31.83 g (80 %) of the pure salt was obtained as a white solid. $^1$H NMR ($D_2O$): 4.48 (s, 2H), 1.41 (t, 3H).

**2,5-Bis[ethoxy(thiocarbonyl)thiomethyl]thiophene (5b)**

To 80 mL of an acetonitrile/water solution (5 volume % water) of bissulphonium salt **4b** (8 g, 0.0224 mol), ethylxanthic acid potassium salt (**b**) (8.25 g, 0.0515 mol) was added as a solid after which the mixture was stirred at ambient temperature for two hours. Then, water was added and the desired xanthate monomer was extracted with ether (3 x 100 mL) and dried over $MgSO_4$. Evaporation of the solvent yielded 7 g (89 %) of the pure product as a white solid; Mp: 36.0-37.4 °C; $^1$H NMR ($CDCl_3$): 6.80 (s, 2H), 4.65 (q, 4H), 4.48 (s, 4H), 1.41 (t, 6H). $^{13}$C NMR ($CDCl_3$): 213.13, 138.61, 126.74, 70.27, 35.02, 13.77. MS (EI, m/e): 231 ($M^+$ - SC(S)OEt), 110 ($M^+$ - 2 x SC(S)Oet)

**S-octhylthioxanthic acid potassium salt (c)**

The preparation of **c** is analogous to that described for **b** but here octanethiol (50 mL,) was used. Yield: 75 % (0.1875 mol); $^1$H NMR ($D_2O$): 3.10 (t, 2H), 1.58 (m, 2H), 1.20 (m, 10H), 0.78 (t, 3H).

**2,5-Bis[(trithiocarbonic acid octyl ester)thiomethyl]thiophene (5c)**

The preparation of **5c** is analogous to that described for **5b** but here S-Octylxanthic acid potassium salt (**c**) was used. Yield: 70 % of pure compound

as a yellow oil; $^1$H NMR ($CDCl_3$): 6.80 (s, 2H), 4.74 (s, 4H), 3.34 (t, 4H), 1.67 (m, 4H) 1.24 (m, 20H) 0.85 (t, 6H).

**Polymerisation of monomers 4a; 5b and 5c**

All polymerisations were carried out in dry THF at different temperatures, with different bases and different concentrations of the base. A solution of monomer **4a** (or **5b** or **5c**) (250 mg) in dry THF at –78 °C (or R.T. or 0 °C) was degassed by passing through a continuous nitrogen flow. An equimolar LDA solution (a 2 M solution in THF/n-hexane) or LHMDS (Lithium Bis(trimethylsilyl)amide, 1 M solution in THF) was added in one go to the stirred monomer solution. The mixture was kept at –78 °C (or R.T. or 0 °C) for 90 minutes under continuous nitrogen flow. After this time, the solution was allowed to come to 0°C or ethanol (5 mL) was added at -78 °C to stop the reaction (this was not necessary if the polymerisation was performed at R.T. or 0 °C). The polymer was precipitated in ice water (100 mL) and extracted with chloroform (3 x 60 mL). The solvent of the combined organic layers was evaporated under reduced pressure and a second precipitation was performed in a 1/1 mixture (100 mL) of diethyl ether and hexane at 0 °C. The polymer was collected and dried in vacuo. $^1$H NMR of **5a**: 6.56-6.72 (br s, 1H), 6.72-6.36 (br s, 1H), 5.22-5.55 (br s, 1H), 3.81-4.12 (br q, 2H), 3.48-3.81 (br q, 2H), 3.11-3.40 (br s, 2H), 1.01-1.37 (br t, 6H). $^{13}$C NMR ($CDCl_3$): 193.61, 140.77, 140.36, 126.15, 125.89, 52.50, 49.20, 46.73, 38.37, 12.45, 11.60. $^1$H NMR ($CDCl_3$) of **6b**: 6.62-6.69 (br s, 1H), 6.44-6.53 (br s, 1H), 5.01-5.12 (br s, 1H), 4.53-4.66 (br q, 2H), 3.46-3.58 (br m, 1H), 3.25-3.37 (br m, 1H), 1.35-1.41 (br t, 3H); $^{13}$C NMR ($CDCl_3$): 212.16, 140.51, 140.12, 126.24 (2C), 70.13, 51.03, 37.67, 13.83. $^1$H NMR of **6c** is not well resolved because the peaks relative to the monomer covered the peaks of the formed oligomers (small percentage).

**Conversion towards the conjugated polymers (6a)**

The precursor polymer **5a** (300 mg) dissolved in dichlorobenzene (15 ml) was refluxed under stirring for three hours. Then, the solvent was evaporated

and, the slurry so obtained was precipitated in hexane. The precipitated was filtered off and washed several times with hexane.

## 2.8 References


1. H. G. Gilch and W. L. Wheelwright, *J. Polym. Sci.* (4), **1966**, 1337.
2. R. A. Wessling and R. G. Zimmerman, *U.S. Patent No 3401152* ***1968***.
3. R. A. Wessling, *J. Polym. Sci., Polym. Symp*. (72), **1985**, 55.
4. S. Son, A. Dodabalapur, A. J. Lovinger and M. E. Galvin, *Science* (269), **1995**, 376 .
5. F. Louwet, D. Vanderzande and J. Gelan, *Synth. Met.* (52), **1992**, 125.
6. F. Louwet, D. Vanderzande and J. Gelan, *Synth. Met.* (69), **1995**, 509.
7. F. Louwet, D. Vanderzande, J. Gelan and J. Mullens, *Macromolecules* (28), **1995**, 1330.
8. K. Harper and W. J. W. West, *Eur. Pat. Appl*. No 182548 **1985**.
9. K.-Y. Jen, R. Jow, H. Eckhardt and R. L. Elsenbaumer, *Polym. Mater. Sci. Eng.* (56), **1987**, 49.
10. K.-Y. Jen, M. Maxfield, L. W. Shacklette and R. L. Elsenbaumer, *J. Chem. Soc., Chem. Commun.* **1987**, 309.
11. K.-Y. Jen, R. Jow, L. W. Shacklette, M. Maxfield, H. Eckhardt and R. L. Elsenbaumer, *Mol. Cryst. Liq. Cryst* (160), **1988**, 69.
12. S. Yamada, S. Tokito, T. Tsutsui and S. Saito, *J. Chem. Soc., Chem. Commun.* **1987**, 1448.
13. S. Tokito, T. Momii, H. Murata, T. Tsutsui and S. Saito, *Polymer* (31), **1990**, 1137.
14. H. Murata, S. Tokito, T. Tsutsui and S. Saito, *Synth. Met.* (36), **1990**, 95.

15. T. Tsutsui, H. Murata, T. Momii, K. Yoshiura, S. Tokito and S. Saito, *Synth. Met.* (41), **1991**, 327.

16. I. Murase, T. Ohnishi, T. Noguchi and M. Hirooka, *Polym. Commun.* (28), **1987**, 229.

17. I. Murase, T. Ohnishi and T. Noguchi, *Ger. Offen.* No 3704411 **1987**.

18. W. Eevers, D. De Schrijver, T. Dierick, C. Peten, J. Van Der Looy and H. J. Geise, *Synth. Met.* (51), **1992**, 329.

19. W. Eevers, M. De Wit, J. Briers, H. J. Geise, R. Mertens, P. Nagels, R. Callaerts, W. Herrebout and B. Vanderveken, *Polymer* (35), **1994**, 4573.

20. H.-Q. Xie, C.-M. Liu and J.-S. Guo, *Eur. Polym. J.* (32), **1996**, 1131.

21. S. Iwatsuki, M. Kubo and H. Yamashita, *Chem. Lett.* **1989**, 729.

22. W. Ten Hoeve, M. M. de Kok, B.-H. Huisman, P. T. Herwig and A. J. J. M. Van Breemen, PCT *Int. Appl.* No 1290059 **2001**.

23. S. Gillissen, Ph. D. Dissertation, Limburgs Universitair Centrum, Diepenbeek, Belgium, December **2002**.

24. Results obtained within the framework of the "PLASTRONIX" 5th framework EC-project nr.: GRD1-1999-10903, duration: **2000-2001**.

25. A. Henckens, Ph. D. Dissertation, Limburgs Universitair Centrum, Diepenbeek, Belgium, October **2003**.

26. W. J. Mitchell, C. Pena and P. L. Burn, *J. Mater. Chem.* (12), **2002**, 200.

27. G. Padmanaban, K. Nagesh, S. Ramakrishnan, *J. Polym. Sci., Part A: Polym. Chem.* 41, (24), **2003**, 3929.

28. A. Henckens, L. Lutsen, D. Vanderzande, M. Knipper, J. Manca, T. Aernouts, J. Poortmans, Proceedings of SPIE - Strasbourg, France, April 26-30, 2004, *Organic Optoelectronics and Photonics* (5464), **2004**, 52.

29. A. Henckens, K. Colladet, S. Fourier, T.J. Cleij, L. Lutsen, J. Gelan, and D. Vanderzande, *Macromolecules*, (38), **2005**, 19.

30. L. Hontis, V. Vrindts, D. Vanderzande, and L. Lutsen, *Macromolecules* (36), **2003**, 3035.

31. P. M. Lahti, D. A. Modarelli, F. R. Denton, R. W. Lenz, and F. E. Karasz, *J. Am. Chem. Soc.* (110), **1988**, 7258

32. F. Banishoeib, A. Henckens, S. Fourier, G. Vanhooyland, M. Breselge, J. Manca, T.J.Cleij, L. Lutsen, D. Vanderzande, Le Huong Nguyen, H. Neugebauer, N. S. Sariciftci, *Thin Solid Films* **2007** accepted

33. D. B. Collum *, A. J. McNeil, A. Ramirez, *Angewandte Chemie International Editino,* 46, (17), **2006**, 3002

34. P. G. Williard, J. M. Salvino, *J. Org. Chem.*, 58 (1), **1993**, 1

35. N. D. R. Barnett, R. E. Mulvey, W. Clegg, and P. A. O'Neil, *JACS*, 113 (21), **1991**, 8187

36. Y.-J. Kim, M. P. Bernstein, A S. Galiano Roth, F. E. Romesberg, *J. Org. Chem.*, 56, **1991**, 4435

37. For an extensive review of structure studies on N-Li species, see: G. K. Schleyer, P. v. R. Snaith, Adv. *Organomet. Chem.*, in press.

38. For an excellent review on the effects of aggregation and mixed aggregation on the structure and reactivity of organolithium compounds, see: D. Seebach, *Angew. Chem., Int. Ed. Engl.*, 27, **1988**, 1624.

39. J. D'Angelo, *Tetrahedron*, 32, **1976**, 2979

40. E. C. Ashby and J. N. Argyropoulos, J. *Org. Chem.*, 51, **1986**, 3593

41. A.-S. Rebstock, F. Mongin, F. Trécourt and G. Quéguiner, *Org. Biomol. Chem.*, 1, **2003**, 3064

42. K. J. Singh and D. B. Collum, *J. AM. CHEM. SOC.*, 128, (42), **2006**, 13753

43. Private discussion with John E. Anthony, University of Kentucky, Department of Chemistry, Lexington, KY 40506 USA

44. S. Son, A. Dodabalapur, A. J. Lovinger, M. E. Galvin, *Science*, (269), **1995**, 376.

45. For a more detailed review on the methods of calculation of energy band gaps in CV measurements see S. Fourier, Ph. D. Dissertation, University of Hasselt, Belgium, May **2007**

46. M. Onoda, H. Nakayama, K. Amakawa and K. Yoshino, *Ieee Transactions on Electrical Insulation*, (27), **1992**, 636

47. G. Janssen, A. Aguirre, E. Goovaerts, *EUROPEAN PHYSICAL JOURNAL-APPLIED PHYSICS* 37, (3), **2007**, 287

48. V. I. Krinichnyi, H. K. Roth, A. L. Konkin, *Physica B,* 344, **2004**, 430

49. M. Al-Ibrahim, H. K. Roth, M. Schroedner, A. Konkin, U. Zhokhavets, G. Gobsch, P. Scharff, S. Sensfuss, *Org. Electron.*, 6, **2005**,65

50. V. Dyakonov, G. Zoriniants, M. Scharber and C. J.Brabec. *Phys Rev. B.*, 59, **1999**, 8019

51. J. De Ceuster, E. Goovaerts, A. Bowen, J. C. Hummlen, and V. Dyakonov. *Phys Rev. B*., 64, **2001**, 195206

52. L. H. Nguyen, S. Günes, H. Neugebauer, N. S. Sariciftci, F. Banishoeib, A. Henckens, T. Cleij, L. Lutsen and D. Vanderzande, *Solar Energy Materials & Solar Cells* (90), **2006**, 2815

53. a) R Joseph Kline, M. D. McGehee, E N Kadnikova, J. Liu, J M.J. Frechet, *Adv. Mater.* (15), **2003**, 1519; b) P. Schilinsky, U Asawapirom, U. Scherf, M. Biele, C.J.Brabec, *Chem. Mater.* (17), **2005**, 2175

54. B. S. Furniss, A. J. Hannaford, P. W. G. Smith, A. R. Tatchell, *Vogel's Textbook of Practical Organic Chemistry, 5th ed.*, Longman: New York, **1989**, 793.

55. F. Zhang, E. Perzon, X. Wang, W. Mammo, M. R. Anderson and O. Inganäs, *Adv. Funct. Mater.* (15), **2005**, 745

56. L. M. Campos, A. Tontcheva, S. Günes, G.Sonmez, H. Neugebauer and N. S. Sariciftci, F. Wudl, *Chem. Mater.* (17), **2005**, 4031

57. S.-C. Lo, A. K. Sheridan, D. W. Samuel, P. L. Burn, *J. Mater. Chem.*, 9, (9), **1999**, 2165.

58. E. Kesters, S. Gillissen, F. Motmans, L. Lutsen, D. Vanderzande, *Macromolecules*, 35, (21), **2002**, 7902.

# Chapter Three

# Synthesis of 3-alkyl substituted derivatives of poly(2,5-thienylene vinylene) PTVs

## *3.1 Introduction*

A feature of most conjugated polymer systems is not only that they do absorb within a narrow region of the solar spectrum, but they also do not overlap with the maximum solar photon flux (~ 1.8 eV).

Among the most investigated classes of conjugated polymers, alkyl substituted polythiophene received special attention. This because starting from about 1992 reductive coupling *via* organo-zinc or Grignard carbanions was developed as a synthetic route towards said polythiophene derivatives. Conjugated polymers so obtained showed low structural defect levels, high mobility of charge carriers, a band gap at the borderline of low band gap materials and an appreciable thermochromism. The latter phenomenon, although widely observed within the material class of conjugated polymers, is especially well documented for poly(3-alkylthiophene) derivatives. From literature it is clear that the length of the alkyl substituents has a pronounced influence on the thermochromic transition of the polymer. Furthermore, molecular aggregates are responsible for the colour changes[1,2] of the final polymer. Temperature-dependent optical absorption measurements have revealed important thermochromic effects in poly(3-alkylthiophene) between 25 and 150 °C which are related to a planar to non-planar transition of the main polymer chain. This conformational transition is caused by an increase of the repulsive intrachain steric interactions upon heating, which then force the thiophene backbone to adopt a non-planar conformation. On the other hand, as observed with poly(3-alkylthiophene), if the side chains do not lead to large steric interactions, the polymer can maintain a highly conjugated structure even at high temperatures while, if

the steric interactions are too strong, no co-planar conformation can be adopted[3].

Poly(2,5-Thienylene Vinylene) derivatives (PTV's) can be considered as derivatives of poly(thiophene)s with the presence of a vinylene bond between the thiophene units. They show interesting potential as low band gap polymers. Indeed, $E_g$ as low as 1.5 eV were predicted on the basis of PTV oligomers[4-7]. However the high reactivity of the corresponding monomers and/or the harsh conditions (strong acid) used for the conversion of the precursor polymers precluded important progress.

Since plain PTVs are insoluble in their conjugated forms it is necessary to move towards soluble derivatives. The alkyl substituted PTVs with band gap energies in the range of $E_g$ = 1.5-1.8 eV could allow for an improved overlap of the polymer absorption spectrum with the solar emission. In addition, regioregular poly(thienylene vinylene)s may show a relatively high degree of intermolecular ordering, which may improve film morphology and lead to an enhanced charge transport capability of the active layer in the device, thereby improving its performance[8,9].

## *3.2 Synthesis of alkyl substituted PTVs via the dithiocarbamate precursor route*

### 3.2.1 Monomer synthesis

The alkyl substituted thiophene monomers were obtained starting from the commercially available 3-bromothiophene (towards **7a** and **7b**) or 3, 4-dibromothiophene (towards **7c**). They were prepared as described in **Scheme 3.1**.

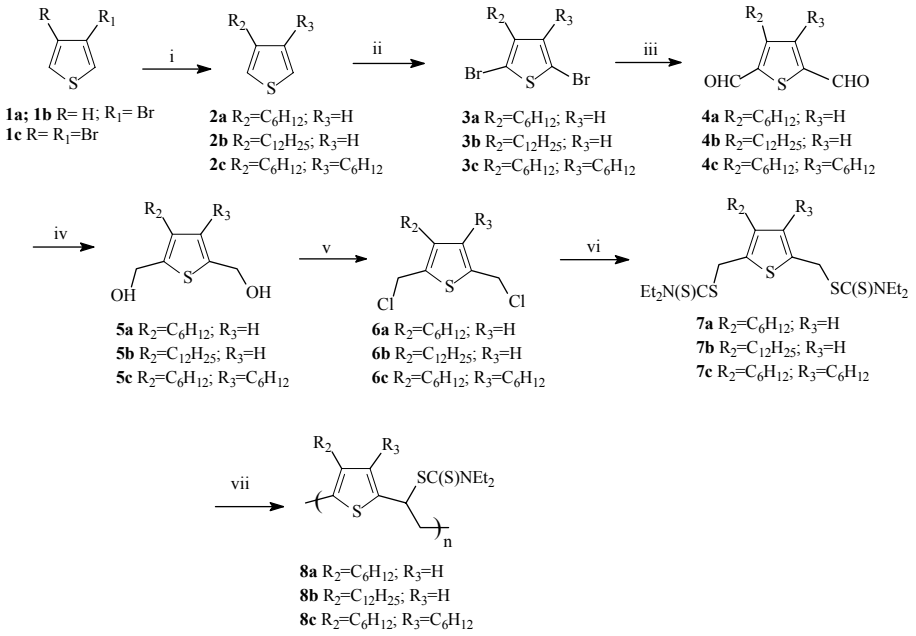


***Scheme 3.1*** *Synthesis of dithiocarbamate monomers 7a, 7b and 7c: i) $BrMgR_2/NiCl_2(dppp)$; ii) b: NBS/DMF, c: NBS/$CHCl_3$/AcOH; iii) 1. BuLi, 2. formylpyperidine; iv) $LiAlH_4$, THF; v) $SOCl_2$, THF; vi) $NaSC(S)NEt_2.3H_2O$ vii) LDA/or LHMDS, THF*

The first reaction step is represented by a Grignard reaction that was carried out according to Kumada *et al.*[10-13] under vacuum. The metal promoted coupling reactions of organic halides are one of the most attractive and useful procedures for formation of the carbon-carbon σ bond. Nickel phosphine complexes, here used, catalyse the selective cross-coupling of Grignard reagents with aryl and alkenyl halides as shown by the general reaction reported hereafter:

$$RMgX + R_1X_1 + NiL_2Cl_2 \rightarrow R\text{-}R_1 + MgXX_1$$

A dihalodiphosphinenickel reacts with a Grignard reagent (**Scheme 3.2**) to form the intermediate, di-organonickel complex, which is subsequently converted into the halo (organo) nickel complex by an organic halide.

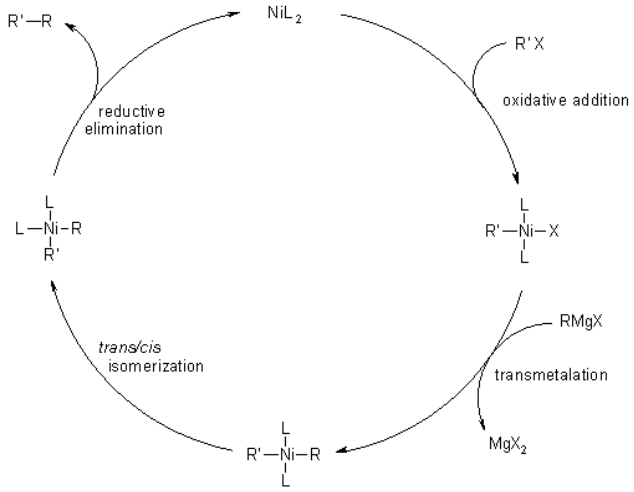


***Scheme 3.2*** *General Mechanism of Grignard reaction according Kumada*

The catalytic activity of the nickel complexes depends strongly upon the nature of the ligands. The catalytically active species does contain phosphine ligands on the nickel atom. Furthermore, the bidentate phosphines as ligands exhibit much higher catalytic activity compared to the monodentate derivatives. The efficiency of the catalytic activity decreases roughly in the sequence: dppp > dppe > dmpe > dppb > cis-dpen. It seems of particular interest to note that the catalytic activity depends on the length of the methylene bridge between two diphenylphosphino groups in a homologous series. For reasons of clarity, the diphosphine ligands mentioned, are given in **Scheme 3.3** with their abbreviations.

| $Ph_2P(CH_2)_nPPh_2$ | $Me_2P(CH_2)_2PMe_2$ | *cis*-$Ph_2PCH{=}CHPPh_2$ |
|---|---|---|
| $n$ = 2, dppe<br>$n$ = 3, dppp<br>$n$ = 4, dppb | dmpe | *cis*-dpen |

***Scheme 3.3*** *Diphosphine ligands used for ordinary cross-coupling with their abbreviations.*

The three alkyl derivatives were obtained in a yield between 75 and 95 %.
The conversion of the 3-alkylthiophene, **2a** and **2b** into the 2, 5-dibromo-3-alkylthiophene[14] **3a** and **3b** is very sensitive to the presence of light, which

might induce over-bromination reactions on the alkyl side chain[15]. Therefore, we carried out all the bromination in the dark. The di-bromo compounds were purified either *via* column chromatography or by a vacuum distillation giving the desired compounds in a yield of ~ 80 – 90 %.

In the formation of di-aldehyde derivatives[16] (**4a**, **4b** and **4c**), special attention was given to the use of extreme dry reaction conditions in order to avoid the formation of large amount of side products, e.g. mono-aldehyde. The di-aldehydes could be obtained in yield ranging from 60 – 80 %.

After the formation of the di-aldehyde the follow-up reaction steps were analogous to the ones described for the synthesis of the plain PTV (chapter 2). The obtained alkylated dithiocarbamate monomers behaved as hygroscopic oils so, it was necessary to freeze dry them before using them in the polymerisation reaction which is very sensitive to traces of water.

### 3.2.2 Polymerisation

A solution of monomer (**7a**, **7b** or **7c**) in dry THF was degassed by passing through a continuous nitrogen flow. The concentration of the monomer was set to 0.2 M or 0.4 M. The solution of base: lithium diisopropyl amide (LDA 2 M solution in THF/n-hexane) or lithium Bis(trimethylsilyl)amide (LHMDS 1 M solution in THF) was added in one go to the stirred monomer solution. The mixture was kept for 90 minutes under continuous nitrogen flow at a given temperature. After this time, the polymer was precipitated in ice water and the water layer was neutralised with diluted HCl before extraction with chloroform. The solvent of the combined organic layers was evaporated under reduced pressure and a second precipitation was performed in pure cold methanol in order to separate the formed polymer from the unreacted monomer. The polymer was collected and dried in vacuo. The $M_w$ were determined by GPC against Poly(Styrene) (PS) standards using THF as eluent.

| Polymer | Entry | # eq. LDA | $\lambda_{max}$ (nm) | $M_w$ g/mol | PD | Temp. (°C) | Yield (%) |
|---|---|---|---|---|---|---|---|
| **8a** | 1 | 1.0 | 535 | 14200 | 1.1 | -78 | <5 |
| | 2 | 1.2 | 382 | 16200 | 3.7 | 0 | <5 |
| | 3 | 1.5 | 380 | 15700 | 4.1 | 0 | <5 |
| **8c** | 4 | 1.0 | 480 | 3200 | 1.2 | -78 | <5 |
| | 5 | 1.2 | -* | 6900 | 2.7 | 0 | <5 |
| | 6 | 1.5 | 537 | 17200 | 1.4 | 0 | <5 |

** The absorption spectrum was featureless, with no clear maximum*

***Table 3.1*** *Polymerisation results for 8a and 8c with the use of LDA*

All the data depicted in the table are averaged values relative to duplo experiments, which showed good reproducibility.

The polymerisation (**Table 3.1**) of the alkyl substituted monomers **7a** and **7c** with LDA, led only to very low $M_w$ polymers ($M_w$ < 14000) and low yield (< 5%). Side reactions were already occurring when one equivalent of base was added. The residual fractions were analysed by GC-MS and the main products formed were found to be the results of the cleavage of the alkyl side chains on the thiophene rings. In some cases side products were observed, which imply the transfer of isopropyl groups from LDA to the thiophene ring [MS (EI, m/e): 210 ($M^+ - C_{13}H_{22}S$)]. The precise mechanism of such transfer reaction is not yet completely clear. Anyhow it was already explained (chapter two) that relates to the use of LDA as a base, which is responsible of several side reactions that compete with the polymerisation reaction.

The use of an alternative base as lithium bis(trimethylsilylamide) (LHMDS) in the polymerisation reaction may open a very efficient pathway to 3-alkyl and 3,4-di-alkyl substituted PTVs. Former studies on the unsubstituted monomer (chapter two) showed that the use of LHMDS instead of LDA gave the precursor polymer PTV in excellent yield and high molecular weight especially at 0 °C and room temperature[17]. Also the alkyl substituted dithiocarbamate monomers **7a**, **7b** and **7c** were polymerised using similar conditions[18]. The results are presented hereafter in **Table 3.2**.

| Polymer | Entry | # eq. LHMDS | $\lambda_{max}$ (nm) | $M_w$ g/mol | PD | Temp. (°C) | Yield (%) |
|---|---|---|---|---|---|---|---|
| **8a** | 7 | 1.5 | 545 | 50100 | 9.6 | 0 | 51 |
| | 8 | 2.0 | 550 | 58300 | 7.7 | 0 | 84 |
| | 9 | 1.5 | 566 | 32000 | 3.6 | R.T. | 56 |
| | 10 | 2.0 | 574 | 35000 | 3.7 | R.T. | 55 |
| | 11 | 2.0* | 560 | 97100 | 10.1 | 0 | 50 |
| **8b** | 12 | 2.0* | 558 | 65400 | 12.7 | -10 | 41 |
| | 13 | 2.0* | 570 | 71800 | 4.5 | 0 | 50 |
| | 14 | 2.0* | -** | 64000 | 4.2 | R.T. | 15 |
| **8c** | 15 | 2.0 | 592 | 17000 | 4.4 | 0 | 40 |
| | 16 | 2.0* | 586 | 31000 | 5.4 | 0 | 47 |
| | 17 | 2.0* | 604 | 71400 | 6.2 | 0 | 42 |

** The concentration of the monomer was set to 0.4 M, instead of 0.2 M*

*** A lot of defects were present; the same behaviour was observed for the plain PTV*

***Table 3.2*** *Polymerisation results for the alkyl PTVs with the use of LHMDS*

The data listed in the table are average values relative to experiments carried out in duplo. The experiments carried out in the same conditions showed a very good reproducibility. The rest fractions after the polymerisation reaction contained only unreacted monomer.

The absorption maxima values depicted in **Table 3.2** are very important for an evaluation of the quality of the conjugated system. They are values at high temperature (typically 130 °C < T < 150 °C) obtained during to *in-situ* conversion experiments of the precursor polymer in an UV-Vis spectrometer. Values of 550 nm and more point to a high effective conjugation lengths for the conjugated PTV so obtained. A further discussion will be given in the characterisation and in the experimental sections.

It can be clearly seen, looking at the **Table 3.2**, that high molecular weight precursor polymers were obtained in good yield. In particular, increasing the initial monomer concentration from 0.2 M to 0.4 M, leads to higher molecular weight. This observation is consistent with the hypothesis of a radical chain polymerisation mechanism for the true monomer, an *in situ* formed quinodimethane system[19]. Operating in this way, a molecular weight of almost 100000 g/mol can be obtained for the precursor polymer **8a**.

The dodecyl derivative **8b** was then polymerised choosing only a monomer concentration in the reaction mixture of 0.4 M varying the reaction temperature from -10 °C till R.T.
Comparison on the $M_w$ distributions of the synthesised materials reveals some specific features (**Figure 3.1**).

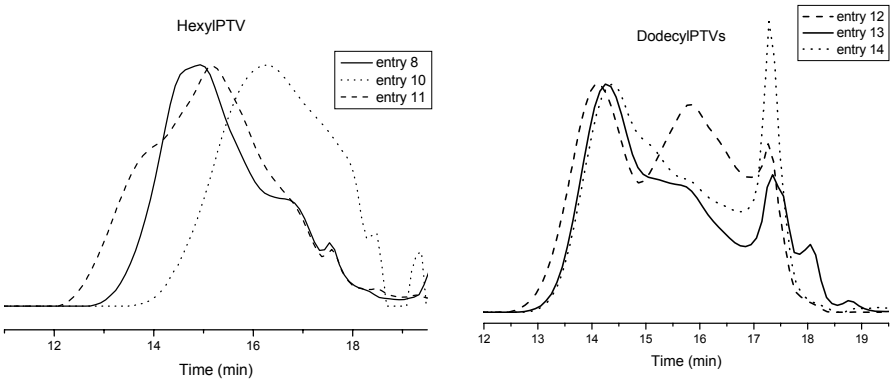


***Figure 3.1*** *GPC chromatograms for hexylPTV (left) and dodecylPTV (right)*

For the polymerisation of **8b**, a clear tendency to have a bimodal distribution of $M_w$ is recognised for the dodecyl PTV (graph on the right). Furthermore, this behaviour seems to decrease with increasing reaction temperature. Apparently these observations point to the presence of two polymerisation mechanisms competing which each other. Although p-quinodimethane based polymerisations have been investigated by a number of research groups, the nature of the underlying polymerisation mechanism — radical or anionic — is still under discussion. Actually, the exact nature of the initiating species is a long standing issue of controversy. In the conditions typically used for polymerisations of p-quinodimethane systems no high molecular weight polymer is formed by anionic processes. Rather they result from a self-initiating radical chain process, which shows features consistent with the occurrence of a termination reaction. Anionic polymerisation, when observed for such p-quinodimethane systems, typically shows rather low molecular weights. This is a result of high concentration of potential nucleophiles (solvent, base). Consequently anionic processes can not be excluded

completely, but taken the results obtained as a whole, the main polymerisation mechanism operating is of radical nature and yields high molecular weight polymers[20]. It should be also remarked that the presence of these two mechanisms of polymerisation give rise to the high values of polydispersities index (PD) observed. Such competition was observed and studied in some detail earlier for the Sulphinyl route. Also here we can assume that such competition is at hand. This implies that we assume that a radical polymerisation mechanism is responsible for the high molecular weight part and an anionic mechanism for the lower molecular weight fraction. Actually in the case of the Sulphinyl route, it was indeed observed that decreasing of the reaction temperature leads to an increase of the contribution of the anionic mechanism. This is attributed to a lower activation energy typical for the anionic polymerisation mechanism compared to the radical polymerisation mechanism.

In the case of the synthesis of the hexyl PTV precursor (graph on the left) the bimodal behaviour seems not so pronounced, indeed, only some tailing is observed.

The same strategy used for the 3-hexyl PTV, was also applied to the 3,4-dihexyl PTV **8c** and, as a result, the doubled monomer concentration led to a $M_w$ value two times higher (compare entry 15 with entry 16 **Table 3.2**). Looking at the $M_w$ distribution for the di-hexyl PTV (**8c Figure 3.2**), also here a broad polydispersity index is observed. Furthermore, the difference in $M_w$ between entry 17 and entry 16, although the two experiments were carried out in the same conditions, may relate to the use of different batches of monomer. In the case of entry 17 the monomer was purified by a second column chromatography. This may point to a definite influence of the purity of the monomer on the polymerisation process.

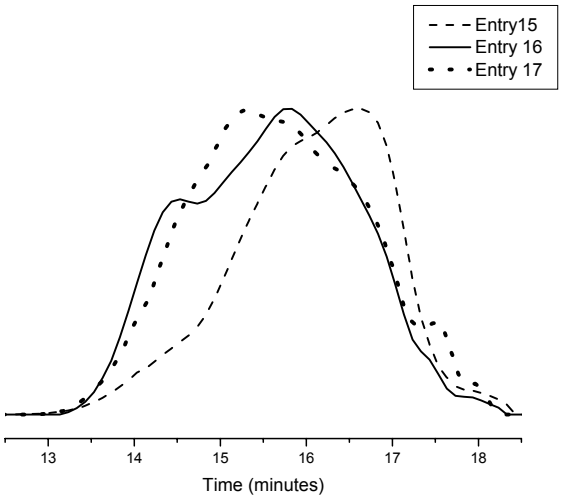


***Figure 3.2*** *GPC chromatogram for di-hexylPTV*

It is known that a radical mechanism in a polymerisation is not very sensitive to the presence of impurities which conversely play an important role in the case of an anionic mechanism. . It may lead to an increased initiation for the anionic polymerisation and in this way to a stronger competition with the radical pathway.

In order to draw some conclusions, it can be stated that the use of LHMDS as the base in the dithiocarbamate precursor route opens an efficient pathway towards a broad range of soluble PTV derivatives.

## *3.3 Characterisation*

### 3.3.1 Structural characterisation of Alkyl PTVs

As an example the NMR spectra of monomers **7a** and **7b** will be analysed.

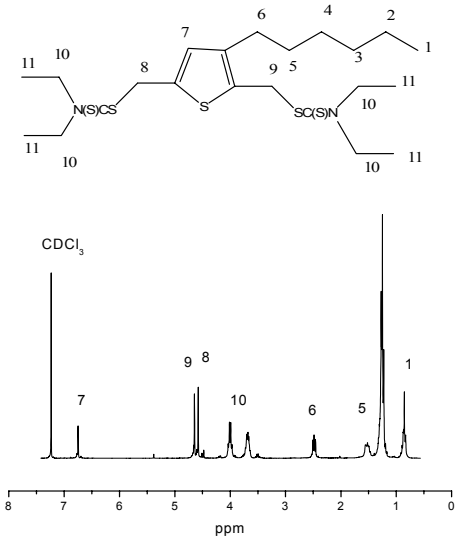


***Figure 3.3*** *$^1$H-NMR of 7a in $CDCl_3$*

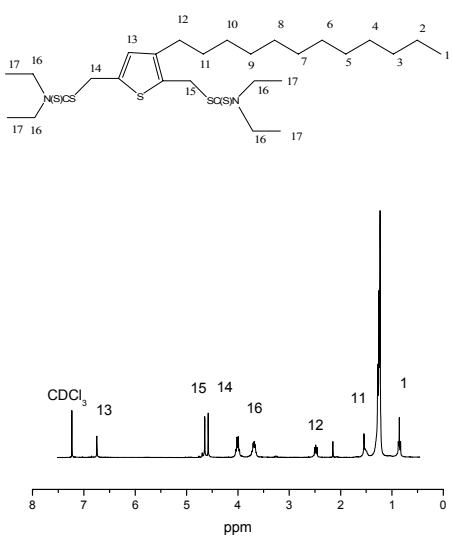


***Figure 3.4*** *$^1$H-NMR of 7b in $CDCl_3$*

The assignment of the protons was done (**Figure 3.3** and **Figure 3.4**) and the chemical shifts values are reported in the experimental section.

The $^1$H-NMR spectra of the hexyl precursor polymer is also reported. The assignment of the characteristic peaks of the precursor polymer **8a** was also accomplished by comparing the chemical shift values with those of the monomer (**Figure 3.5**).

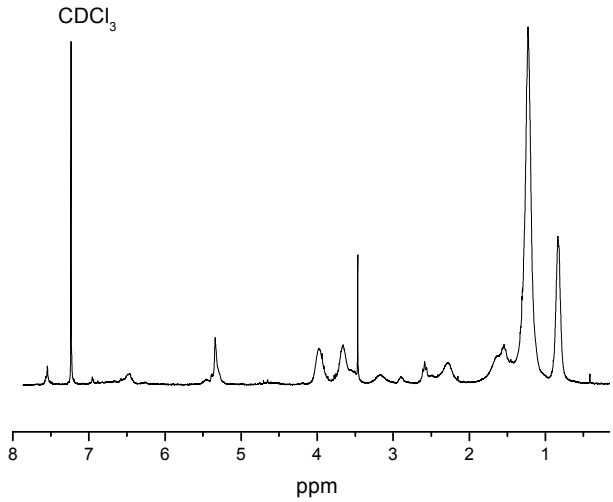


***Figure 3.5*** *$^1$H-NMR of 8a in $CDCl_3$*

The $^1$H-NMR spectra showed broadened peaks, compared to those of the monomer, as expected in the case of polymers, some traces of monomer can also be observed as well.

### 3.3.2 Study of thermal conversion of the precursor polymers to the conjugated structure

The thermal elimination of the dithiocarbamate group of the precursor polymer, as well as the thermal stability of the conjugated polymer, were studied by means of *in situ* techniques. Indeed an *in-situ* UV-Vis and a complementary *in-situ* FT-IR study were carried out in order to deduct the conversion reaction protocol of the precursor polymers towards their conjugated forms (**Scheme 3.4**).

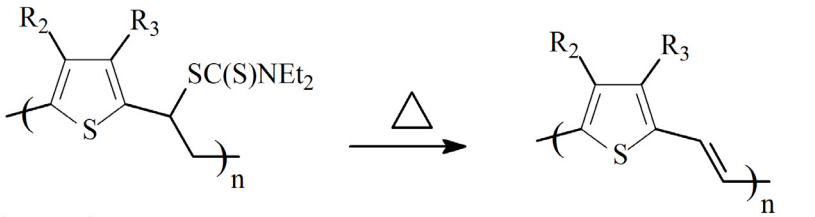


**8a** $R_2=C_6H_{12}$; $R_3=H$
**8b** $R_2=C_{12}H_{25}$; $R_3=H$
**8c** $R_2=C_6H_{12}$; $R_3=C_6H_{12}$

**9a** $R_2=C_6H_{12}$; $R_3=H$
**9b** $R_2=C_{12}H_{25}$; $R_3=H$
**9c** $R_2=C_6H_{12}$; $R_3=C_6H_{12}$

***Scheme 3.4*** *Conversion towards the conjugated polymers.*

In **Figure 3.6** is represented the UV-Vis spectrum at different temperatures of the hexyl PTV derivative. A chloroform solution of precursor polymer was coated on a quartz disk which was placed into an oven purged with a nitrogen flow and positioned in the spectrometer in order to collect all the spectra at different temperatures.

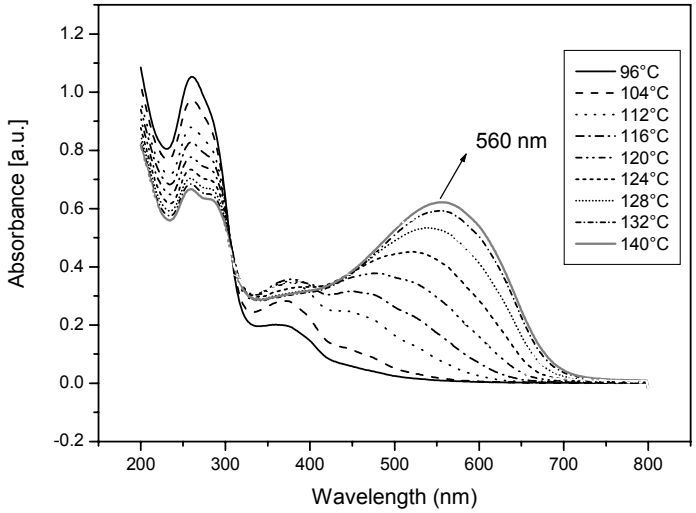


***Figure 3.6*** *In situ UV-Vis spectrum for 8a entry 11 at specific temperatures*

The highest $\lambda_{max}$ values, relative to the precursor polymers are depicted In **Table 3.2**. Comparing for example the *in situ* thermally converted 3-hexyl PTV with $\lambda_{max}$ = 560 nm (**Table 3.2**, entry 11), with the absorption spectrum of the same material at room temperature, a redshift of almost 70 nm is

observed (**Figure 3.10**). This is mainly a consequence of a thermochromic effect and it is more clearly visible in the analysis of the conversion profiles. The absorption profile at fixed wavelength as a function of temperature shows, after finalising conversion to the conjugated system (T > 130 °C), a sharp decrease of the absorption as temperature (**Figure 3.7**) increases.

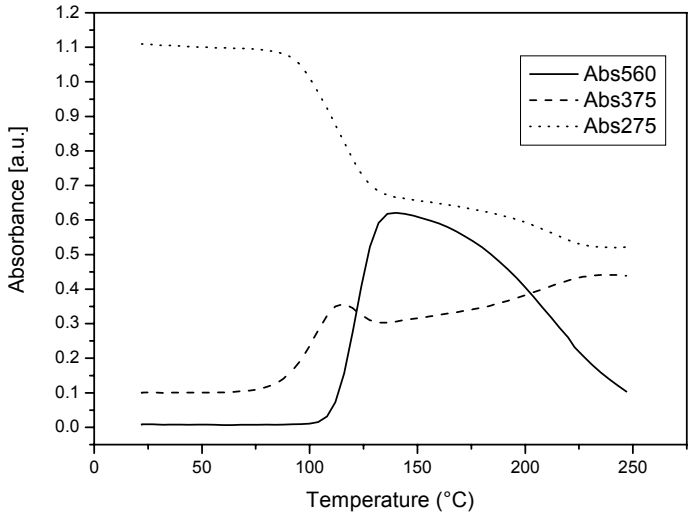


***Figure 3.7*** *UV-Vis profile for 8a entry 11*

This thermochromic effect is also well documented in literature for poly(3-alkylthiophene) (P3HT)[21-24]. As a consequence of heating a conjugated polymer, the maximum wavelength in the UV-Vis spectrum shifts because of the increased molecular motions of the polymer chain induced by the temperature increase. In particular the torsion angles between the monomer segments increase and so a decrease of the optimal overlap in the conjugated system is induced. This implies a shorter effective conjugation length resulting in a shift to lower wavelengths. Besides this blueshift, a decrease in absorbance also occurs, caused by the lower extinction coefficient.

In order to give another prove of the fact that the sharp change in the absorbance profile (**Figure 3.7**) is not due to poor thermal stability of the polymer several heating-cooling experiments were done. A film of precursor polymer was casted on a quartz disk and heated at 2 °C/min. up to different

temperatures. After this heating cycle the film was cooled down back at R.T. Several further heating-cooling cycles under nitrogen flow while taking continuously UV-Vis spectra (**Figure 3.8**) were performed.

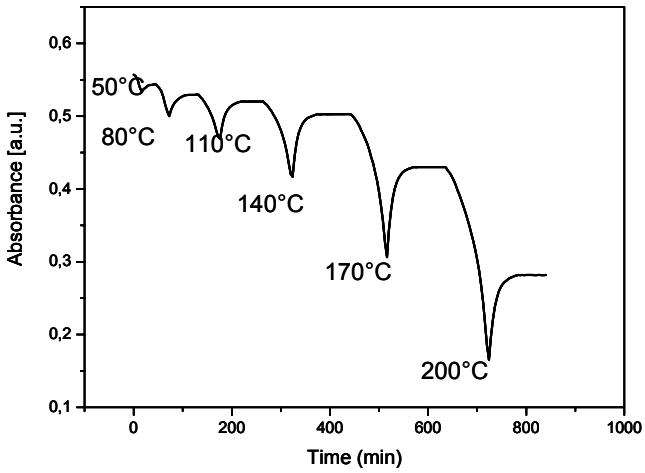


***Figure 3.8*** *Heating-Cooling experiment for 8a entry 9*

In the above reported experiment, the same film was heated up to 50 °C, 80 °C, 110 °C, 140 °C, 170 °C and 200 °C and cooled down to R.T. for six cycles. Monitoring the $\lambda_{max}$ values a decrease (shift to lower wavelength) is detected when the temperature increases, as the temperature goes down, the signal recovered to a large extent (**Table 3.3**). Beyond 170 °C a much larger change in $\lambda_{max}$ is observed.

| Polymer | Temperature (°C) | $\lambda_{max}$ (nm) at high T | $\lambda_{max}$ (nm) at R.T. after cooling |
|---|---|---|---|
| **8a** | 50 | 564 | 572 |
| | 80 | 551 | 566 |
| | 110 | 538 | 566 |
| | 140 | 529 | 561 |
| | 170 | 493 | 555 |
| | 200 | 465 | 476 |

***Table 3.3*** *$\lambda_{max}$ values at high temperature and at R.T. after heating-cooling cycles for 8a entry 9*

It can be concluded that the decrease in the absorbance between 50 °C and 170 °C is due mainly to the thermochromic effect. Instead, the fast decrease shown at temperature higher than 170 °C is most probably due to degradation of the polymer chain.

Thermochromism will also affect the colour of the polymer films. Indeed, upon slow heating, the colour of the conjugated polymer **9a** changes from purple to a dark burgundy followed by a final change to yellow at higher temperature. Cooling down the sample slowly, the purple colour is restored. Whereas high cooling rates confers to the polymer a final colour that is red-orange (**Figure 3.9**).

***Figure 3.9*** *Colour of the polymer thin films at different temperatures*

The precursor polymer **8a** was also converted in solution by refluxing it in ortho-dichlorobenzene for 12 hours. The conjugated polymer **9a** (entry 11) obtained in this way displays a $\lambda_{max}$ value in thin film up to 621 nm at room temperature (**Figure 3.10**). In order to summarise, it can be said that after conversion in solution, polymer thin films analysed by means of UV-Vis technique showed $\lambda_{max}$ values between 590 and 621 nm when the $M_w$ values

are beyond 50.000 g/mol. Whereas, for polymer with $M_w$ inferior to this value a $\lambda_{max}$ value ≤ 580 nm was found.

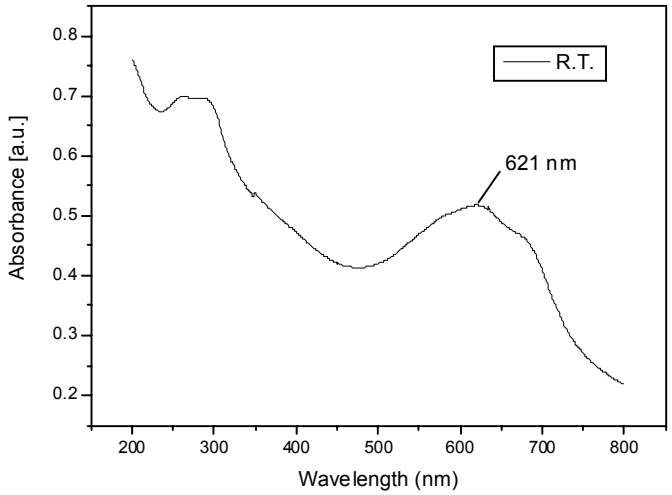


***Figure 3.10*** *UV-Vis spectrum in film at R.T. for 9a entry 11*

From the UV spectrum, an optical band gap of 1.65 eV was derived. The presence of a shoulder at higher wavelength in the UV-Vis spectrum of the conjugated polymer was also noticed. Typically this behaviour denounces the formation of aggregates and this may be due to the presence of an ordered structure. The high wavelength shoulder was observed in the polymers **9a** prepared at 0 °C (not the ones prepared at R.T.) and is more pronounced for the polymers with highest molecular weight values. For example, comparing the UV-Vis spectrum in solution (chloroform) and in solid state (film) of the polymer **9a**-(entry 11), a bathochromic shift was observed upon going from solution to thin film (**Figure 3.11**).

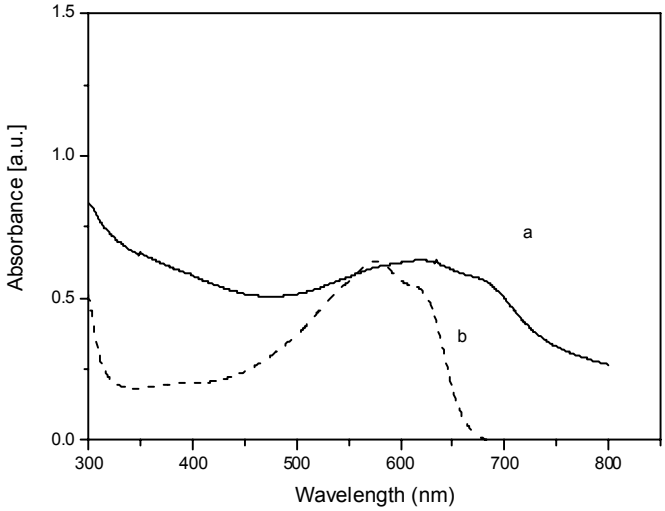


***Figure 3.11*** *UV-Vis spectra for entry 11 after conversion in solution: film (a), solution (b)*

Furthermore, a large degree of vibronic coupling is found both in the solution and in the solid state spectra. Both observations are indicative of structural order in solution as well as in film.

For the conjugated polymer **9a**-(entry 8) no vibronic coupling can be seen and only a small bathochromic shift is observed between the UV-Vis spectra in solution and in thin film (**Figure 3.12**). This suggests that little structural order exists even in film for this polymer.

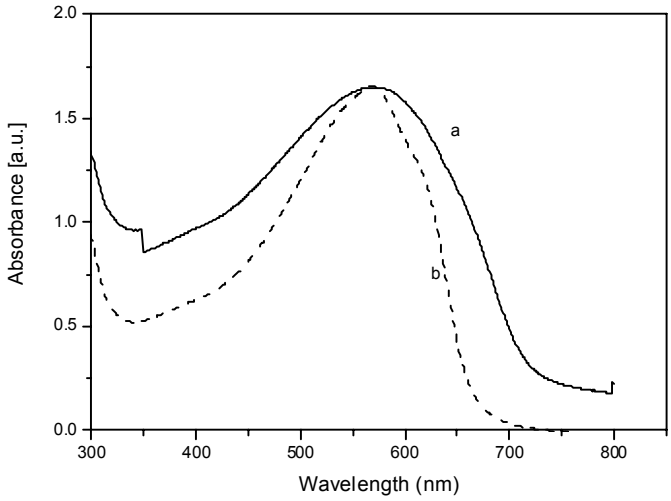


***Figure 3.12*** *UV-Vis spectra for entry 8 after conversion in solution: film (a), solution (b)*

These observations may point to a rather regio-regular structure of the 3-hexyl PTV **9a-11** and a rather regio-random polymer structure of 3-hexyl PTV **9a-8**.

Loewe *et al*. reported similar observations for regio-regular and regio-random poly(3-dodecylthienylene vinylene) synthesized by Stille coupling[9].

Compared with the latter synthetic procedure the dithiocarbamate precursor route seems to enable the synthesis of 3-alkyl PTVs with higher molecular weight and in higher yield. Actually the main observation here is the existence of experimental conditions which lead to a regio-regular polymerisation of the monomer **7a**.

An *in-situ* UV-Vis and a complementary *in-situ* FT-IR study were carried out also for **8b** and **8c** (**Figure 3.13** and **Figure 3.14** respectively).

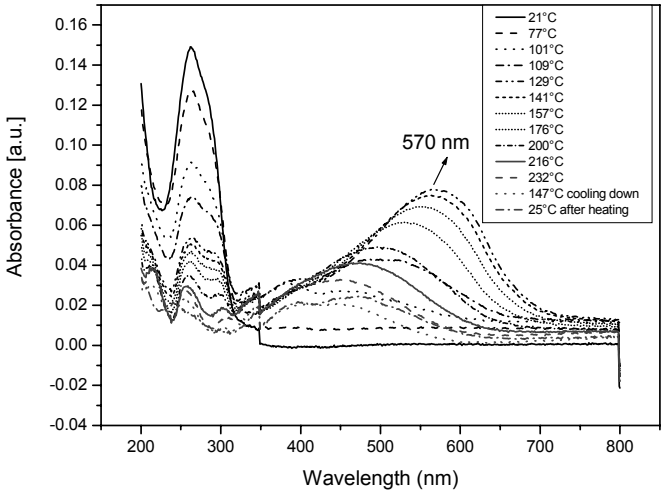


***Figure 3.13*** *In situ UV-Vis spectrum for 8b entry 13 at specific temperatures*

The di-hexyl PTV (**8c**) shows a very high $\lambda_{max}$ value compared to the other two alkyl PTV derivatives presented earlier in this chapter. This behaviour may point possibly to a better ordered structure with low defect content as the monomer has a symmetric structure. On the other hand also a substituent effect may influence the $\lambda_{max}$ value.

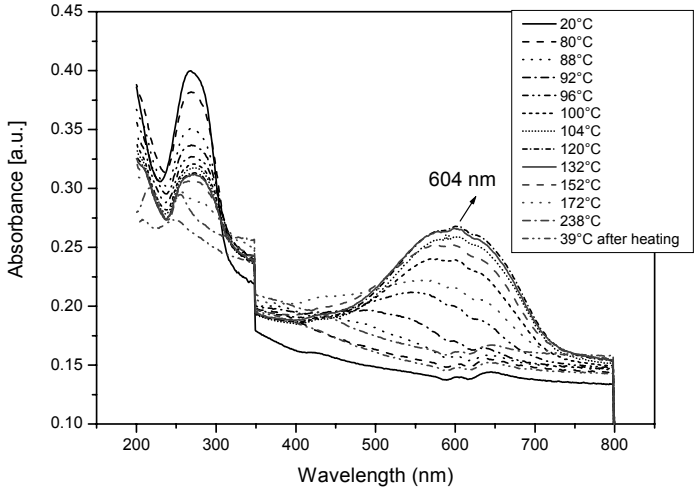


***Figure 3.14*** *In situ UV-Vis spectrum for 8c entry 17 at specific temperatures*

The thermochromic effect is also observed for the 3-dodecyl PTV (**8b**) and to a smaller degree for the 3,4-dihexyl PTV (**8c**) as is clear from the absorption profiles reported hereafter (**Figure 3.15** and **Figure 3.16**).

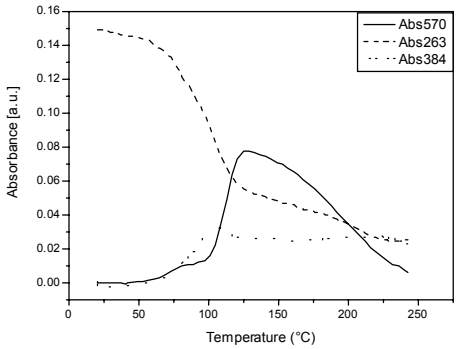


***Figure 3.15*** *UV-Vis profile for 8b*

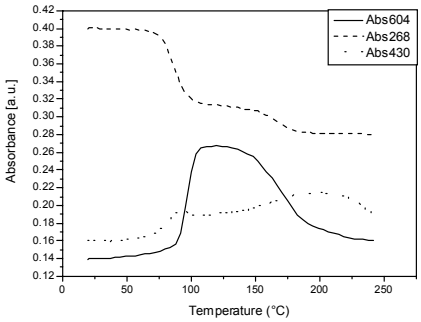


***Figure 3.16*** *UV-Vis profile for 8c*

After conversion of the precursor polymers in o-dichlorobenzene at reflux for 12 h UV-Vis spectra in film of the conjugated polymer were taken at R.T. An increased $\lambda_{max}$ value was observed in both cases as a consequence of the characteristic thermochromic behaviour possessed by these materials (**Figure 3.17** and **Figure 3.18**).

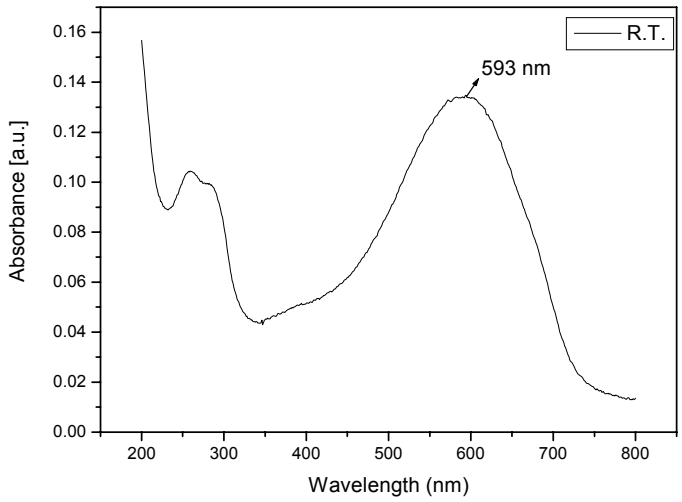


***Figure 3.17*** *UV-Vis spectrum for 9b entry 13*

The fact that the UV-Vis of the hexyl PTV shows a higher value of $\lambda_{max}$ (621 nm) compared to the UV-Vis spectrum of the dodecyl PTV ($\lambda_{max}$ = 593 nm) might be due to the presence of a higher content of low $M_w$ fractions as also seen in the $M_w$ distribution of the two polymers (**Figure 3.1**).

The presence of a shoulder observed at high wavelength for the polymer **9c** (682 nm) is certainly an indication for the presence of an ordered structure of the polymer. Indeed, because of di-substitution, we are in the presence of a symmetric monomer, and so regio-regularity is not an issue.

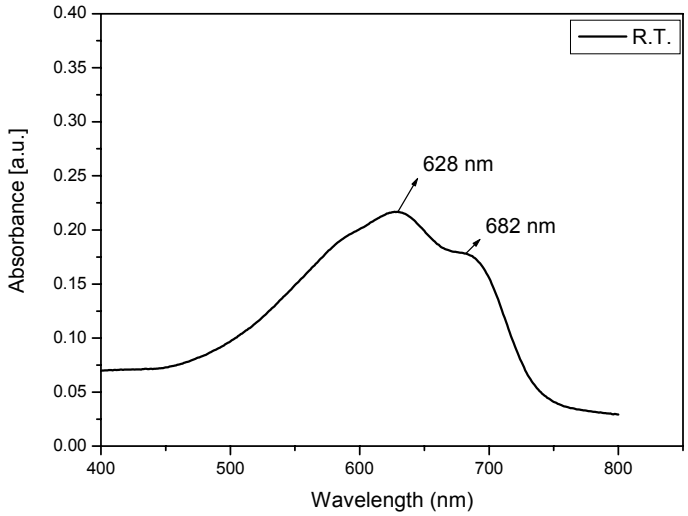


***Figure 3.18*** *UV-Vis spectrum for 9c entry 17*

Summarising, the optical band gaps, which have been determined from the absorption edge of the polymer thin films are reported in **Table 3.4**.

| Polymer | Optical Band gap (eV) |
|---|---|
| **8a** | 1.65 |
| **8b** | 1.67 |
| **8c** | 1.64 |

***Table 3.4*** *Calculated optical band gap values for alkyl PTVs*

Consequently, the alkyl PTV derivatives show the characteristics of low band gap polymers.

*In situ* FT-IR measurements were also performed for all the alkyl PTV derivatives synthesised. Here only the spectra relative to **8b** are reported since, the alkyl PTV derivatives did not show significant differences in the infra-red characteristic bands.

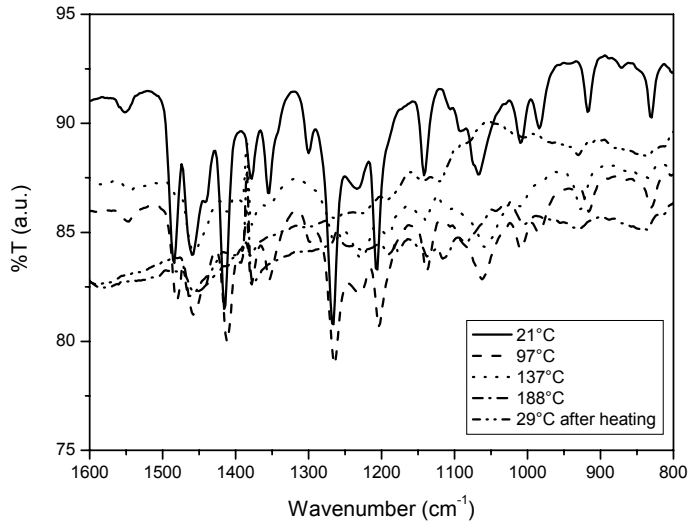


***Figure 3.19*** *FT-I.R. spectra at different temperatures for 8b*

The formation of the double bond can be seen by the appearance of a peak at 928 $cm^{-1}$ (**Figure 3.19**).

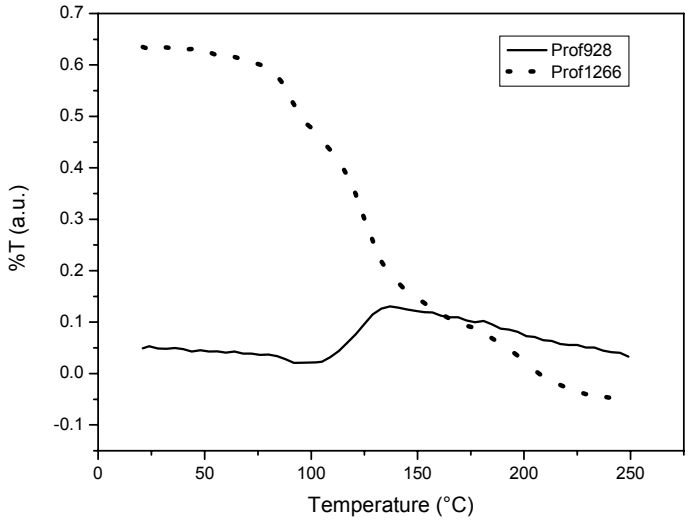


***Figure 3.20*** *FT-I.R. profile for 8b*

The appearance of the double bond as well as the disappearance of the dithiocarbamate groups can be better follow in the FT-IR profile (**Figure**

**3.20**). The elimination starts at ~ 100 °C and seems to be complete at 140 – 145 °C under these heating conditions. These values are comparable to those of plain PTVs

### 3.3.3 Cyclic voltammetry measurements

A detailed understanding of the doping process of conjugated polymers remains a scientific challenge. Electrochemical doping is complex and consists of several simultaneous and/or consecutive chemical and physical processes like swelling of the polymer, charge transfer between the electrode and the polymer, insertion of compensating ions into the bulk of the polymer, conformational changes of the polymer chain and change of conductivity. The strong development of polymer electronics during the last decade has made cyclic voltammetry, (CV), an established method to assess the energy position of the highest occupied molecular orbital (HOMO) and the lowest unoccupied molecular orbital (LUMO). This is an alternative to methods based on surface photoelectron spectroscopy. Cyclic voltammetry requires that electrochemical potentials are related to the vacuum level, something associated with both fundamental and practical problems. Although frequently used, the methodological basis for electrochemical band edge determination is not very well established. The relevance and generality of electrochemical characterisation of conjugated polymers can be estimated by comparison to other methods. This is frequently done by calculating the electrochemical band-gap, $E_{g,EC,}$ and comparing it with the optical band-gap, $E_{g,opt.}$ Many interesting problems of conjugated polymer electrochemistry can be addressed without the exact knowledge of the relation between the vacuum level and the electrochemical reference system in use. The study of the electrochemical behaviour of polymers as a function of substitution and sample preparation can shed some light on the understanding of the doping process, but it is also the basis for the development of applications[25].
The method used for the calculation of the $E_g$ *via* a CV measurement was already reported in chapter 2.

The polymers **9a** and **9c** were casted on a Pt working-electrode from a chloroform solution of them. The cyclic voltammogram for 3-hexyl PTVs (**9a**) in 0.1 M $TBAPF_6$ in acetonitrile solution, recorded during the potential cycling between -2 V and 0.6 V vs. Ag/Ag+ quasi reference electrode, is depicted in **Figure 3.21.**

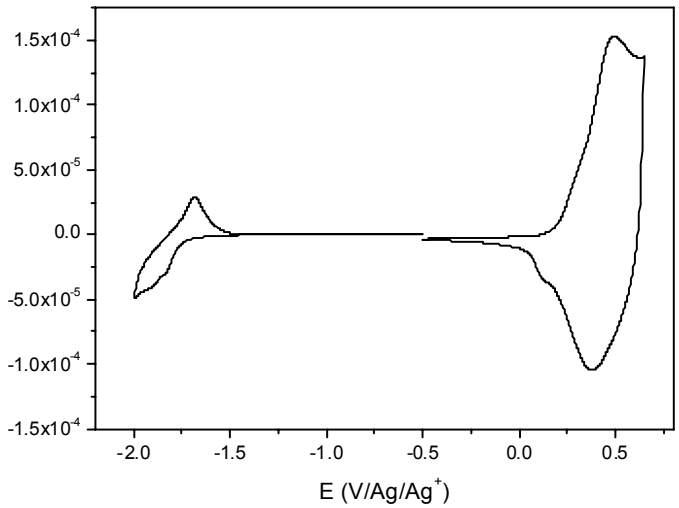


***Figure 3.21*** *CV measurement for 9a*

It can be seen that the material can be both oxidized and reduced with a p-doping/de-doping onset potential at about 0.26 V and a n-doping/de-doping onset potential at about -1.74 V *versus* the quasi Ag/Ag+ reference electrode. Both p- and n-doping signal are quasi-reversible. The energy levels of the highest occupied molecular orbital and the lowest unoccupied molecular orbital of 3-hexyl PTV (**9a**) are estimated to be -5.17 eV and -3.24 eV respectively. The electrochemical band gap can be calculated (see chapter 2) as the difference between the HOMO and the LUMO energy levels, thus resulting in a value of 1.93 eV. The difference between the optical and electrochemical band gap is most probably due to the difficult ion-transport through the polymer film.

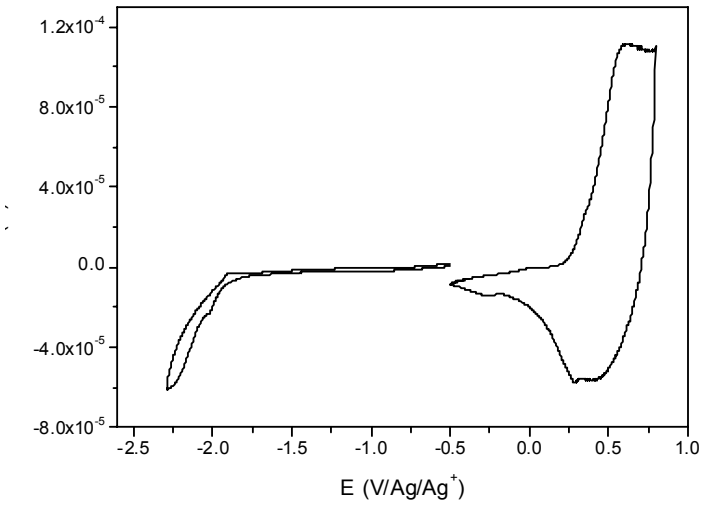


***Figure 3.22*** *CV measurement for 9c*

**Figure 3.22** shows the cyclic voltammogram of the 3,4-di-hexyl-PTV (**9c**) film on the Pt electrode. It can be seen that there is also a reversible p-doping/dedoping at positive potential range and an irreversible n-doping/dedoping processes at negative potential range. The oxidation peak potential is 0.61 V vs. Ag/Ag+. The onset reduction potential ($E^{red}$) and onset oxidation potential ($E^{ox}$) of the polymer are −1.91 V and 0.32 V (*versus* Ag/Ag+), respectively. From the $E_{onset}{}^{red}$ and $E_{onset}{}^{ox}$ values, the LUMO and HOMO energy levels of −3.07 eV and −5.30 eV were obtained. Therefore, the electrochemically determined band gap of 3,4-di-hexyl-PTV derived from the equation reported below is 2.23 eV.

$$E_g = E_{onset}{}^{ox} - E_{onset}{}^{red}$$

This value does not coincide with the calculated optical energy gap of 1.67 eV. Therefore, for both polymers, there is a big difference between the optical and electrochemical band gap. The reason is, most probably, related to a difficult ion-transport through the polymer film due to the presence of apolar side chains.

Amorphous polymer films and chain flexibility could lower the oxidation potential. But there are also arguments that crystalline parts of the film can tune the potential in the same direction. However, it is probably more reasonable to use regio-regularity as the starting point for a discussion. Crystallites are generally formed in polymers with a regio-regular coupling of the monomers and where steric interactions of the side chains promote an ordered (often more or less planar) conformation of the backbone. The quinoidal state that follows upon doping is favoured by the planar conformation. Thus, crystallinity may promote doping[26]. Recent studies have been able to separate redox conversion of different phases in films of highly regio-regular poly(alkylthiophene) in which the well-ordered, crystalline domains have the lowest oxidation potential[27,28]. Conditions during film formation can have a strong influence on film quality, also on a molecular level. This is highly relevant for the influence of conformational effects on the electrochemical behaviour, which has been demonstrated by Skompska *et al*.[25] Injection properties at the metal–polymer interface in electronic devices can be affected by the processing of the polymer film.[29]. This is something that could eventually also tune the redox potentials. To draw some conclusions we can say that band-gaps calculated from the electrochemical potentials for redox conversion have often been found to be higher than optical band-gaps. As a kind of final remark, the lack of standards in reporting and translating redox potentials suggest that the now well-established method of evaluating HOMO and LUMO positions by cyclic voltammetry may be used only in a relative way.

### 3.3.4 X-ray diffraction spectroscopy (XRD)

The XRD measurement was performed by Jan D'Haen at IMO-IMOMEC, University of Hasselt.

The XRD profile of the soluble 3-hexyl PTV **9a-11** is given in **Figure 3.23**. This conjugated polymer was obtained, as stated before, by conversion of the precursor polymer (entry 11) in ortho-dichlorobenzene under reflux for 12 hours. After precipitation in cold methanol, the conjugated polymer was

filtered off and dried under vacuum in a desiccator. The material was then analysed in the solid state, as a powder.
Since parallel beam geometry is recommended for XRD studies of irregular shaped surfaces, a Bruker D8 Discover with a divergence of less than 0.05° was used for the measurements.

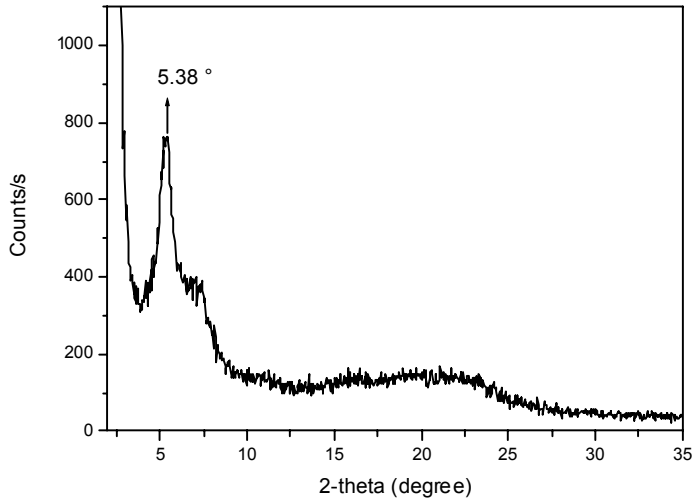


***Figure 3.23*** *XRD measurement for 9a entry 11*

The diffractogramm shows some crystallographic order in the material, indeed the peak at 2θ = 5.38° corresponds with an interplanar distance of d = 1.6 nm[30] (Bragg law hereafter reported):

$$n\lambda = 2d / \sin 2\theta$$

The evidence of some crystallinity substantiates the regio-regular structure of the PTV[31] **9a-11**.

### 3.3.5 Atomic Force Microscopy (AFM) measurements

To further investigate the molecular organisation present in these materials, the UV-Vis spectra of solutions in different solvents (p-xylene and chlorobenzene) were prepared and evaluated. Very diluted solutions were

prepared and heated below the boiling point of the solvents used until complete dissolution of the conjugated polymer. After using a very slow cooling rate at room temperature, UV-Vis spectra in solution at R.T. were taken.

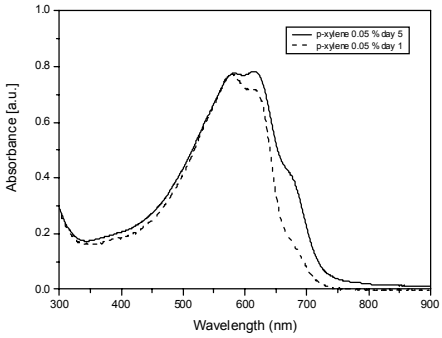


***Figure 3.24*** *UV-Vis spectrum for 9a-11*

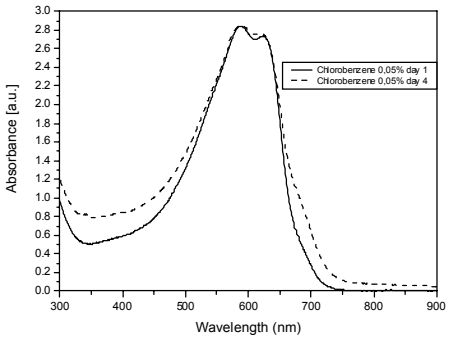


***Figure 3.25*** *UV-Vis spectrum for 9a-11*

As shown in the above reported UV-Vis spectra, the presence of some structural organization in solution is clear and it evolves as time passes (**Figure 3.24** and **Figure 3.25**). For the samples prepared in p-xylene, which is a poorer solvent than chlorobenzene, at R.T., an extra shoulder at ~ 675 nm is observed: it was assigned to aggregation as a consequence of a $\pi$-$\pi$ stacking interaction.

With the aim to investigate further the microstructure, a silicon oxide substrate was dipped in the solutions and analysed by tapping mode AFM (**Figure 3.26**). Contrasts of nano-particles were specifically evidenced in the phase images. These nano-clusters, with a dimension of 20-30 nm, have most probably a nano-crystalline structure. (The AFM measurements were performed by Dr. Olivier Douheret at IMO division, University of Hasselt).

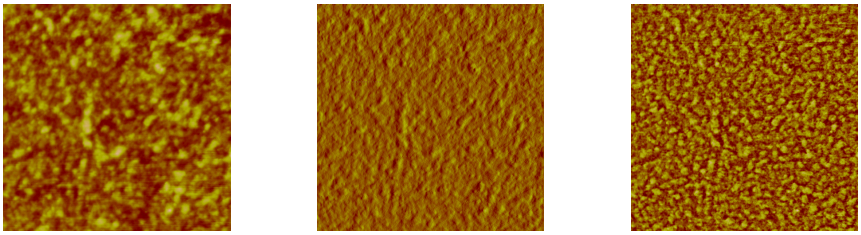

*a* *b* *c*

***Figure 3.26*** *a) AFM image for 9a entry 11 (0.05 % solution in chlorobenzene) 1×1 µm² Height; b) Amplitude; c) Phase*

### 3.3.6 Characterisation of the conjugated polymers by NMR spectroscopy ($T_1$ and $T_2$ determination)

The NMR investigation was performed in collaboration with Dr. Peter Adriaensens at University of Hasselt.

Due to the rather low solubility of the conjugated 3-hexyl PTV **9a**, the polymers obtained by thermal conversion of **8a** entry 11 (**9a-11**) and entry 8 (**9a-8**) were studied by means of $^{13}$C-CP/MAS NMR spectroscopy.

Under normal circumstances, two relaxation processes of proton nuclei are possible: spin-spin relaxation and spin-lattice relaxation. Two factors mainly determine the spin-lattice relaxation time: i) the environment i.e. the number of protons: the more protons are present, the faster the relaxation can occur; and ii) the mobility: the more mobile the chain segment, the shorter the relaxation time. The same consideration is true for the relaxation of carbon nuclei.

The $T_1$ decay times of all proton (or carbon) resonances of a material can be determined by means of an inversion recovery experiment. Here a series of $^1$H NMR spectra were recorded using the pulse sequence shown in **Figure 3.27**.

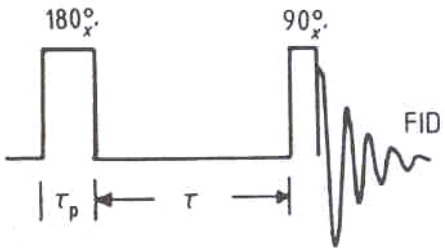


***Figure 3.27*** *Pulse sequence for determining the spin-lattice relaxation time $T_1$*

After the 180° pulse, $M_0$ lies along the (-z) direction. (Figure 3.28) During the variable time $\tau$ the system relaxes with the rate constant $k = T_1^{-1}$ (the spin-lattice relaxation is a first-order process). When $\tau = 0$, $M_z \sim - M_0$, but $M_z$ tends to be more and less negative when $\tau$ becomes longer. The situation in which $M_z = 0$, is important for the quantitative measurement of $T_1$ and here $\tau = \tau_0$. For greater values of $\tau$, $M_z$ again becomes positive and gets more and more positive until the system has finally returned to the equilibrium value $M_z = M_0$.

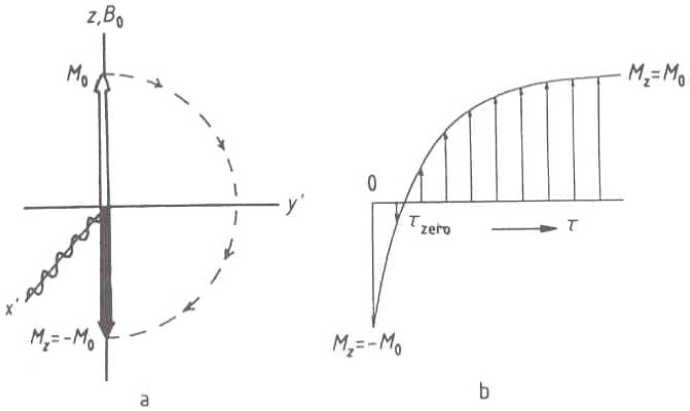


***Figure 3.28*** *Evolution of the magnetisation $M_z$ with time $\tau$ after a 180° pulse*

In view of the fact that $M_0$ and $M_z$ are not directly measurable quantities, the magnetisation component $M_z$ is rotated into the direction of the y'-axis by a 90° pulse in the second phase of the pulse sequence after the delay $\tau$. In this way a transverse magnetization component $M_{y'}$ is given which can be

observed. The intensities (I) of the NMR signals obtained after the Fourier transformation are proportional to the components $M_{y'}$. The spin-lattice relaxation process can therefore be described by **equation 3.1** from which $T_1$ can be calculated as:

$$I = I_0 (1 - 2 \exp(-\tau/T_1)) \qquad \textbf{eq.3.1}$$

Solid-state NMR spectroscopy and relaxometry are powerful non-invasive and non-destructive techniques to investigate the segmental chain dynamics and molecular miscibility of polymers on the nanometre level[32, 33]. **Figure 3.29** shows the $^{13}C$ spectra.

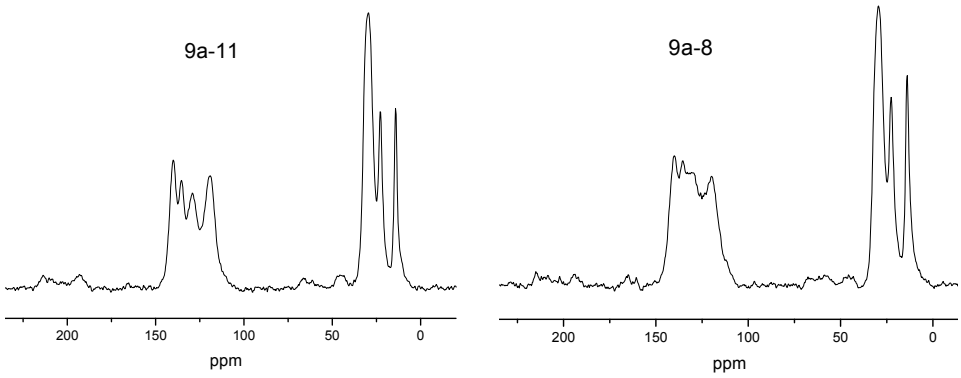


***Figure 3.29*** *$^{13}C$-CP/MAS NMR spectroscopy of 9a-11 and 9a-8*

It is clear that the resonances of **9a-11** are well resolved, pointing to a regio-regular microstructure. For **9a-8**, the lines are clearly broadened due to chemical shift dispersion (different chemical environments). This reflects more random like microstructures. To confirm the more ordered structure of **9a-11**, the $T_{1H}$ relaxation decay times were measured for both conjugated polymers. At temperatures below $T_g$, the $T_{1H}$ relaxation is averaged out over a distance of several tens to hundreds of nm due to the process of spin-diffusion[34]. Moreover, since $T_{1H}$ is dependent on fast MHz motions it will be determined mainly by the mobile side chains. While an average $T_{1H}$ decay

time of 0.68 ± 0.07 sec is obtained via the chemical shift selective $^{13}C$ resonances of **9a-11**, a value of only 0.33 ± 0.05 sec is measured for **9a-8**. From this observation, it can be concluded that the side chains of **9a-11** have higher degree of organisation as compared to those of **9a-8**. This is in agreement with the structural information obtained from the $^{13}C$-CP/MAS spectra. This conclusion was further confirmed by determination of the $T_{1H}$ and $T_{1\rho H}$ relaxation decay times by means of solid state $^{1}H$ wide-line NMR. The results are presented in **Table 3.5**.

| Polymer | $T_{1H}$ (sec) | $T_{1\rho H}$ (ms) |
|---|---|---|
| **9a-11** | 0.64 | S: 1.4 (23%)<br>L: 5.3 (77%) |
| **9a-8** | 0.36 | S: 1.3 (20%)<br>L: 6.0 (80%) |

***Table 3.5*** *$T_{1H}$ and $T_{1\rho H}$ values*

The $T_{1H}$ decay times, now obtained directly *via* the sensitive but chemical shift unselective proton resonance (broad signal of several tens of kHz), are completely in agreement with those obtained via $^{13}C$-CP/MAS. The $T_{1\rho H}$ relaxation, which is sensitive to more slowly kHz motions of the polymer backbone, had to be analysed bi-exponentially with a short (S) and long (L) decay time. The short decay time, and its fraction, mainly represents the backbone protons while the long decay time mainly represents the side chain protons. No significant differences are observed between both polymers. So, it can be concluded that the two polymers can only be differentiated based on their $T_{1H}$ relaxation. This confirms that the main difference between the two polymers is situated in their side chain mobility. Polymer **9a-11** has restricted side chain motions since the more regio-regular structure allows stronger side-chain Van der Waals interactions and so improved π-stacking. Last but not least, the stronger side-chain interactions confirm the lower solubility of **9a-11** as compared to **9a-8** emphasizing the delicate balance between solubility on one hand and high conjugation length and structural order on the other.

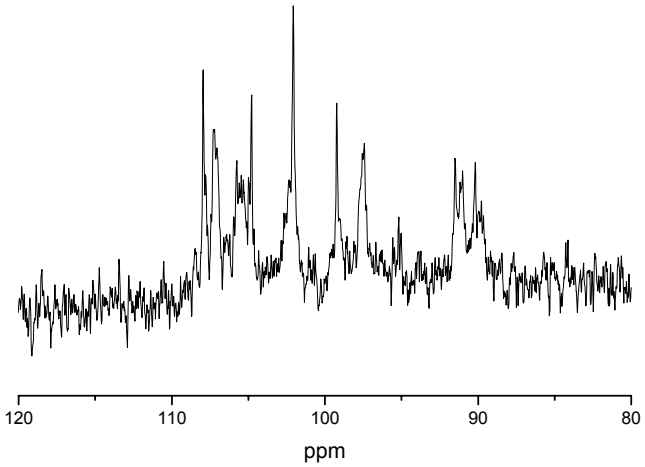


***Figure 3.30*** *$^{13}$C-NMR spectroscopy of 9b (detail of aromatic region) in $CDCl_3$*

The dodecyl PTV (**9b**) was also analysed by NMR and it presented more or less the same characteristic as **9a-8**. Many environments can be seen looking at **Figure 3.30**. This points to a possible more random like structure. It might be due to the presence of a very long alkyl side chain which can fold on itself and that this does not allow for the formation of a regio-regular configuration[35-39]. The variations of polymer chain folding also may show different conformations, dependent upon the interchain packing as was investigated for different series of alkyl substituted poly(thiophene)[40].

### 3.3.7 Charge transfer processes

Charge transfer processes were studied in collaboration with the University of Antwerp, by Aranzazu Aguirre and Griet Janssen of the group of Prof. Etienne Goovaerts.

A light induced Electron Paramagnetic Resonance (Li-EPR) measurement was used to investigate the photoinduced charge transfer (the method was already described in chapter 2).

The hexyl-PTV, which is not easily soluble in chlorobenzene, was then stirred under reflux (3 h at 145 °C). Solutions containing double amounts of PCBM as

compared to those of polymer were prepared afterwards. The solutions were spin-coated and, the so prepared films showed a thickness of ~ 100 nm.
The blend of hexyl-PTV/PCBM showed a clear light-induced signal (Figure 3.31), attributed to the appearance of the polaron and the PCBM radical.

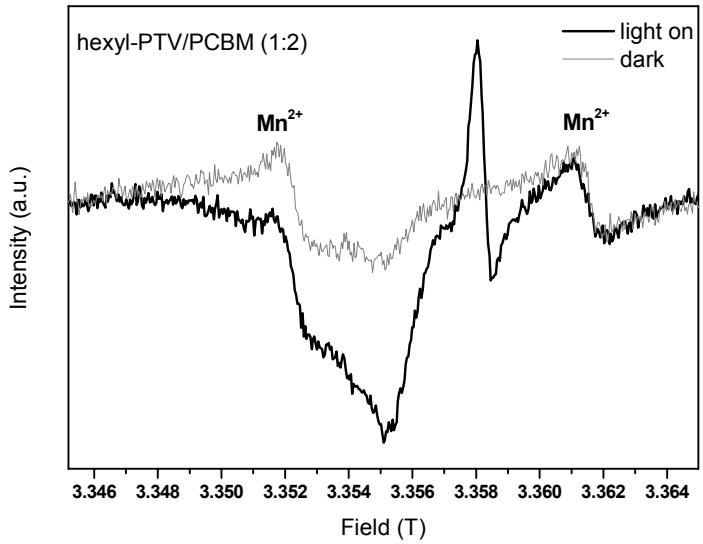


***Figure 3.31*** *W-band EPR (~95 GHz) spectrum of hexyl-PTV/ PCBM obtained at 18dB (microwave power 70μW), before and during illumination (excitation at 488nm) at 100K. Inset: absorption spectrum and cw-EPR simulations of hexyl-PTV.*

Iodine doping was performed in a number of cases in conjugated polymers in order to induce the polaron chemically and be able to study it separately from the PCBM radical. This approach was also attempted for the hexyl-PTV, but at doping level with sufficient signal-to-noise ratio, the line broadening due to dipolar interactions between spins was too important to be able to resolve the anisotropy in the polaron spectra.

## *3.4 Application in solar cells*

Photovoltaic studies on solar cell devices were performed by Le Huong Nguyen and Helmut Neugebauer from the group of Serdar Sariciftci at Linz

Institute for Organic Solar Cells (LIOS)* in Austria and, by Claudio Girotto and Tom Aernouts from the group of Jef Poortmans at IMEC Leuven**.

The dihexyl and the dodecyl PTVs were dissolved in o-dichlorobenzene (p.a.), while the hexyl PTV, due to its difficult solubility, was dissolved in chlorobenzene (p.a.) under reflux condition. The concentration of the solutions was set at 2 % for dihexyl and dodecyl PTVs, and 1 % for the hexyl PTV.

Then, blends in a 1:1 ratio with PCBM were prepared for all three samples. Spin coating was done on quartz at 2000 RPMs for dodecyl and dihexyl PTVs, and at 1000 RPMs for hexyl PTV. UV-Vis of the pristine samples and of the blends were taken for comparison (**Figure 3.32**).

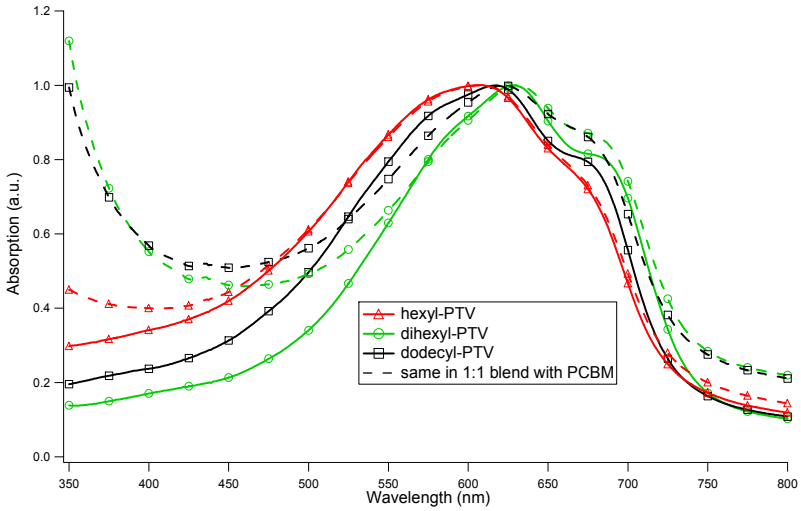


***Figure 3.32*** *UV-Vis spectra of alkyl PTV derivatives (pristine sample and in 1:1 blends with PCBM)*

Based on the absorption edge of the different polymers an optical band gap can be derived of about 1.68 eV as was also reported in **Table 3.4**. Another interesting observation is the red shift from the hexyl to the dodecyl and the dihexyl PTV derivatives. Moreover, the development of the shoulders gets higher with the same trend. The spectrum of the blend hexyl PTV:PCBM is almost identical to the pristine one, with only the superposition of the PCBM spectrum. The other two are a little modified, with attenuation of the

maximum peak and of the high energy spectrum of the PTVs. The shoulders are still clearly visible, especially the one around 680-700nm.

It should be noticed that the difference observed in the UV-Vis spectra of the dodecyl PTV (compare **Figure 3.17** with **Figure 3.32**) may relate to the method of preparation of the films. The spin-coating can induces order in the film compared to simply casted film. This induced order is responsible of the increased absorption maximum value observed for the dodecyl PTV.

The best PV devices were obtained by preparing solutions of polymers as donor component and the $C_{60}$-derivative 1-(3-methoxycarbonyl) propyl-1-phenyl [6,6] $C_{61}$ (PCBM) as acceptor in the bulk heterojunction concept at different weight ratio. Poly(3,4-ethylenedioxythiophene) : poly(styrenesulfonate) (PEDOT:PSS) (Baytron P, Bayer Germany) was spin-coated on top of indium-tin oxide (ITO) (Merck, Germany) coated glass (~25 W/sq) which had been cleaned in an ultrasonic bath with acetone and isopropyl alcohol. The active layer was spin-coated on the PEDOT: PSS layer. 6 Å of lithium fluoride (LiF) and an 80 nm thick Al electrode was then deposited onto the blend film by thermal evaporation at ~5x $10^{-6}$ mbar. All current-voltage (I-V) characteristics of the photovoltaic devices were measured using a Keithley SMU 2400 unit under inert atmosphere (argon) in a dry glove box. A Steuernagel solar simulator was used as the excitation source with a power of 100 $mWcm^{-2}$ white light illumination (AM 1.5 conditions). A lock-in technique was used to measure the incident photon-to current efficiency (IPCE). With this technique the number of electrons produced from the cell under short-circuits conditions are related to the number of incident photons. Light intensity correction was performed using a calibrated Si photodiode.

I-V characteristics of ITO/PEDOT/PTV: PCBM/LiF/Al for the polymer devices are shown in **Figure 3.33** both in dark and under AM 1.5 illumination.

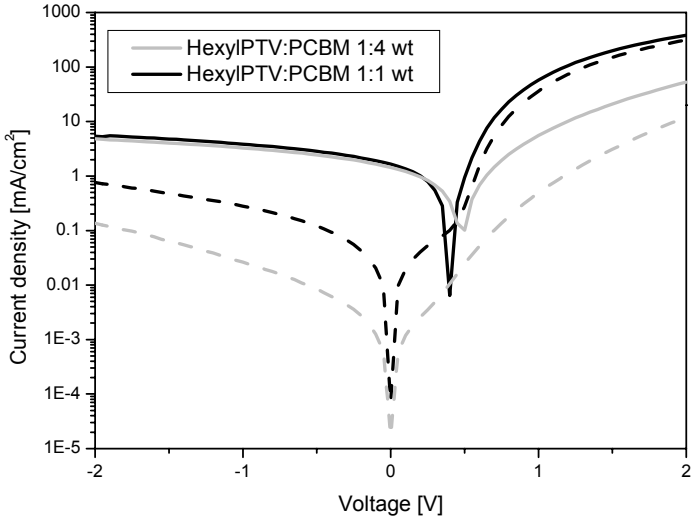


***Figure 3.33*** *I-V characteristics (AM 1.5, 100 mW/cm2) of the hexylPTV: PCBM in different ratios**

In the **Table 3.6** the characteristic values found for the solar cells are reported.

| Best devices | $V_{oc}$ [mV] | $I_{sc}$ [mA/cm$^2$] | FF | Efficiency [%] |
|---|---|---|---|---|
| **9a/PCBM (1:4)*** | 500 | 1.43 | 0.29 | 0.21 |
| **9a/PCBM (1:1)*** | 400 | 1.65 | 0.31 | 0.20 |
| **9a/PCBM (1:1)**** | 590 | 0.07 | 0.24 | 0.01 |
| **9b/PCBM (1:1)**** | 520 | 1.04 | 0.31 | 0.17 |
| **9c/PCBM (1:1)**** | 590 | 1.17 | 0.54 | 0.38 |

***Table 3.6*** *Listed open-circuit voltage ($V_{OC}$), short-circuit current ($I_{SC}$), fill factor (FF) and conversion efficiency (h) for 9a, 9b and 9c*

The results are promising although rather low efficiency values were found. On the base of the results obtained for **9c**, a $V_{oc}$ of ~ 590 mV can be predicted also for the hexyl and the dodecyl PTV.

Further optimisations are still necessary for the solar cells; it might be interesting to evaluate the effect of heat treatment on the performance as well.

## *3.5 Conclusions*

The use of Lithium Bis(trimethylsilyl)amide (LHMDS) as base in the dithiocarbamate precursor route, opens up a highly efficient synthetic route towards the synthesis of 3 and 3,4 alkyl substituted derivatives of Poly(2,5-Thienylene Vinylene). The conjugated polymers obtained after conversion are superior in yield, molecular weight and optical absorption characteristics compared to the ones produced with the earlier synthetic routes towards this class of soluble conjugated polymers.

In case of the synthesis of a precursor toward the 3-alkyl (hexyl) PTV, it seems that a regio-regular polymerisation process can occur. In order to get regio-regular polymers also the purity of the starting monomers may be of a crucial importance, besides specific polymerisation conditions.

Evidence for the formation of an ordered structure was pointed out by optical absorption spectroscopy, XRD, AFM and solid state NMR.

Future work will focus on the optimisation of the polymerisation reaction. This implies a better understanding of the extent of regio-regularity and the polymerisation mechanisms occurring. Furthermore, these soluble PTV derivatives will be further evaluated for application as low band gap materials in photovoltaic devices.

## *3.6 Experimental part*

**Materials**. Unless stated otherwise, all reagents and chemicals were obtained from commercial sources (Acros and Aldrich) and used without further purification. Tetrahydrofuran (THF) was dried by distillation from sodium/benzophenone.

**Characterisation**. Nuclear magnetic resonance (NMR) spectra were recorded on a Varian Inova 300 spectrometer at 300 MHz for $^{1}H$ NMR and at 75 MHz for $^{13}C$ NMR using a 5 mm probe. Solid-state $^{13}C$ CP/MAS NMR spectra were recorded at room temperature on an Inova 400 Varian spectrometer operating at a static magnetic field of 9.4 T. Magic angle spinning was performed at 7.4 kHz, making use of ceramic $Si_3N_4$ rotors. The aromatic signal of hexamethylbenzene was used to determine the Hartmann-Hahn condition for cross-polarization and to calibrate the carbon chemical shift scale (132.1 ppm). Other spectral parameters used were a 90° pulse length of 2.2 μs, a spectral width of 50 kHz, a preparation delay of 3 s and an acquisition time of 20 ms. High power decoupling was set to 85 kHz during the acquisition time.

Solid-state proton wide-line $T_{1H}$ and $T_{1\rho H}$ relaxation measurements were carried out on the same spectrometer in a wideline probe equipped with a 5 mm coil. A spectral width of 2 MHz was used and a preparation delay time equal to 5 times the longest $T_{1H}$ relaxation time was always maintained between successive pulses. The $T_{1H}$ relaxation decay times were measured by means of a modified solid echo pulse sequence in which an inversion recovery filter was placed in front of the solid echo part. The solid echo part had a total echo delay of 7 μs. The $T_{1H}$ analysis of the integrated signals was according the equation: $I(t) = I0\ (1 - 2.\ \exp(-t/T_{1H})$ where t is the variable evolution time and I0 the intensity of the resonance at equilibrium. The $T_{1\rho H}$ decay times were measured by applying a spin-lock field (50 kHz) of variable duration after the initial 90° pulse of the solid-echo part. The $T_{1\rho H}$ analysis of the integrated signals was according the equation: $I(t) = I0.\ \exp(-t/\ T_{1\rho H})$

where t is the variable spin-lock time and I0 the intensity of the resonance at equilibrium.

Gas chromatography/mass spectrometry (GC/MS) analyses were carried out with TSQ – 70 or Voyager mass spectrometers (Thermoquest); the capillary column was a Chrompack Cpsil5CB or Cpsil8CB.

Analytical Size Exclusion Chromatography (SEC) was performed using a Spectra series P100 (Spectra Physics) pump equipped with two mixed-B columns (10 μm, 2 x 30 cm, Polymer Labs) and a Refractive Index detector (Shodex) at 70 °C. THF was used as the eluent at a flow rate of 1.0 mL/min. Molecular weight distributions are given relative to polystyrene standards.

FT-IR spectra were collected with a Perkin Elmer Spectrum One FT-IR spectrometer. UV-Vis spectroscopy was performed on a VARIAN CARY 500 UV-Vis-NIR spectrophotometer. Samples for temperature dependent thin film FT-IR and UV-Vis Characterisation were prepared by spin-coating the precursor polymer from a $CHCl_3$ solution (10 mg/mL) onto NaCl disks at 500 rpm or quartz disks at 700 rpm. The disks were heated in a Harrick high temperature cell (heating rate: 2 °C/min), which was positioned in the beam of either the FT-IR or the UV-Vis spectrometer to allow *in-situ* measurements. Spectra were continuously acquired under a continuous flow of $N_2$.

Thin film electrochemical properties were measured with an Eco Chemie Autolab PGSTAT 20 Potentiostat/Galvanostat using a conventional three-electrode cell (electrolyte: 0.1 mol/L $LiClO_4$ in anhydrous $CH_3CN$) with an $Ag/Ag^+$ reference electrode (0.01 mol/L $AgNO_3$, 0.1 mol/L $LiClO_4$ and $CH_3CN$), a platinum counter electrode and an Indium-Tin Oxide (ITO) coated glass substrate as working electrode. Cyclic voltamograms were recorded at 50 mV/s under $N_2$ atmosphere and all potentials were referenced using a known standard (ferrocene/ferrocinium, 0.099 V vs. $Ag/Ag^+$). Solution electrochemistry was performed using the same setup (electrolyte: 0.1 mol/L tetra-n-butyl ammonium hexafluorophosphate ($TBAPF_6$) in anhydrous $CH_2Cl_2$) and a Pt working electrode.

A Bruker D8 Discover diffractometer equipped with a Göbel mirror (copper target K$\alpha$1 and K $\alpha$2 lines) and centric cradle was used to obtain 1-D X-ray

diffraction (XRD) profiles. The spectra were taken under a step-scan rate of 0.04 ° per 40 s in the scattering angle range of 2θ = 2 °- 35 °.

A Bruker ELEXSYS E680 spectrometer in conjunction with a split-coil 6-T superconducting magnet was used for W-band (95 GHz) light-induced Electron Paramagnetic Resonance (Li-EPR). These measurements were performed at 100 K using an Oxford flow cryostat and with a Bruker cylindrical cavity which allows optical access to the sample via an optical fibre. Optical excitation was performed with the 488 nm line of an $Ar^+$ laser. The results presented here are recorded with a modulation frequency and amplitude of 100 kHz and 3 G respectively and a microwave frequency and microwave power of 94.0795 GHz and 7x10-2 mW. The samples were prepared from dried drop cast films of the 1:1 ratio polymer/PCBM solution.

**Synthesis of 3-hexylthiophene (2a)**

To a stirring solution of 3-bromothiophene **1a** (1 g, 7.4 mmol) ether (6.5 ml) and $NiCl_2$ 1,3-bis(diphenylphosphino) propane (dppp) catalyst (5 %), in a three-necked flask under vacuum, the hexyl magnesium bromide (2.0 M in diethyl ether 7.4 ml, 37 mmol) was added dropwise via a cannula at 0 °C. After complete addition the mixture was stirred at room temperature (RT) overnight. Then, the mixture was quenched with diluted HCl (1 M) and extracted with dichloromethane; the organic layer was dried over $MgSO_4$ and the obtained product was purified via flash chromatography using hexane as eluent to give **2a** as colourless oil in a yield of 95 %. $^1$H NMR ($CDCl_3$): 7.3 (dd, 1H, J=3Hz, J=2Hz), 7.03 (m, 1H), 6.96 (dd, 1H, J=1Hz, J=3.8Hz), 2.26 (t, 2H, J=7.6Hz), 1.62 (m, 2H), 1.28 (m, 6H), 0.88 (t, 3H, J=4.7Hz).

$^{13}$C NMR ($CDCl_3$, 200 MHz) 143.2, 128.2, 125.0, 119.7, 31.7, 30.5, 30.3, 29.0, 22.6, 14.1.

FT-I.R. (NaCl, $cm^{-1}$) 3105, 3073, 3051, 2956, 2929, 2856, 1750, 1558, 1537, 1465, 1409, 1378, 1350, 1328, 1234, 1153, 1079, 936, 920, 856, 834, 772, 681, 661, 633, 577

**Synthesis of 3-hexyl-2,5-di-bromo-thiophene (3a)**

In a round-bottom flask 3-hexylthiophene **2a** (1 g, 6 mmol) and DMF were stirred at 0 °C and a solution of N-bromosuccinimide (NBS) (2.3 g, 13 mmol) in DMF was added slowly via a dropping funnel (the concentration of 3-hexylthiophene in the final reaction mixture is 0.3 M). The mixture was stirred for 3 days at RT in the darkness. Then, the reaction mixture was poured onto an equal volume of ice and extracted with ether. Afterwards the organic layer was washed with NaOH 2.5 M and saturated NaCl solution. The solvent was evaporated and the product (**3a**) was obtained as a colourless oil (yield 82 %). $^{1}$H NMR ($CDCl_3$): 6.66 (s, 1H), 2.40 (t, 2H, J=7.54Hz), 1.43 (m, 2H), 1.19 (m, 6H), 0.78 (t, 3H, J=6.3Hz).

$^{13}$C NMR ($CDCl_3$, 200 MHz) 142.74, 130.70, 110.08, 107.70, 31.34, 29.26, 28.56, 22.33, 13.83.

FT-I.R. (NaCl, $cm^{-1}$) 3091, 2954, 2926, 2856, 1648, 1542, 1466, 1459, 1419, 1377, 1344, 1189, 1095, 998, 963, 924, 825, 772, 725, 698, 686, 651, 577, 472.

**Synthesis of 3-hexyl-2,5-thiophenedicarboxaldehyde (4a)**

In a three-necked round-bottom flask 2,5-dibromo-3-hexylthiophene **3a** (1 g, 3 mmol) and THF (10 ml) were stirred under vacuum at -78 °C. A solution of n-butyllithium (n-BuLi) 1.6 M in ether (4.1 ml, 6.6 mmol) was slowly added with a cannula, the mixture was stirred for 30 minutes and afterwards 1-formylpiperidine, previously distilled, (0.76 g, 6.7 mmol) was slowly added. The reaction mixture was left at 25 °C under continuous stirring for 12 hours. HCl 2 M was added to quench the excess of BuLi followed by extraction with chloroform. The oily compound so obtained was purified via column chromatography on silica gel (chloroform/hexane 5:5), yielding the di-aldehyde as an orange oil (96 %).$^{1}$H NMR ($CDCl_3$): 10.02 (s, 1H), 9.98 (s, 1H), 7.62 (s, 1H), 3.02 (t, 2H, J=5Hz), 1.67 (m, 2H), 1.38 (m, 6H), 0.88 (t, 3H, J=4.7Hz)

**Synthesis of 3-hexyl-2,5-bis(hydroxymethyl)thiophene (5a)**

In a 100 mL round-bottom flask $LiAlH_4$ was added (0.34 g, 9 mmol) to dry THF (50 ml, dried over sodium) under argon atmosphere. This slurry was cooled to 0 °C and the di-aldehyde **4a** (1 g, 4.5 mmol) in THF (10 ml) was slowly added via a dropping funnel. When the addition was completed a reflux condenser was fitted and the slurry was heated at reflux temperature for 5 hours. After cooling down, air was allowed to get in the system and the reaction mixture was placed in an ice bath. Then, it was quenched by cautious sequential addition of water, aqueous 15 % NaOH solution, and again water until no more gas development could be detected. This solution was filtered and the residue was extracted with ether. The combined organic layers were dried over $MgSO_4$ and the solvent was evaporated under reduced pressure. The pure diol **5a** was obtained as yellowish oil in a yield of 80 %. $^1$H NMR ($CDCl_3$): 6.75 (1H), 4.41 (4H), 3.73 (2H), 1.84 (2H), 1.54 (2H), 1.24 (4H), 0.87 (3H)

**Synthesis of 3-hexyl-2,5-bis(chloromethyl)thiophene (6a)**

To a cooled (0 °C), stirred solution of diol **5a** (0.8 g, 3.5 mmol) in THF (10 ml) was slowly added a solution of $SOCl_2$ (0.64 ml, 1.04 g, 8.9 mmol) in THF (5 ml). The temperature of the reaction mixture was allowed to increase to RT under continuous stirring for 1 hour. Then, the mixture was cooled down again at 0 °C and a saturated sodium carbonate solution was added dropwise until neutral. The mixture was extracted with ether and dried over $MgSO_4$. The solvent was evaporated and the highly reactive dichloride **6a** was obtained as an orange oil. Because of the highly reactivity of **6a**, the di-chlorine was used as it was in the next reaction step without purification.

**Synthesis of thiophene 3-hexyl-2,5-diylbismethylene N,N-diethyl dithiocarbamate (7a)**

To a solution of bischloromethyl (0.93g, 3.5 mmol) **6a** in ethanol (10 ml), sodium diethyldithiocarbamate trihydrate (or diethyldithiocarbamic acid sodium salt trihydrate) (1.61 g, 10.5 mmol) was added as a solid. The mixture was stirred at ambient temperature overnight. Then, water was added and the desired monomer was extracted with ether (3 x 100 mL) and dried over

$MgSO_4$. Column chromatography (chloroform/hexane 5:5) yielded the monomer as a yellow oil (70 %). $^1$H NMR ($CDCl_3$): 6.75 (s, 1H), 4.65 (s, 2H), 4.58 (s, 2H), 4.04 (q, 4H), 3.73 (q, 4H), 1.52 (m, 2H), 1.27 (m, 20H), 0.87 (t, 3H)

**Synthesis of 3-dodecylthiophene (2b)**

The synthesis was done in the same way as for **2a** but, here dodecyl magnesium bromide (2.0 M in diethyl ether) was added instead of hexyl magnesium bromide. **2b** was obtained as colourless oil in a yield of 75 %. $^1$H NMR ($CDCl_3$): 7.3 (dd, 1H), 7.03 (m, 1H), 6.90 (d, 1H), 2.67 (t, 2H), 1.64 (m, 2H), 1.28 (m, 18H), 0.87 (t, 3H).

**Synthesis of 3-dodecyl-2,5-di-bromo-thiophene (3b)**

The synthesis was done in the same way as for **3a**. **3b** was obtained as a colourless oil (yield 87 %). $^1$H NMR ($CDCl_3$): 6.76 (s, 1H), 2.49 (t, 2H), 1.52 (m, 2H), 1.25 (t, 18H), 0.87 (t, 3H).

$^{13}$C NMR ($CDCl_3$) 143.0, 130.9, 110.3, 107.9, 31.9, 29.7, 29.6, 29.1, 25.4, 22.7, 14.1.

**Synthesis of 3-dodecyl-2,5-thiophenedicarboxaldehyde (4b)**

The formation of the dicarboxaldehyde was carried out in the same way of **4a**. The oily compound was obtained pure in a yield of 80%. .$^1$H NMR ($CDCl_3$): 10.12 (s, 1H), 9.95 (s, 1H), 7.62 (s, 1H), 2.97 (t, 2H), 1.67 (m, 2H), 1.23 (m, 18H), 0.85 (t, 3H)

**Synthesis of 3-dodecyl-2,5-bis(hydroxymethyl)thiophene (5b)**

The synthesis was done in the same way as for **5a.** The pure diol was obtained as a yellowish oil in a yield of 85%. $^1$H NMR ($CDCl_3$): 6.76 (s, 1H), 4.70 (m, 4H), 3.72 (t, 2H), 1.83 (br t, 2H), 1.52 (t, 2H), 1.23 (m, 18H), 0.85 (t, 3H)

**Synthesis of 3-dodecyl-2,5-bis(chloromethyl)thiophene (6b)**

The synthesis was done in the same way as for **6a**. The highly reactive dichloride **6b** was converted in situ into the monomer **7b**.

**Synthesis of thiophene 3-dodecyl-2,5-diylbismethylene N,N-diethyl dithiocarbamate (7b)**

The synthesis was done in the same way as for **7a**. The monomer was obtained as orange oil and purified via column chromatography using a mixture of hexane/ethylacetate (8:2) as eluent. The pure product was obtained in a yield of 60%. $^1$H NMR ($CDCl_3$): 6.75 (s, 1H), 4.65 (s, 2H), 4.58 (s, 2H), 4.02 (q, 4H), 3.68 (q, 4H), 2.48 (t, 2H), 1.54 (m, 2H), 1.27 (m, 30H), 0.85 (t, 3H)

**Synthesis of 3,4-dihexylthiophene (2c)**

Hexyl magnesium bromide (2.0 M in diethyl ether, 12 ml, 62 mmol) was added dropwise via a cannula to a stirred solution of 3,4-dibromothiophene (3 g, 12 mmol) and $NiCl_2$ (dppp) catalyst (5 %) in ether, under vacuum, at 0 °C. After complete addition the mixture was refluxed for 20 hours. It was then cooled down again to 0 °C and quenched with diluted HCl. The mixture was extracted with dichloromethane; the organic layer was dried over $MgSO_4$ and the solvent evaporated under pressure. The product of the reaction mixture was purified via flash chromatography in hexane to give the pure 3,4-dihexylthiophene as colourless oil in a yield of 95 %. $^1$H NMR ($CDCl_3$): 6.87 (s, 2H), 2.50 (t, 4H), 1.64 (m, 4H), 1.31 (m, 12H), 0.90 (t, 6H)

**Synthesis of 3,4-dihexyl-2,5-dibromo-thiophene (3c)**

In a round-bottom flask 3,4-dihexyl-thiophene **2c** (3.2 g, 12 mmol) and a mixture of chloroform/acetic acid 50:50 (50 ml) were stirred and heated at 30 °C; NBS (4.48 g, 25.2 mmol) was then slowly added. After complete addition, the reaction mixture was refluxed for 15-20 min, then cooled down again and diluted with an equal volume of water; the chloroform layer was separated and washed (3 times) with sodium carbonate solution and once with water. The di-bromo derivative **3c** was obtained as a yellow oil (yield 90 %). $^1$H NMR ($CDCl_3$): 2.51(t, 4H), 1.31 (m, 12H), 0.89(t, 6H)

**Synthesis of 3,4-dihexyl-2,5-thiophenedicarboxaldeyde (4c)**

In a three-necked round-bottom flask 3,4-dihexyl-2,5-dibromothiophene (4.79, 11.7 mmol) and THF were stirred under vacuum at -78 °C. A solution 1.6 M of n-BuLi (16.1 ml, 25.74 mmol) was slowly added via a cannula and the mixture stirred for 30 minutes. Afterwards 1-formylpiperidine, previously distilled, was slowly added (2.92 g, 25.8 mmol) and the reaction mixture was then stirred at 25 °C for 12 hours. HCl 2 M was added to quench the excess of BuLi followed by extraction with chloroform. The obtained compound was purified via column chromatography with chloroform/hexane (5:5) as the eluent and the pure product was obtained as an orange oil in a yield of 70 %. $^1$H NMR ($CDCl_3$): 10.09 (s, 2H), 2.9(t, 4H), 1.55 (m, 4H), 1.31 (m, 12H), 0.87 (t, 6H)

**Synthesis of 3,4-dihexyl-2,5-bis(hydroxymethyl)thiophene (5c)**

The synthesis was done in the same way as for **5a**. The pure diol **5c** was obtained as a yellowish oil in a yield of 70 %. $^1$H NMR ($CDCl_3$): 4.73(s, 4H), 2.5 (t, 4H), 1.29 (m, 12H), 0.89 (t, 6H)

**Synthesis of 3, 4-dihexyl-2, 5-bis (chloromethyl) thiophene (6c)**

The synthesis was done in the same way as for **6a**.

**Synthesis of thiophene 3,4-dihexyl-2,5-diylbismethylene N,N-diethyl dithiocarbamate (7c)**

Compound **6c** was converted *in situ* in the diethyl dithiocarbamate monomer as described in **7a**. The pure monomer was obtained after purification via column chromatography in ether as an orange – red oil in a yield of 70 %. $^1$H NMR ($CDCl_3$): 4.56 (s, 4H), 3.98 (s, 4H), 3.66 (q, 4H), 2.45(q, 4H), 1.33 (t, 12H), 0.84(t, 6H)

**Polymerisation**

A solution of monomer (**7a**, **7b** or **7c**) in dry THF (the monomers were previously freeze dried) was degassed by passing through a continuous

nitrogen flow. The concentration of the monomer was set to 0.2 M or 0.4 M. A solution of base, (Lithium di-isopropyl amide (LDA) 2.0 M solution in THF or Lithium Bis(trimethylsilyl)amide (LHMDS) 1 M solution in THF) was added in one go to the stirred monomer solution. The mixture was kept for 90 minutes under continuous nitrogen flow at a given temperature. The polymer was precipitated in ice water and the water layer was neutralized with diluted HCl before extraction with chloroform. The solvent of the combined organic layers was evaporated under reduced pressure and a second precipitation was performed in pure cold methanol. The polymer was collected and dried in vacuo. **8a** $^1$H NMR ($CDCl_3$): 6.72-6.36 (br s, 1H), 5.24-5.58 (br s, 1H), 3.86-4.15 (br q, 2H), 3.42-3.75 (br q, 2H), 2.21-2.40 (br m, 2H), 1.01-1.55 (br m, 8H), 0.91-0.82 (br t, 3H).

**8b** $^1$H NMR ($CDCl_3$): 6.78-6.36 (br s, 1H), 5.40-5.21 (br s, 1H), 3.86-4.15 (br q, 2H), 3.42-3.75 (br q, 2H), 2.18-2.42 (br m, 2H), 1.01-1.62 (br m, 18H), 0.91-0.83 (br t, 3H).

**8c** $^1$H NMR ($CDCl_3$): 5.25-5.60 (br s, 1H), 3.86-4.15 (br q, 2H), 3.42-3.75 (br q, 2H), 2.24-2.36 (br m, 4H), 1.05-1.60 (br m, 16H) 0.91-0.82 (br t, 6H).

**Conversion reaction towards the conjugated polymer**

The precursor polymer **8a** (**8b** or **8c**) (300 mg) was dissolved in ortho-dichlorobenzene (15 ml) and refluxed for 12 hours. Then, the solvent was evaporated and the slurry obtained was precipitated in methanol. The precipitate was filtered off and washed several times with methanol. The conjugated polymer was obtained as a deep blue/purple powder with a golden luster.

**9a**: 570 ≤ $\lambda_{max}$ ≤621 nm; $M_w$ = 30000 – 100000 g/mol; $^1$H NMR ($CDCl_3$): 6.71-6.39 (br s, 1H), 5.24-5.60 (br s, 1H), 2.20-2.40 (1H), 1.01-1.55 (br m, 8H), 0.91-0.82 (br t, 3H).

**9b**: 580 ≤ $\lambda_{max}$ ≤593 nm; $M_w$ = 60000 – 80 000 g/mol; $^1$H NMR ($CDCl_3$): 6.78-6.34 (br s, 1H), 5.40-5.21 (br s, 1H), 2.15-2.42 (br d, 1H), 1.00-1.60 (br m, 18H), 0.91-0.83 (br t, 3H).

**9c**: 600 ≤ $\lambda_{max}$ ≤628 nm; $M_w$ = 15000 – 80000 g/mol; 5.25-5.60 (br s, 1H), 2.24-2.36 (br m, 2H), 1.05-1.60 (br m, 16H) 0.91-0.82 (br t, 6H).

## 3.7 References


1. A. Zen, J. Pflaum, S. Hirschmann, W. Zhuang, F. Jaiser, U. Asawapirom, J. P. Rabe, U. Scherf, and D. Neher, *Adv. Funct. Mater.*, 14, (8), **2004**, 757.
2. B. L. Lucht, W. B. Euler, O. J. Gregory, *Polymer Preprints*, 43, (1), **2002**, 59.
3. C. Roux, J.-Y. Bergeron, M. Leclerc, *Macromolecular Chemistry and Physics,* 194, (3) **2003**, 869
4. E. H. Elandaloussi, P. Frere, P. Richomme, Orduna, J. Garin, J. Roncali, *J. Am. Chem. Soc.*,119, **1997**, 10774
5. I. Jestin, P. Frère, P. Blanchard, J. Roncali, *Angew. Chem. Int. Ed.*, 37, (7), **1998**, 942
6. I. Jestin, P. Frère, N. Mercier, E. Levillain, D. Stievenard, J. Roncali, *J. Am. Chem. Soc.*, 120, **1998**, 8150
7. J. Roncali, *Accounts of Chemical Research*, 33, **2000**, 147
8. A. P. Smith, R.R. Smith, B. E. Taylor, and M. F. Durstock, *Chem. Mater.,* 16, **2004**, 4687
9. R. S. Loewe, R. D. McCullough, *Chem. Mater.*, 12, **2000**, 3214
10. K. Tamao, K. Sumitani, Y. Kiso, M. Zembayashi, A. Fujioka, S. Kodama, I. Nakajima, A. Minato, and M. Kumada, *Bull. Chem. Soc. of Japan*, 49, (7), **1976**, 1958
11. K. Tamao, K. Sumitani, M. Kumada, *J. of Am. Chem. Soc.*, 94, (12), **1972**, 4374
12. Y. S. Seo, H. S. Yun, K. Park, *Bull. Korean Chem. Soc.*, 20, (11), **1999**, 1345
13. J. W. Dankwardt, *Angew. Chem. Int. Ed.*, 43, **2004**, 2428

14. P. Bauerle, F. Pfau, H. Schlupp, F. Wurthner, K. U. Gaudl, M. Balparda Caro, P. Fisher, *J. Chem. Soc. Perkin Trans.*, 2, **1993**, 489

15. A. Donat-Bouillud, I. Lèvesque, Y. Tao, M. D'Iorio, *Chem. Mater.*, 12, **2000**, 1931

16. J. Frey, A. D. Bond, A. B. Holmes, Chem. Comm., **2002**, 2424

17. F. Banishoeib, S. Fourier, T.J.Cleij, L. Lutsen, D. Vanderzande, *Eur. Phys. J. Appl. Phys.*, 37, **2007**, 237

18. F. Banishoeib, P. Adriaensens, S. Berson, S. Guillerez, O. Douheret, J. Manca, S. Fourier, T.J. Cleij, L. Lutsen, D. Vanderzande, *Solar Energy Materials & Solar Cells,* 91, **2007**, 1026

19. L. Hontis, V. Vrindts, D. Vanderzande, and L. Lutsen, *Macromolecules*, 36, **2003**, 3035.

20. a) L. Hontis, V. Vrindts, L. Lutsen, D. Vanderzande, and J. Gelan, *Polymer*, 42, (13), **2001**, 5793; b) D. J. M. Vanderzande, L. Hontis, A. Palmaerts, D. Van Den Berghe, J. Wouters, L. Lutsen and T. Cleij, Proc. of SPIE Vol. 5937, **2005**, 59370Q

21. H. Xie, S. O'Dwyer, J. Corish, D. A. Morton-Blake, *Synth. Met.*, 122, **2001**, 287

22. S.-A. Chen, and J.-M. Ni, *Macromolecules*, 25, **1992**, 6081

23. Y. Wang, N. Archambault, A. Marold, L. Weng, B. L. Lucht, and W. B. Euler, *Macromolecules*, 37, **2004**, 5415

24. T. Johansson, W. Mammo, M. Svensson, M. R. Andersson and O. Inganäs, *J. Mater. Chem.*, 13, **2003**, 1316

25. M. Skompska and A. Szkurlat, *Electrochim. Acta*, 46, **2001**, 4007

26. A. R. Hillman, I. Efimov and M. Skompska, *Faraday Discuss.*, 121, **2002**, 423

27. J. Liu, T.-F. Guo, Y. Shi and Y. Yang, *J. Appl. Phys.*, 89, **2001**, 3668

28. C. Yang, S. Holdcroft, *Synth. Met.*, 84, **1997**, 563

29. C.Y. Yang, C. Soci, D. Moses and A.J. Heeger, *Synth. Met.*, 155, (3), **2005**, 639

30. T. Yamamoto, D. Komarudin, M. Arai, B. L. Lee, H. Suganuma, N. Asakawa, Y. Inoue, K. Kubota, S. Sasaki, T. Fukuda, H. Matsuda, *J. Am. Chem. Soc.*, 120, **1998**, 2047

31. H. Friebolin, Basic One- and Two-Dimensional NMR Spectroscopy, (1991), Weinheim, 149.

32. R. A. Komoroski, High Resolution NMR spectroscopy of Synthetic Polymers in Bulk (1986) VCH: Florida.

33. K. Schmidt-Rohr; H. Spiess, W. Multidimensional solid-state NMR and polymers (1996) Academic Press, 402

34. V. D. Fedotov; H. Schneider, Structure and dynamics of bulk polymers by NMR-methods Springer-Verlag, Berlin (1989)

35. Yuhei Shimoyama, *Thin Solid Film*, 464, **2004**, 403

36. R. Azumi, E. Mena-Osteritz, R. Boese, J. Benet-Buchholz and P. Bäuerle, *J. Mater. Chem.*, 16, **2006**, 728

37. S. Malik, A. K. Nandi, *J. polym. sci., Part B, Polym. phys.*, 40, (18), **2002**, 2073

38. S. Malik, A. K. Nandi, *J. Appl. Polym. Sci.*, 103, (4), **2006**, 2528

39. M. Al-Ibrahim, H.-K. Roth, M. Schroedner, A. Konkin, U. Zhokhavets, G. Gobsch, P. Scharff and S. Sensfuss, *Organic Electronics*, 6, (2), **2005**, 65

40. E. Mena-Osteritz, A. Meyer, B. M. W. Langeveld-Voss, R. A. J. Janssen, E. W. Meijer, and P. Bauerle, Angew. Chem. Int. Ed., 39, (15), 2000, 2679

# Chapter Four

# The polar derivatives of Poly(2,5-thienylene vinylene) PTVs

## *4.1 Introduction*

Polythiophene, synthesised with linkages through the 2 and 5 positions, has a symmetric repeat unit and is a highly crystalline polymer. Due to the rigidity of the backbone, and to the strong inter-chain interactive forces, polythiophene is completely insoluble and infusible. On the other hand, its substituted derivatives have attracted significant attention because of their resulting solution and melt processability when flexible side groups are introduced onto the thiophene ring.

Polar conjugated polymers have become a very interesting topic in the last years. Various side groups have been added to the polymer backbone in order to make them more soluble and processable[1-4]. The capability to further fine tune the solubility properties of these polymers is important in order to make them soluble in environmentally friendly solvents like alcohols and/or water. It has been proved that, for example, the use of alkoxy-substituted thiophenes is advantageous over the alkyl derivatives, because the oxygen atom is sterically less demanding than the methylene group[5]. In addition, the oxygen directly attached to the thiophene ring lowers the oxidation potential of the monomer and of the polymer. In general, it can be stated that, the introduction of strong electron-donating groups, lowers the HOMO-LUMO gap with respect to unsubstituted or alkyl substituted PTVs[6-12].

Since the observation that doped and conductive thin films of alkoxy substituted poly(thienylene vinylene)s exhibit a high degree of transparency in the visible region, attempts have been made to develop polymerisation routes to prepare them and related processable polymers with high molecular masses[13]. These systems have shown low ionization potentials and good p-

type doped stabilities. With the appropriate improvements in mechanical properties, processability and conductivity, it is quite conceivable that this class of conductive polymers could function as replacement for ITO transparent electrodes providing access to flexible LEDs, LCDs, transparent EMI shields etc. Many attempts to prepare such electron rich polymers by the precursor route using the bis(sulphoniummethyl) or the bis(chloromethyl) monomers have not been generally successful because of the high reactivity/instability of the corresponding monomers[14].

As part of our work towards new functionalised, polar PTV derivatives, we are interested in the preparation of PTV-type polymers bearing alkoxy and triethylene glycol derived side chain.

## *4.2 Polar PTV bearing alkoxy and triethylene glycol side chains*

### 4.2.1 The 3,4 di-hexyloxy-2,5-thienylenevinylene derivatives

In this section we will report on a new type of thienylene vinylene derivatives consisting of a 3,4-dialkoxy substituted thienylene vinylene. Since the 3,4-dialkoxy derivatives (**Scheme 4.1**) are more electron rich than the unsubstituted thienylene vinylene, they are expected to show a narrow energy gap between the highest occupied molecular orbital (HOMO) and lowest unoccupied molecular orbital (LUMO). Furthermore, the S-O intramolecular interaction may contribute to reduce the HOMO-LUMO energy gap. As matter of fact, fine tuning of the HOMO and LUMO energies of molecular wires is essential for efficient electron transport over a long distance.

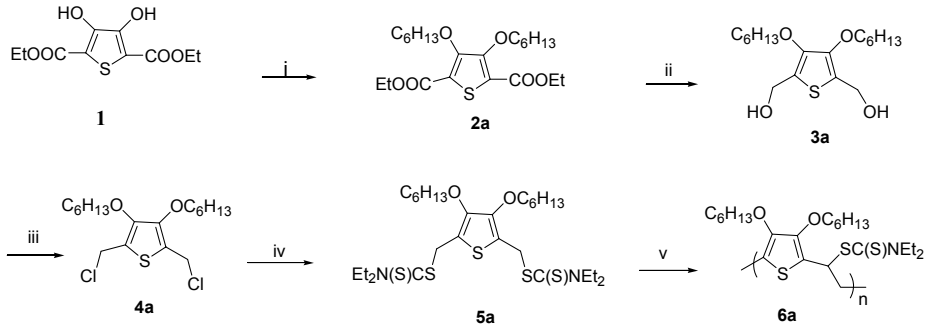


***Scheme 4.1*** *Synthesis of 3,4-di-hexyloxy-2,5-thienylenevinylene 6a: i) $K_2CO_3$/bromohexane; ii) $LiAlH_4$/THF; iii) $SOCl_2$/THF iv) $NaSC(S)NEt_2.3H_2O$; v) base/ THF*

The 3,4-dihydroxythiophene (**1**) was prepared by the Hinsberg[15,16] method using thiodiglycolic acid and diethyl oxalate according to the reaction pathway reported in **Scheme 4.2**.

The mechanism of the reaction consists of a Claisen type condensation between a 1,2-dicarbonyl compound and a thiodiacetate in order to give the thiophene ring in a quantitative yield.

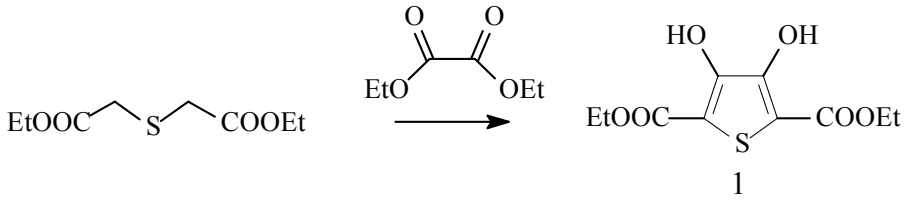


***Scheme 4.2*** *Synthesis of 2,5-dicarboethoxy-3,4-dihydroxythiophene*

The alkylation of the di-hydroxy compound **1** was carried out in basic environment in the presence of a large excess of alkyl-bromide[6]. Since the reaction proceeds *via* a $S_N2$ mechanism, the chosen halide should be a methyl halide or a primary halide. The yield of the reaction showed to be around 80 %.

The following reaction steps: the reduction of the ester into a di-alcohol (**3a**), the chlorination (**4a**), and the formation of the dithiocarbamate monomer (**5a**) were carried out according the same procedures described for

the synthesis of the plain PTV (chapter 2) and for the alkyl substituted PTV derivatives (chapter 3).

It is noteworthy that the presence of the oxygen directly attached to the thiophene ring makes the dichloromethyl derivative (**4a**) more unstable. Because of the electron-donating character of the oxygen atom, the chlorination of the alcohol **3a** is then the critical step in the synthetic pathway earlier described. As a result, it is very important to convert directly the chloromethyl derivative (**4a**) *in situ* into the dithiocarbamate monomer **5a** to avoid degradation. Indeed the overall yield for the formation of the dithiocarbamate monomer (**5a**) starting from the di-alcohol (**3a**) is attested to be around 20 %.

### 4.2.2 The 2,5-dicarboethoxy-3,4-Bis-{2-[2-(2-methoxy-ethoxy)-ethoxy]-ethoxy}-thiophene

The synthesis of thiophene capped oligo(ethylene oxide) was carried out according the same procedure used for the synthesis of the di-alkoxy substituted thienylene vinylene (**Scheme 4.3**).

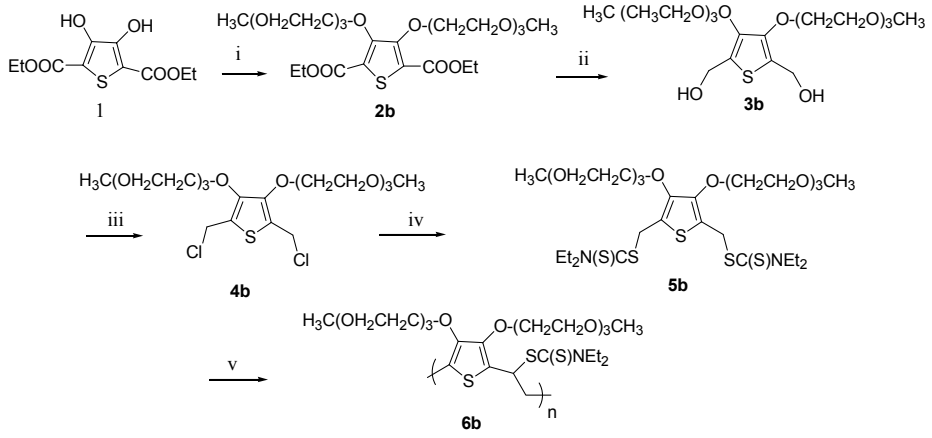


***Scheme 4.3*** *Synthesis of 3,4-Bis-{2-[2-(2-methoxy-ethoxy)-ethoxy]-ethoxy}-thiophene 6b: i) $K_2CO_3$/ bromo-triethylene glycol; ii) $LiAlH_4$/THF; iii) $SOCl_2$/THF iv) $NaSC(S)NEt_2.3H_2O$; v) base/ THF*

The difference here, was the introduction of an ethylene glycol side chain instead of an alkoxy one (step 1 of the synthetic **Scheme 3.3**).
The oligo(ethylene glycol) side chains were synthesised according the **Scheme 4.4** hereafter reported[17, 18].

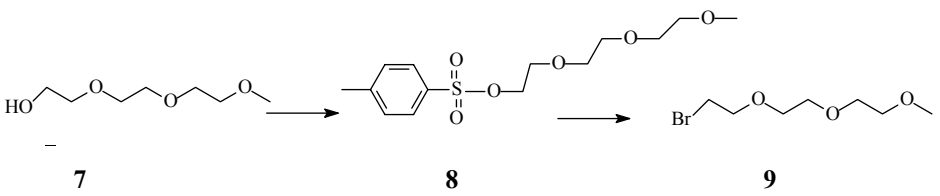


**7** **8** **9**

***Scheme 4.4*** *Synthesis of oligo(ethylene glycol) of formula 9*

It is known that, alcohols do not undergo the same $S_N2$ reactions commonly observed with alkyl halides. This is the reason why it was decided to convert the alcohol into a better leaving group. In this regard, the synthesis of tosylate compounds is particularly useful. Indeed, they may be used in substitution reactions with a wide variety of nucleophiles. In the first reaction step, the glycol **7** was tosylated in the presence of p-toluensulphonyl chloride. The reaction step proceeds quantitatively. The so formed tosylate (**8**) will react with nucleophiles in the same way as alkyl halides do. Although tosyl groups are good leaving groups, it was decided to convert the compound **8** into a bromo derivative according to standard literature procedures for the synthesis of this kind of compounds. So, the tosyl-ethylene glycol was brominated with lithium bromide yielding **9** almost quantitatively.
Because ethylene glycols are very hygroscopic compounds, it was very difficult to extract them from the water layer during the work up. This characteristic behaviour explains the lower yields observed in comparison to those obtained for the synthesis of the alkoxy derivatives, although the reactions were carried out using the same protocol.

### 4.2.3 Polymerisation

The monomers **5a** (**Scheme 4.1**) and **5b** (**Scheme 4.3**) were freeze dried before being used in the polymerisation process because of their high hygroscopic behaviour.

The polymerisation reactions were performed in a three-necked flask. The monomer was dissolved in dried THF and degassed by passing through a continuous stream of nitrogen. The solution of base (1 M LHMDS solution in THF/n-hexane or phosphazene base $P_2$-t-Bu 2.0 M solution in THF) was added in one go through a septum. Then, the reaction was stirred at a given temperature for 90 minutes under nitrogen atmosphere. Afterwards, the mixture was poured out in ice water and extracted with chloroform; finally the combined organic layers were concentrated with the use of a rotary evaporator. The crude product was then, dissolved again in chloroform and precipitated in a non-solvent (i.e. methanol) at 0 °C. The polymers so obtained were collected and dried in vacuo.

The polymerisation results are presented in **Table 4.1**. The molecular weights were determined by SEC using THF as eluent.

| Polymer | Entry | # eq. LHMDS | $M_w$ g/mol | Temp. (°C) | [monomer] (M) |
|---|---|---|---|---|---|
| **6a** | 1 | 2.0 | / | 0 | 0.4 |
| | 2 | 2.0 | 29900 | R.T. | 0.4 |
| **6b** | 3 | 2.0 | / | 0 | 0.2 |
| | 4 | 2.0 | / | 0 | 0.4 |
| | 5 | 3.0 | / | 0 | 0.4 |

***Table 4.1*** *Polymerisation results for 6a and 6b*

The polymerisation reactions were carried out in duplo experiments to check the reproducibility. They did not lead to polymers although an excess of base was used. Only in the case of **5a** by the use of an excess of base (*i.e.* 2.0 eq) and at R.T. rather oligomers with $M_w$ ~ 30000 g/mol, (PD = 4.9) were obtained in a yield of 20 %. Increasing the monomer concentration **5b** in the reaction mixture did also not lead to the formation of a polymer fraction.

The residual fractions of the polymerisation were also analysed in order to check the presence of products due to possible side reactions. The analyses showed just the presence of the unreacted monomer **5a** or **5b**. This fact, in a certain way, points to the impossibility of the base to abstract the proton and carry on to the formation of the true monomer.

The reason of the failure of the expected polymerisation reactions might be found in the increased electron donor property of the side chain of the monomers. This implies decreased acidity of the proton that needs to be extracted by the base as compared to PTVs with an alkyl side chain or compared to a non substituted monomer. It is then necessary to use a much stronger base in order to achieve the formation of the true monomer, the p-quinodimethane system in an efficient way.

Furthermore, a double substitution in the position 3 and 4 of the thiophene ring may induce higher steric hindrance that can limit the accessibility of the base.

In the case of monomer **5b** potential additional effects of glycol side chain can be considered. It is well known that PEO solvates a wide variety of metal ions ranging from alkali metal to transition metals forming PEO-salt complexes. The complexation occurs primarily by the coordination of the backbone ether oxygen atoms to the metal ions. It seems also that there is a rapid exchange occurring between the complexed and un-complexed states[19-21]. The formation of cross-linked forms due to the association of the PEO tails with the $Li^+$ ions of the base has been reported in literature as well. It has also been proved that, this ion association, increases with the total salt concentration content.

All the afore mentioned factors, may have a negative effect on the polymerisation reactions thus competing and inhibiting them.

With the aim of finding a more appropriate base, polymerisation tests were carried out in the presence of 1-tert-butyl-2,2,4,4,4-pentakis(dimethylamino)-2$\Lambda^5$,4$\Lambda^5$-catenadi(phosphazene) also called phosphazene base $P_2$-t-Bu, as 2.0 M solution in THF. This is an extremely strong and hindered neutral nitrogen base (**Scheme 4.5**). Indeed, it is about

$10^9$ times more basic than DBU [$pk_a$ (DMSO) 21.45]. It is stable to hydrolysis and unaffected by alkylating agents and, it is also highly selective[22, 23].

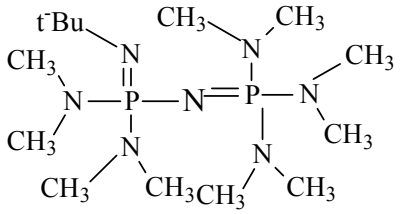

***Scheme 4.5*** *Structure of the phosphazene base*

Attempts were done to polymerise the di-alkoxy thienylene vinylene derivatives but, unfortunately without any success (**Table 4.2**).

| Polymer | Entry | # eq. $P_2$-t-Bu | $M_w$ g/mol (THF) | Temp. (°C) |
|---|---|---|---|---|
| **6a** | 6 | 1.0 | / | 0 |
| | 7 | 2.0 | / | 0 |

***Table 4.2*** *Polymerisation results for 6a with a phosphazene base*

The lack of an appropriate base for the polymerisation reaction did not allow for the synthesis of the polar derivatives of PTV *via* the dithiocarbamate precursor route. Further investigation on the polymerisation mechanism might be necessary.

## *4.3 Synthesis of the ethyl alkyl ether derivatives of PTV*

It is known that the introduction of an ether function at a "phenolic" position of the thiophene ring leads to an increase of the monomer oxidation potential and to a decrease of the stability of the resulting polymer films. Conversely, the use of two or three $CH_2$ groups as spacer allows the synthesis

of highly stable polymers having one or more ether functions[24-26]. It has also to be considered that the location and the number of oxygen atoms in the side chain have significant effects on the optical and electrical properties of the substituted polythiophenes[27]. More specifically, depending on its position in the side chain, an ether function can diversely affect the electronic density in the thiophene ring and thus the oxidation potential of the monomer.

Since the impossibility of synthesising the 3,4-polar substituted PTV polymers, the synthesis of a mono substituted thiophene with an ethyl alkyl ether function has been tried. This approach was used firstly to reduce the steric hindrance around the thiophene ring, secondly to retain the acidity of the proton that has to be abstracted, and thirdly to move away the oxygen from the thiophene ring introducing a spacer for increasing the stability of the monomer.

### 4.3.1 The 3-(3,6,9-trioxy decyl)-2,5-thienylenevinylene

The introduction of ether functions on monomers can be generally performed using different conditions for the Williamson ether synthesis depending on the number of $CH_2$ groups to be introduced between the thiophene ring and the first oxygen atom. The study of such structural modifications is important for the evaluation of the effects of an oxygen atom on chain substituents (i.e. electron withdrawing and hydrophilic effects). The synthesis of the oxyalkyl ether was done using sodium hydride and the appropriate alkyl halide (usually a bromide) in THF (**Scheme 4.6**).

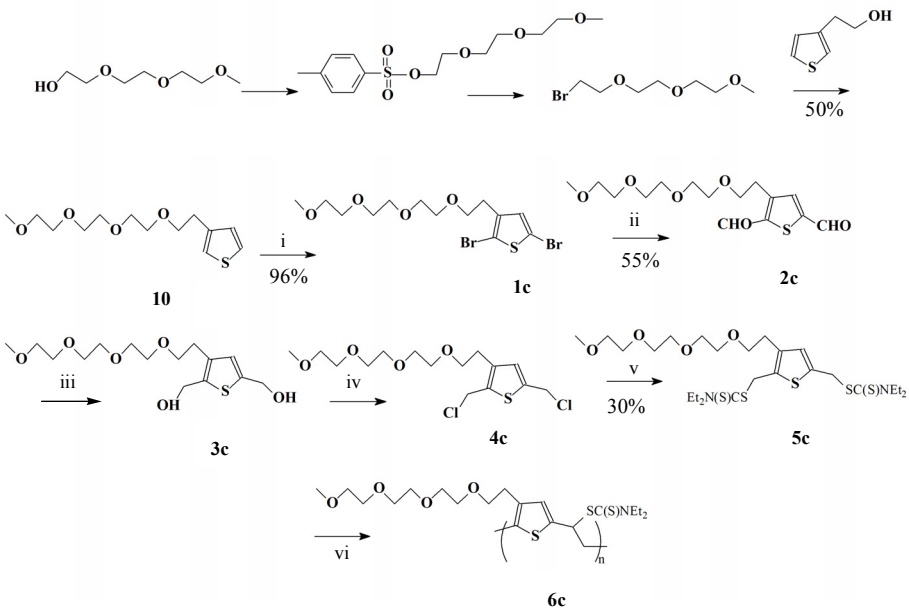


***Scheme 4.6*** *Synthesis of Ethyl alkyl ether derivatives of PTV 6c: : i) NBS/DMF;ii) BuLi/$Et_2O$, formylpiperydine; iii) $LiAlH_4$/THF; iv) $SOCl_2$/THF v) $NaSC(S)NEt_2.3H_2O$; vi) base/ THF*

The synthesis of the bromide tri-ethylenglycol derivative, **9,** has been already discussed in **Scheme 4.4**.

The 3-ethanol-thiophene undergoes a coupling reaction with the ethylene glycol chain in basic environment. The fact that we are not in the presence of a "phenolic" –OH group as in the previous experiments (**Scheme 4.3**), requests a much stronger base compared to the potassium carbonate used earlier. A Williamson ether synthesis involves an $S_N2$ reaction where a halogen group is replaced by an alkoxide ion, which can itself be prepared by a reaction of the alcohol with an active metal such as sodium metal or its hydride (i.e. NaH). The resultant alkoxide salt reacts then with the alkyl halide (which must be a primary halide) to produce an ether via the $S_N2$ mechanism. The Williamson ether synthesis was performed in dry conditions with a yield of around 50 %. All the other steps were carried out as reported in the previous paragraphs of this chapter. The reaction steps presented in **Scheme 4.6** proceeded with good yields.

### 4.3.2 Polymerisation

The monomer **5c** was previously distilled in order to increase its purity and, afterwards, freeze dried since it is hygroscopic and any trace of water would interfere with the polymerisation reaction.
The polymerisation reactions were performed in a three-necked flask. The monomer was dissolved in dried THF and degassed by passing through a continuous stream of nitrogen. The solution of base (1 M LHMDS solution in THF/n-hexane) was added in one go through a septum. Then, the reaction was stirred at a given temperature for 90 minutes under nitrogen atmosphere. The mixture was subsequently poured out in ice water. After performing an extraction with chloroform, the combined organic layers were concentrated in vacuo. The crude product was dissolved again in chloroform, precipitated in a non-solvent at 0 °C, and then collected and dried in vacuo. The polymerisation results are presented in **Table 4.3**. The molecular weights were determined by SEC with THF as eluent.

| Polymer | Entry | # eq. LHMDS | $M_w$ g/mol | PD | Temp. (°C) |
|---|---|---|---|---|---|
| **6c** | 1 | 2.0 | 2800 | 1.3 | 0 |
| | 2 | 2.0 | 2300 | 1.8 | R.T. |

***Table 4.3*** *Polymerisation results for 5c*

Looking at the $M_w$ values depicted in the table, it can be noticed that just oligomers were obtained. In comparison with the disubstituted derivatives, **5a** and **5b**, here the reactivity of the monomer **5c** towards the polymerisation reaction seems indeed restored. TLC analyses of the rest fractions showed the complete consumption of the monomer within the reaction time applied (1.5 hours). The formation of oligomers may be due to the occurrence of an anionic mechanism. Earlier work has shown that typically in case of a switch from a radical to an anionic mechanism a strong reduction of the $M_w$ obtained is observed.

Seemingly, the presence of the PEO side chain seems to have a strong influence on the polymerisation mechanism occurring in the dithiocarbamate route compared to similar experiments as for example for the synthesis toward Poly(3-Hexyl Thienylene Vinylene).

Proton NMR analysis showed only the presence of these oligomers, as clearly visible in **Figure 4.1**.

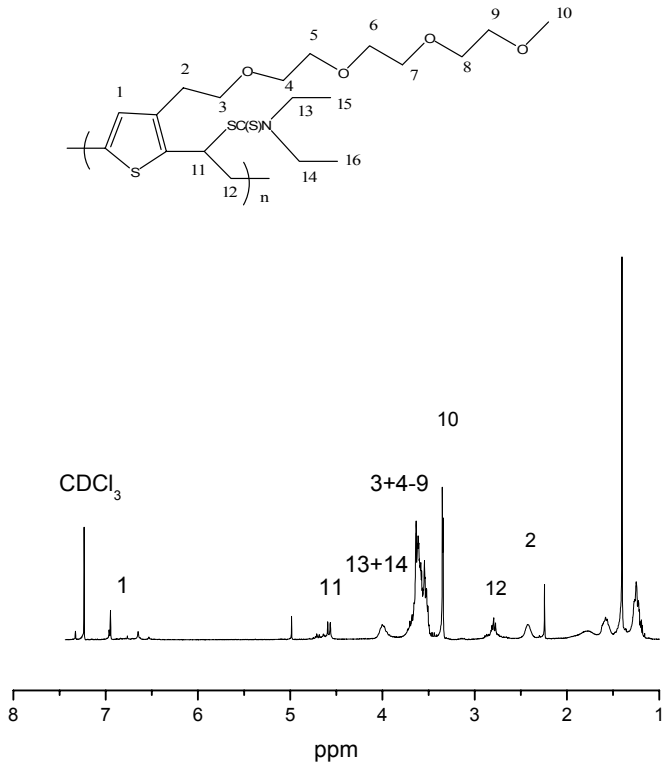


***Figure 4.1*** *$^1$H-NMR of 6c in $CDCl_3$*

The reason why a PEO side chain can favour the anionic polymerisation mechanism is still not totally clear.

Possibly, complexation reactions between the ethylene glycol side chain and the $Li^+$ ions of the base may be related to the observed results.

## *4.4 Characterisation*

### 4.4.1 Structural Characterisation of 3,4-di alkoxy PTV

As an example the NMR spectrum of **7a** is also reported in **Figure 4.2**.

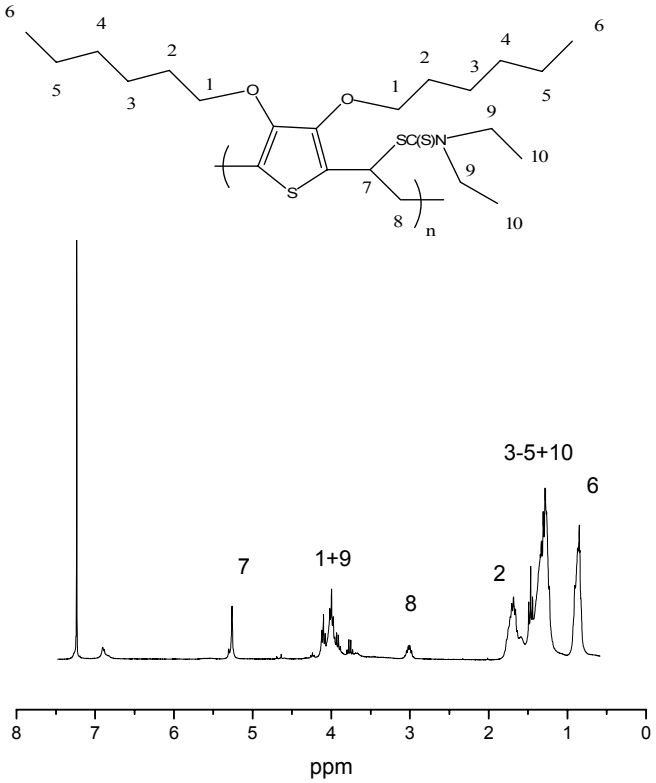


***Figure 4.2*** *$^1$H-NMR of 6a in $CDCl_3$*

The assignment of the proton signals was achieved by comparison with the NMR data of the Poly(3-alkyl)TVs described in chapter 3. The chemical shifts are reported in the experimental section.

### 4.4.2 Conversion towards the conjugated polymer

The precursor polymer **6a** (entry 2 **Table 4.1**) was dissolved in 1,2-dichlorobenzene and heated at a reflux temperature of 185 °C for 5 hours.

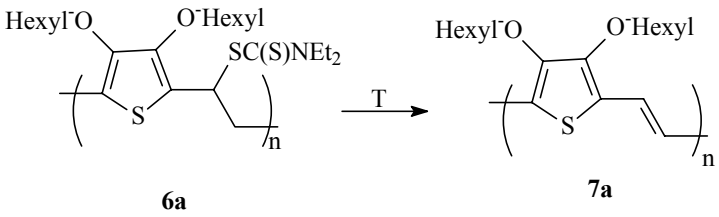


**6a** **7a**

***Scheme 4.7*** *Conversion reaction of precursor polymer 6a towards 7a*

The colour of the solution turned from orange into deep blue: after precipitation in cold methanol a very fine blue powder corresponding to the conjugated material was obtained (**7a**; **Scheme 4.7**).

UV-Vis spectroscopy measurements were done to evaluate the thermal elimination of the dithiocarbamate groups towards the conjugated systems and to have more information about the quality of the conjugated system.

An *in-situ* UV-Vis and FT-I.R. study was carried out in order to deduct the conversion reaction protocol of the precursor materials. A solution of precursor in chloroform was casted on a quartz disk (or a NaCl disk, respectively) and consequently placed in an oven continuously purged with nitrogen. The oven was directly connected to the apparatus for the spectroscopic measurements.

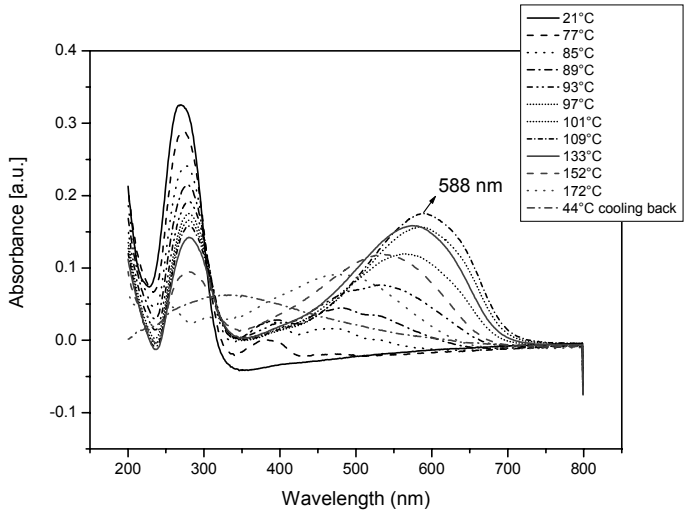


***Figure 4.3*** *UV-Vis. spectra at different temperature for 6a*

The $\lambda_{max}$ value observed (**Figure 4.3**) is quite high (i.e. 588 nm) although we are in the presence of rather oligomers. Apparently, a good ratio of effective conjugated length and low defect content was achieved for this material.
As shown in the UV-Vis spectrum at R.T. in thin film (**Figure 4.4**) of the thermally converted polymer, in refluxing o-dichlorobenzene, no increase of the $\lambda_{max}$ value was observed.

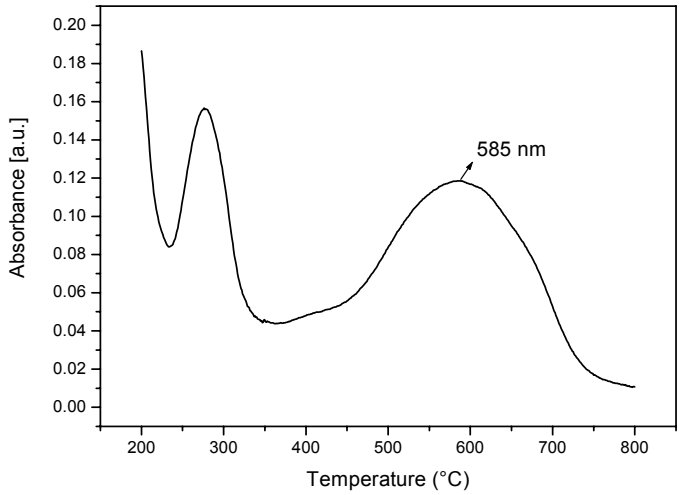


***Figure 4.4*** *UV-Vis spectrum at R.T. in film after conversion*

The absorption profile at fixed wavelength as a function of temperature (**Figure 4.5**) shows that the formation of the double bond starts already at 80 °C and is complete at 100 °C for the heating program used. This is quite low compared with the conversion temperature we observed for example for Poly(3-hexylTV) under the same heating conditions (start at 115 °C). Possibly this point to a substituent effect on the thermal elimination reaction of dithiocarbamate groups. Seemingly, electron donor substituents would facilitate elimination. This temperature range is much lower as compared with alkyl derivatives and plain PTV. This difference is maybe due to substitution effect.

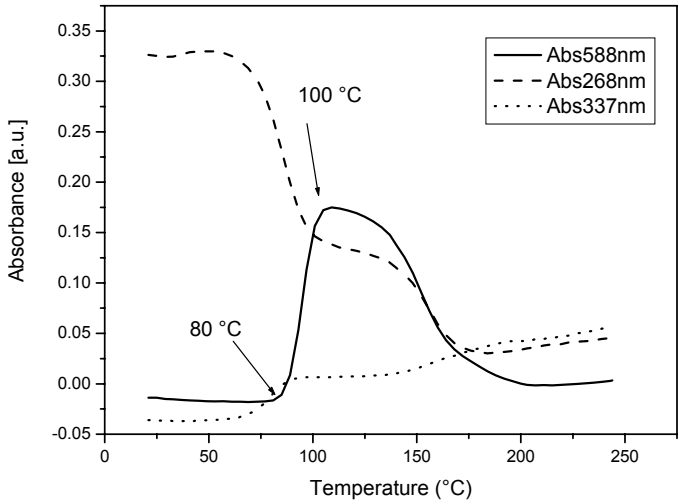


***Figure 4.5*** *UV-Vis profile for 6a*

Beyond 140 °C, a decrease of the absorption as temperature increases is observed. This may point to the degradation of the polymer **6a.**

An *in situ* FT-I.R. (**Figure 4.6**) measurement was also performed in order to evaluate the formation of the conjugated system by following the characteristic absorption band of the double bond.

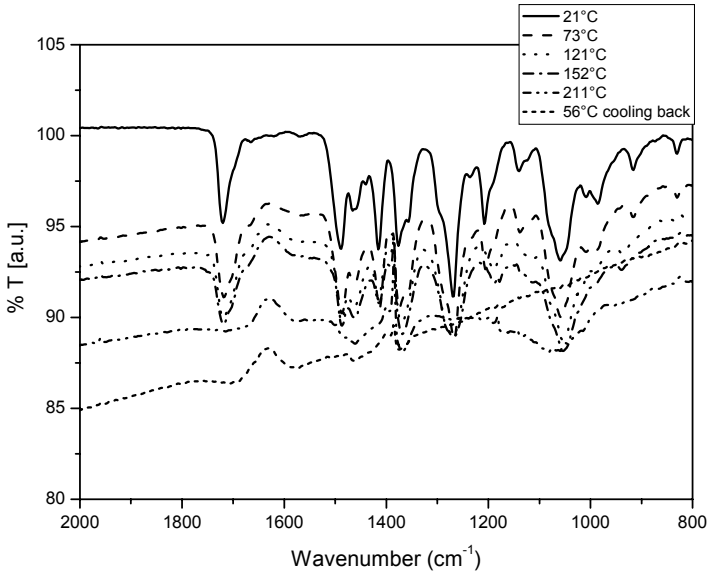


***Figure 4.6*** *FT-I.R. spectra at different temperature for 6a*

The formation of the double bond can be seen by the appearance of a peak at 938 $cm^{-1}$. The disappearance of the dithiocarbamate groups is also observed at the same time.

The presence of aromatic ethers is confirmed by the peak at 1055 $cm^{-1}$ which corresponds to the symmetric stretching C-O-C and by the presence of a peak at 1270 $cm^{-1}$ which corresponds to the unsymmetrical stretching C-O-C.

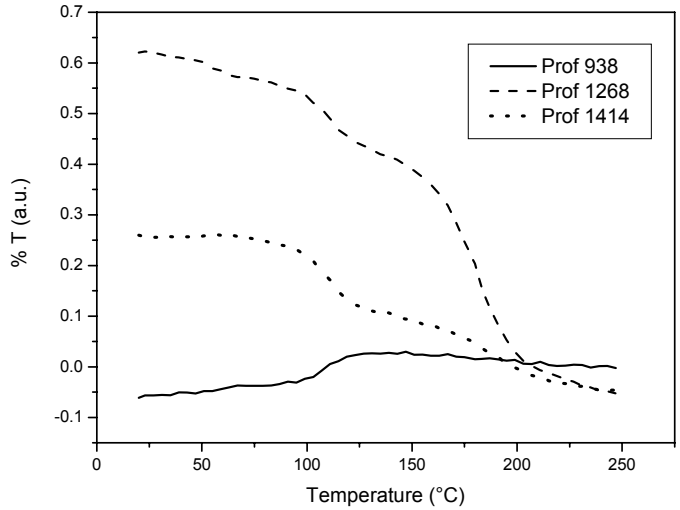


***Figure 4.7*** *FT-I.R. profile for 6a*

The formation of the double bond can be observed more clearly in the FT-I.R. profile (**Figure 4.7**).

## *4.5 Conclusions*

In this chapter we have tried to introduce polar side chains on the thiophene ring. The presence of these chains played a significant role in the polymerisation of those derivatives *via* the dithiocarbamate route.

It was observed that the formation of the quinodimethane system, for the disubstituted alkoxy derivatives seems to be inhibited or substantially suppressed, leading only to rather oligomers, in the best case.

On the other hand, for the monosubstituted alkyl derivative, the reactivity seems restored. Indeed, all the monomer was consumed. Again only oligomers could be obtained. In this case, it seems that the PEO side chain plays a crucial role in the sense that an anionic polymerisation mechanism seems to be exclusive. The reason of such behaviour is still under investigation.

In this regard, the oligomers can be used as model compounds for a better understanding of the polymerisation mechanism. Further investigations towards the polymerisation conditions should be planned. Certainly, the dithiocarbamate precursor route offers the possibility of making electron-rich conjugated polymers in an efficient way and with improved properties compared to the already existing precursor routes. Surprising results or even apparently contradictory results should not be interpreted as a failure but rather taken into account as a consequence of the novelty of the route. A further exploration of the chemistry behind this route and especially gaining more insight in the polymerisation mechanism at hand is indispensable.

## *4.6 Experimental part*

**Materials:** All solvents used in the synthesis were distilled before use. Tetrahydrofuran (THF) was refluxed under nitrogen with sodium metal and benzophenone until a blue colour persisted and was then distilled. All the commercially available products were purchased from Acros or Aldrich.

**Characterisation:** $^{1}H$ NMR spectra were taken on a Varian Inova 300 spectrometer. For all synthesized compounds, spectra were recorded in deuterated chloroform; the chemical shift at 7.24 ppm (relatively to TMS) was used as reference.

Average molecular weights and molecular weight distributions were determined relative to polystyrene standards (Polymer Labs) by Size Exclusion Chromatography (SEC). Chromatograms were recorded on a Spectra series P100 (Spectra Physics) equipped with two MIXED-B columns (10 μm, 2 x 30 cm, Polymer Labs) and a relative index (RI) detector (Shodex) at 70°C. A THF solution of oxalic acid (1.1 $10^{-3}$ M) was used as the eluent at a flow rate of 1.0 ml/min. Toluene was used as flow rate marker.

GC/MS analyses were carried out at the TSQ – 70 and Voyager mass – spectrometers (Thermoquest), capillary column: Chrompack Cpsil5CB or Cpsil8CB.

Fourier Transform Infra Red spectroscopy (FT-IR) was performed on a Perkin Elmer Spectrum One FT-IR spectrometer (nominal resolution 4 $cm^{-1}$, summation of 16 scans). Samples for the FT-IR characterisation were prepared by spin-coating the precursor polymer from a chloroform solution (6 mg/ml) onto NaCl disks (diameter 25 mm and thickness 1 mm) at 500 rpm. The NaCl disks were heated in a Harrick oven high temperature cell (purchased from Safir), which was positioned in the beam of the FT-IR to allow *in situ* measurements. The temperature of the sample and the heating source were controlled by a Watlow temperature controller. The heating source was in direct contact with the NaCl disk. Spectra were taken continuously and the heating rate was 2 °C/min from room temperature up

to 350°C. The atmosphere in the temperature cell could be varied from a continuous flow of nitrogen to vacuum (15 mmHg). Timebase software was used to investigate regions of interest.
Ultraviolet visible spectroscopy (UV-VIS) was performed on a VARIAN CARY 500 UV-VIS-NIR spectrophotometer (interval: 1 nm, scan rate: 600 nm/min, continuous run from 200 to 700 nm). The precursor polymer was spin-coated from a chloroform solution (6 mg/ml) onto quartz glass (diameter 25 mm and thickness 3 mm) at 700 rpm. The quartz glass was heated in the same Harrick oven high temperature cell as was used in the FT-IR measurements. The cell was placed in the beam of the UV-Vis spectrophotometer and spectra were taken continuously. The heating rate was 2 °C/min up to 250 °C. All measurements were performed under a continuous flow of nitrogen. Scanning kinetics software was used to investigate the regions of interest.
TLC analyses were made on Merck aluminium sheets, 20 x 20 cm, covered with silica gel 60 $F_{254}$.

**Synthesis of 2,5-dicarboethoxy-3,4-dihydroxythiophene (1).**
The product listed in the title, was prepared according to the Hinsberg method. The pure product was obtained in a quantitative yield. $^1$H NMR ($CDCl_3$): 9.34 (s, 2H), 7.03 (m, 1H), 4.38 (q, 4H), 1.37 (t, 6H).

**Synthesis of 2,5-dicarboethoxy-3,4-dihexyloxythiophene (2a).**
A mixture of 15 g of compound **1**, $K_2CO_3$ (16 g, 2 eq.) and 1-bromohexane (22 eq) was heated at 110-120 °C for 30 h. After cooling down to R.T. the solution was washed with water and the organic phase was dried over $MgSO_4$. Evaporation of the excess of 1-bromohexane gave 82 % of crude product as yellowish oil. $^1$H NMR ($CDCl_3$): 7.3 (dd, 1H), 4.3 (m, 4H), 4.14 (t, 4H), 2.0 (m, 8H), 0.8 (t, 6H); $^{13}$C NMR ($CDCl_3$): 148.2, 112.1, 71.47, 33.5, 25.4, 14.2.

**Synthesis of 2,5-bis(hydroxymethyl)-3,4-dihexyloxythiophene (3a)**
In a three-necked round-bottom flask with dry THF (100 ml, dried over sodium) $LiAlH_4$ (0.27 g, 7.2 mmol) was added under argon atmosphere. This slurry was cooled to 0 °C and the diester **2a** (1.54 g, 4 mmol) was slowly

added *via* a dropping funnel. When the addition was completed a reflux condenser was fitted and the slurry was heated at reflux temperature for 4 hours. After cooling down, the reaction mixture was placed in an ice bath. Then, it was quenched by cautious sequential addition of water, aqueous 15 % NaOH solution, and again water until no more gas development could be detected. This solution was filtered and the residue was extracted with ether. The combined organic layers were dried over $MgSO_4$ and the solvent was evaporated under reduced pressure. The compound **3a** was obtained as orange oil (50 %). $^1$H NMR ($CDCl_3$): 7.3 (dd, 1H), 4.6 (s, 4H), 3.94 (t, 4H), 2.03 (s, 2H), 1.5 (q, 4H) 1.2 (m, 8H), 0.8 (t, 6H).

**Synthesis of 2,5-bis(chloromethyl)- 3,4-dihexyloxythiophene (4a)**

To a cooled (0 °C), stirred solution of diol **3a** (0.6 g, 1.7 mmol) in THF (20 ml) was slowly added a solution of $SOCl_2$ (0.3 ml, 4.3 mmol) in THF (5 ml). The temperature of the reaction mixture was allowed to increase to room temperature under continuous stirring for 1 hour. Then, the mixture was cooled down again at 0 °C and a saturated sodium carbonate solution was added dropwise until neutral. The mixture was extracted with ether and dried over $MgSO_4$. The solvent was evaporated and the highly reactive dichloride **4a** was obtained as orange oil. The dichloride was used as it was in the following reaction step.

**Thiophene-2,5-diylbismethylene N,N-diethyl dithiocarbamate 3,4-dihexyloxythiophene (5a)**

To a solution of bis-chloromethyl (0.64g, 1.7 mmol) **4a** in ethanol (10 ml), sodium diethyldithiocarbamate trihydrate (or diethyldithiocarbamic acid sodium salt trihydrate) (1.53 g, 7 mmol) was added as a solid. The mixture was stirred at ambient temperature overnight. Then, water was added and the desired monomer was extracted with ether and, dried over $MgSO_4$. Evaporation of the solvent followed by purification via column chromatography yielded the pure product as an orange oil. $^1$H NMR ($CDCl_3$): 4.57 (s, 2H), 4.98 (q, 8H), 3.72 (q, 4H), 1.68 (t, 4H); 1.35 (m, 24H), 0.88 (t, 6H).

**Synthesis of 2,5-dicarboethoxy-3,4-Bis-{2-[2-(2-methoxy-ethoxy)-ethoxy]-ethoxy}-thiophene (2b)**

A mixture of 3 g of compound **1**, $K_2CO_3$ (3.19 g, 2 eq.) and bromo-ethyleneglycol (7.6 eq) was heated at 110-120 °C for 30 h. After cooling down to R.T. the solution was washed with water and evaporation of the excess of the ethyleneglycol gave quantitatively the crude product as orange oil. $^1$H NMR ($CDCl_3$): 4.2 (m, 8H), 3.7 (t, 4H), 3.4 (m, 16H), 3.2 (m, 6H), 1.3 (t, 6H).

**Synthesis of 2,5-bis(hydroxymethyl)- 3,4-Bis-{2-[2-(2-methoxy-ethoxy)-ethoxy]-ethoxy}-thiophene (3b)**

In a three-necked round-bottom flask with dry THF (100 ml, dried over sodium) $LiAlH_4$ (3.92 g, 10 mmol) was added under argon atmosphere. This slurry was cooled to 0 °C and the diester **2b** was slowly added via a dropping funnel. When the addition was completed a reflux condenser was fitted and the slurry was heated at reflux temperature overnight. After cooling down, the reaction mixture was placed in an ice bath. Then, it was quenched by cautious sequential addition of water, aqueous 15 % NaOH solution, and again water until no more gas development could be detected. This solution was filtered and the residue was extracted with ether. The solvent was evaporated under reduced pressure. The compound **3b** was obtained as orange oil (55 %). $^1$H NMR ($CDCl_3$): 3.7 (t, 4H), 3.6 (m, 24H), 3.4 (m, 6H), 1.8 (s, 2H).

**Synthesis of 2,5-bis(chloromethyl)- 3,4-Bis-{2-[2-(2-methoxy-ethoxy)-ethoxy]-ethoxy}-thiophene (4b)**

To a cooled (0 °C), stirred solution of diol **3b** (5 g, 10 mmol) in THF (20 ml) was slowly added a solution of $SOCl_2$ (1.94 ml, 27 mmol) in THF (5 ml). The temperature of the reaction mixture was allowed to increase to room temperature under continuous stirring for 1 hour. Then, the mixture was cooled down again at 0 °C and a saturated sodium carbonate solution was added dropwise until neutral. The mixture was extracted with ether the

solvent was evaporated. The highly reactive dichloride **4b** was obtained as orange oil.

**Thiophene-2,5-diylbismethylene N,N-diethyl dithiocarbamate 3,4-Bis-{2-[2-(2-methoxy-ethoxy)-ethoxy]-ethoxy}-thiophene (5b)**

To a solution of bischloromethyl (5.4g, 11 mmol) **4b** in ethanol (10 ml), sodium diethyldithiocarbamate trihydrate (or diethyldithiocarbamic acid sodium salt trihydrate) (9.62 g, 43 mmol) was added as a solid. The mixture was stirred at ambient temperature overnight. Then, water was added and the desired monomer was extracted with ether. Evaporation of the solvent followed by purification via column chromatography yielded the pure product as an orange oil. $^1$H NMR ($CDCl_3$): 3.56 (m, 36H), 3.35 (s, 6H), 1.19 (t, 12H).

**Synthesis of methoxy tri-ethylene glycol bromide (9)**

A three necked flask equipped with mechanical stirrer, thermometer and nitrogen inlet was charged with the tri-ethylene glycol monomethylether (**7**), p-toluensulphonyl chloride (1.02 eq) and $CH_2Cl_2$. The homogeneous mixture was cooled at -78 °C and KOH (4 eq.) was added portionwise under vigorous stirring while maintaining the reaction temperature below 5 °C. The mixture was stirred at 0 °C for 3 h after which $CH_2Cl_2$ and iced-water were added. The organic phase was separated and the aqueous phase was extracted with $CH_2Cl_2$. The combined organic phase was then washed with water, dried and the solvent evaporated. The reaction was quantitative and the colourless oil so obtained was used as it was in the following step without further purification. A three necked flask equipped with a mechanical stirrer, a reflux condenser and thermometer was charged with the tosylate (**8**) and freshly distilled THF. Under vigorous stirring a solution of lithium bromide (2.16 eq) in THF was added. A white suspension was obtained that was stirred at 50 °C for six days. Filtration of the reaction mixture gave a light brown filtrate which was concentrated under vacuum. Extraction of the crude product with toluene followed by filtration and concentration yielded the bromine (**9**) as a pure compound in a quantitative yield. $^1$H NMR ($CDCl_3$): 3.736 (t, 2H), 3.57 (m, 8H), 3.47 (t, 2H), 3.29 (s, 3H).

**Synthesis of 3-(2-{2-[2-(2-Methoxy-ethoxy)-ethoxy]-ethoxy}-ethyl)-thiophene (10)**

In a three necked flask with a nitrogen inlet, to a stirred suspension of NaH (1 eq) in dry THF at 0 °C, was added dropwise via a cannula a solution of 2-(3-thienyl)ethanol. After the complete evolution of the hydrogen, the methoxy-tri-ethyleneglycol bromide **9** was added dropwise and a catalytic amount of macrocycle 18C6 was also added. The resulting mixture was refluxed over night. After cooling down to R.T., the suspension was treated with HCl 1N. The organic layer was washed with water and run over silica. The colourless oil so obtained was distilled with a Kugelrohr apparatus (130-150 °C); the final yield was 50 %. $^{1}$H NMR ($CDCl_3$): 7.3 (dd, 1H), 7.06 (d, 1H), 6.99 (dd, 1H), 3.70 (q, 2H), 3.54 (m, 12H), 3.24 (s, 2H), 2.72 (t, 2H). $^{13}$C NMR ($CDCl_3$): 30.6, 59.0, 70.2, 70.5 (4×), 71.4, 71.9, 121.1, 125.1, 128.5, 139.1.
IR ($cm^{-1}$): 3099, 2871, 1537, 1455, 1350, 1329, 1297, 1246, 1199, 1111, 1042, 941, 858, 833, 778, 690, 666, 636. GC-MS: m/z [$M^+$] 274; 93.9 % pure, 1.7 % remaining alcohol.

**Synthesis of 2,5-di-bromo- 3-(2-{2-[2-(2-Methoxy-ethoxy)-ethoxy]-ethoxy}-ethyl)-thiophene (1c)**

In a three-necked round-bottom flask with the compound **10** and DMF was added slowly a solution of NBS (2.2 eq) in DMF at 0 °C in the darkness. After complete addition, the reaction mixture was stirred at R.T. for 72h. Then, it was poured over a solution of NaOH 2.5 M and extracted with ether. After evaporation of the solvent the excess of succinimide was eliminated by filtering over glass woole and the pure product was obtained in a yield of 96 % as a yellowish oil. $^{1}$H NMR ($CDCl_3$): 6.99 (s, 1H), 3.64 (q, 2H), 3.61 (m, 12H), 3.54 (s, 2H), 2.72 (t, 2H). $^{13}$C NMR ($CDCl_3$): 29.8, 59.0, 69.8, 70.2, 70.4, 70.5, 70.5 (2×), 71.8, 108.9, 110.3, 131.4, 139.5.
IR ($cm^{-1}$): 3091, 2872, 1717, 1643, 1542, 1453, 1419, 1350, 1325, 1298, 1248, 1199, 1111, 1003, 983, 966, 928, 851, 656, 473. GC-MS: m/z [$M^+$] 432; 89.7 % pure.

**Synthesis of 3-(2-{2-[2-(2-Methoxy-ethoxy)-ethoxy]-ethoxy}-ethyl)-2,5-thiophene dicarboxaldehyde (2c)**

A three necked flask equipped with a nitrogen inlet, was charged with the dibromo compound (**1c**, 1.0 eq) and dry THF. The mixture was cooled at -78 °C and BuLi (2.18 eq.) was added dropwise via a cannula under continuous stirring. The mixture was stirred at -78 °C for 30 minutes after which formylpyperidine (2.2 eq) previously distilled was added. The mixture was then stirred for 12 h at R.T. Afterwards, HCl 1N was added very carefully to stop the reaction. An extraction in chloroform was then performed. The combined organic phase was dried and the solvent evaporated. The dicarboxaldehyde compound (**2c**) was obtained as a pure compound after column chromatography in ether as yellow/orange oil (55 %). $^1$H NMR ($CDCl_3$):10.1 (s, 1H); 9.95 (s, 1H), 6.76 (s, 1H), 3.76 (t, 2H), 3.54 (m, 12H), 3.24 (s, 3H), 2.80 (t, 2H).

**Synthesis of 2,5-bis(hydroxymethyl)- 3-(2-{2-[2-(2-Methoxy-ethoxy)-ethoxy]-ethoxy}-ethyl)-thiophene (3c)**

In a three-necked round-bottom flask with dry THF (100 ml, dried over sodium) $LiAlH_4$ (3 eq) was added under argon atmosphere. This slurry was cooled to 0 °C and the di-aldehyde **2c** was slowly added via a dropping funnel. When the addition was completed a reflux condenser was fitted and the slurry was heated at reflux temperature overnight. After cooling down at R.T., the reaction mixture was placed in an ice bath. Then, it was quenched by cautious sequential addition of water, aqueous 15 % NaOH solution, and again water until no more gas development could be detected. This solution was filtered and the residue was extracted with ether. The solvent was evaporated under reduced pressure. The compound **3c** was obtained as orange oil (65 %). $^1$H NMR ($CDCl_3$): 6.74 (s, 1H), 4.72 (s, 2H), 4.63 (s, 2H), 3.63 (m, 14H), 3.52 (s, 2H), 2.79 (s, 3H), 1.69 (br s, 2H).

**Synthesis of 2,5-bis(chloromethyl)- 3-(2-{2-[2-(2-Methoxy-ethoxy)-ethoxy]-ethoxy}-ethyl)-thiophene (4c)**

To a cooled (0 °C), stirred solution of diol **3c** in THF was slowly added a solution of $SOCl_2$ (2.5 eq) in THF. The temperature of the reaction mixture was allowed to increase to room temperature under continuous stirring for 1 hour. Then, the mixture was cooled down again at 0 °C and a saturated sodium carbonate solution was added dropwise until neutral. The mixture was extracted with ether the solvent was evaporated. The highly reactive dichloride **4c** was obtained as orange oil and used as it was in the following step.

**Thiophene-2,5-diylbismethylene N,N-diethyl dithiocarbamate 3-(2-{2-[2-(2-Methoxy-ethoxy)-ethoxy]-ethoxy}-ethyl)-thiophene (5c)**

To a solution of bischloromethyl **4c** in ethanol, sodium diethyldithiocarbamate trihydrate (or diethyldithiocarbamic acid sodium salt trihydrate) (4 equivalents) was added as a solid. The mixture was stirred at ambient temperature overnight. Then, water was added in order to stop the reaction and, the desired monomer was extracted with ether. Evaporation of the solvent followed by purification via column chromatography yielded the pure product as an orange oil (overall yield 30 %). $^1$H NMR ($CDCl_3$): 6.95 (s, 1H), 4.76 (s, 2H), 4.71 (s, 2H), 4.02 (q, 4H) 3.58 (m, 18H), 3.34 (s, 2H), 2.79 (s, 3H), 1.22 (m, 12H).

**Polymerisation of monomers 5a; 5b and 5c**

All polymerisations were carried out in dry THF at different: temperatures, with different bases and different concentrations of the base. A solution of monomer **5a** (or **5b** or **5c**) (250 mg) in dry THF at 0 °C or R.T. was degassed by passing through a continuous nitrogen flow. An equimolar solution of LHMDS (Lithium Bis(trimethylsilyl)amide, 1 M solution in THF) or $P_2$-t-Bu (2 M solution in THF) was added in one go to the stirred monomer solution. The mixture was kept at the desired temperature for 90 minutes under continuous nitrogen flow. After this time, the solution was precipitated in ice water (100 mL) and extracted with chloroform (3 x 60 mL). The solvent of the

combined organic layers was evaporated under reduced pressure and a second precipitation was performed in a non solvent at 0 °C (methanol). **6a** $^{1}$H NMR ($CDCl_3$): 4.98-3.98 (br s, 2H), 3.94-3.81 (br s, 1H), 3.72-2.8 (br q, 2H), 2.29 (q, 2H), 2.21-1.75 (br t, 4H), 1.35-1.29 (br m, 8H), 1.00-0.91 (br m, 6H), 0.88 (s, 3H). $^{13}$C NMR ($CDCl_3$): 197.4, 149.1, 148.1, 114.8, 108.3, 73.6, 44.2, 38.8, 32.5, 32.1, 26.3, 23.1, 14.0, 12.5.

**6c** The NMR peaks are the same as for the monomer since we are in the presence of oligomers with very short repeating lengths.

## 4.7 References


1. H. B. Yildiz, S. Kiralp, L. Toppare, Y. Yagci, K. Ito, *Materials Chemistry and Physics*, 100, **2006**, 124
2. C. Huang, W. Huang, J. Guo, C. Z. Yang, E. T. Kang, *Polymer*, 42, **2001**, 3929
3. L. Qi, M. Sun, S. Dong, *J. of Appl. Pol. Sci*. 102, **2006**, 1803
4. R. A. Silva, L. A. Cury, M. S. Mazzoni, E. Soares, P. S. S. Guimaraes, F. Serein-Spirau, S. Lois, J. Moreau, J. P. Lère-Porte, *Macromol. Symp*. 229, **2005**, 194
5. G. Daoust and M. Leclerc, *Macromolecules*, 24, **1991**, 455
6. S. Akoudad, P. Frère, N. Mercier, J. Roncali, *J. Org. Chem.*, 64, **1999**, 4267
7. J. Lukkari, M. Salomaki, A. Viinikanoja, T. Aaritalo, J. Paukkunen, N. Kocharova, J. Kankare, *J. Am. Chem. Soc.*, 123, **2001**, 6083
8. L. Peeters, H. J. Geise, *TRIP*, 5, (5), **1997**, 161
9. E. E. Havinga, C; M. J. Mutsaers, *Chem. Mater.*, 8, (3), **1996**, 769
10. N. Ono, H. Okumura, T. Murashima, *Heteroatom Chemistry*, 12, (5), 2001, 414
11. Richard D. McCullough, *Adv. Mat.*, 10, (2), **1999**, 93
12. K.-Y. Jen, H. Eckhardt, T. R. Jow, L. W. Shacklette and R. L. Elsenbaumer, *J. Chem. Soc., Chem. Commun.*, **1988**, 215
13. H. S. O. Chan and S. C. Ng, *Progress in Polymer Science*, 23, (7), **1998**, 1167
14. H. Cheng, R. L. Elsenbaumer, *J. Chem. Soc., Chem. Commun.*, **1995**, 1451
15. J. M. McIntosh, H. Khalil, *Can. J. Chem.* 53, **1975**, 209
16. A. Lima, P. Schottland, S. Sadki, C. Chevrot, *Synth. Met.*, 93, **1998**, 33

17. E. M. D. Keegstra, J. W. Zwikker, M. R. Roest, L. W. Jenneskens, J. *Org. Chem.*, 57, **1992**, 6678

18. J. Light, R. Breslow, *Organic Syntheses, Coll.*, Vol. 9, 733, Vol. 72, 199

19. F. P. Wenzl, G. Mauthner, M. Collon, E. J. W. List, C. Suess, A. Haase, G. Jakopic, D. Somitsch, P. Knoll, M. Bouguettaya, J. R. Reynolds, G. Leising, Thin Solid Film, 433, 2003, 287

20. D. Witker, M. D. Curtis, *Journal of Power Sources*, 156, **2006**, 525

21. M. Jayakannan, S. Ramakrishnan, *J. Pol. Sci.: Part A: Pol. Chem.*, 38, **2000**, 2635

22. R. Schwesinger et al, *Liebigs Ann. Chem.*, 1055, **1996**

23. F. Uhlig et al., *Phosphorus, Sulfur Silicon Relat. Elem*. 81, **1993**, 155

24. M. Lemaire, R. Garreau, F. Garnier, J. Roncali, *New J. Chem*., 11, **1987**, 703

25. M. Lemaire, R. Garreau, J. Roncali, D. Delabouglise, H. K. Youssoufi, F. Garnier, *New J. Chem*., 13, **1989**, 863

26. C. Lee, K. J. Kim, S. B. Rhee, Synth. Met., 69, **199**5, 295

27. S.-A. Chen and C.-C. Tsai, Macromolecules, 26, **1993**, 2234

# Chapter Five

# The acid induced conversion of the dithiocarbamate precursor polymers towards PTVs

## *5.1 Introduction*

Highly conjugated polymers are generally insoluble and infusible because of the stiffness of their backbones. This makes it difficult to process these materials into useful objects such as fibres and films. A solution to this problem is the synthesis of these polymers via precursor routes[1]. The precursor polymers so obtained are soluble, and can be processed by conventional methods. Consecutively they can be converted (thermally[2-9], chemically[10-18], via excimer laser[19], with ions[20]) in a last reaction step to the fully conjugated chain. Usually the full conjugation is reached by thermal elimination of leaving groups at relatively high temperatures.

In our laboratory occasional observations showed that solutions of dithiocarbamate precursor polymers in "acid" solvents (*i.e.* chloroform weak acid) changed colour quite quickly. This change of colour might be ascribed to some conversion towards the conjugated form. It was then decided to test the effect of acid on the dithiocarbamate precursor polymer. The fact that we were able to synthesise soluble conjugated polymers (alkyl derivatives of PTV) allowed further investigation of this observation since the conjugated polymers so obtained can be analysed in solution. As a first step, a literature search on the state of the art of the conversion procedures of precursor polymers was done. Many examples were found, since an overview of the existing precursor routes was already given in chapter two, we will focus here only on the elimination procedures involving the use of acids.

## 5.2 Earlier observation in the use of acids in elimination procedures

In the sulphonium precursor route discovered by Wessling and Zimmerman[4, 21, 22] a soluble precursor Poly(p-Phenylene Vinylene) (PPV) was obtained. The solubility of these polymers was due to the presence of the sulphonium leaving groups. These groups can be eliminated by heat treatment of the film at a temperature of 200 °C or 300 °C for more than 2 hours resulting in a yellow free standing film of PPV. However, rapid heating at 220 °C provided a flexible foam structure.

Murase and Gagnon[23] studied more in detail the process involved. The formation of two gaseous molecules [$(CH_3)_2S$ and HCl] that were released during the elimination process was observed. These gasses could interfere with the device fabrication if not complete eliminated.

A major problem in the conversion process is the incomplete loss of all the sulphur and chlorine containing functional groups producing a polymer with $sp^3$ hybridized carbon atoms in the main chain. This reduces the overall conjugation. The optimum conversion temperature for PPV with a minimum amount of sulphur was determined to be beyond 380 °C[24].

Films of PPV were prepared also *via* pyrolysis of a water-soluble sulphonium polyelectrolyte precursor polymer derived from p-xylylene bis (tetrahydrothiophenium chloride)[25] according to the Kanabe[26] and Wessling[27] procedures, which were later modified by Lenz[28]. Use of Tetrahydrothiophene (THT) instead of a dialkylsulphide in the synthesis of the monomer bissulphonium salt, leads to a lower pyrolysis temperature of the precursor polymer. An inert atmosphere in the temperature range of 180-280 °C gives rise to the elimination of THT and hydrochloric acid and leads to the fully conjugated polymer[29]. The thermal elimination of dialkylsulfide and HCl is stated to proceed via $E1_{CB}$ mechanism giving a transconfiguration of the double bond[30,31]. To us this hypothesis is quite improbable as no base is present. Alternatively, the proposal of an E1 mechanism is more appropriate.

The sulphonium precursor polymer was converted into the conjugated polymer by heating treatment of the thin film at a temperature of 220-250 °C for 12 h under vacuum.

More recently, Marletta *et al.* [17] reported on rapid conversion of PPV at low temperatures. The process involved the substitution of the chloride anions of the sulphonium precursor polymer by a long chain sodium dodecylbenzenesulfonate (DBS) anion that was afterwards converted under atmospheric conditions. The resulting conjugated polymer showed conjugation length and optical properties comparable to those of standard films converted at higher temperature.

A pulsed laser beam was used by Paik *et al.*[19] in order to induce the conversion of a sulphonium precursor polymer into the conjugated PPV. The complete conversion was achieved within 20 seconds. The characteristic of the PPV obtained by the laser beam conversion process were almost the same as those observed for the film produced by a thermal process.

A second precursor route, where the solubilising leaving group is rather an alkoxy group, (usually a methoxy), was developed by Burn[32] and led to polymers which are soluble in polar aprotic solvents.

Heat treatment of the methoxy precursor polymer led to a thermally stable, partially conjugated, precursor polymer. In order to prepare the fully conjugated polymer, it was necessary to heat the precursor polymer at 200 °C under a flow of HCl-Ar gas for several hours. This method was incompatible with the fabrication of devices.

An alternative route was developed by the initial replacement of the sulphonium moiety by a butoxy group in order to produce a neutral precursor polymer (PPV) which was soluble in organic solvents[33]. This neutral polymer can be eliminated either thermally or in the presence of a weak acid. When a strong acid is used, the PPV polymer was produced in the doped state.

Ichikawa *et al.*[34] reported on bridged cyclic aryleneethylene polymers having alkoxy groups. Those precursor polymers were converted into the conjugated form by a heat treatment using an acid catalyst such as hydrochloric acid, acetic acid or, concentrated sulphuric acid.

All the afore mentioned methods refer to conversion of precursor polymers not made with the dithiocarbamate precursor route. As we have described already in chapter two; the dithiocarbamate route gives the only prospective towards the synthesis of electron rich conjugated poly(Arylene Vinylene) derivatives[35]. So, in this chapter, we will present an alternative protocol for the conversion of the dithiocarbamate precursor polymers which allows also post-functionalisation of those polymers.

## *5.3 Conversion of the precursor dithiocarbamate polymer in the presence of acid*

All the experiments presented in this chapter, were carried out using a 3-hexyl PTV precursor polymer. The synthesis and the characteristics of the material were already presented in chapter three. This specific material was chosen because it shows a reasonable solubility also in its conjugated form necessary for the characterisation and the evaluation of the conjugated system after conversion in acid.
The precursor polymer was converted by the use of an acid according to the reaction scheme in **Figure 5.1**.

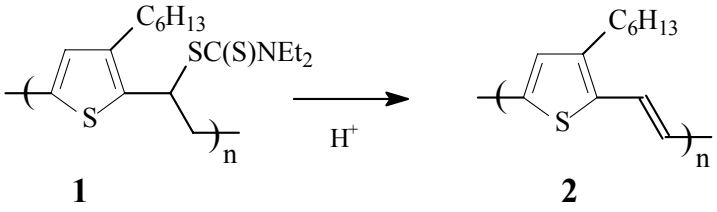


***Figure 5.1*** *Conversion of the precursor polymer 1 into the conjugated for 2*

To a solution of precursor polymer (**1**) dissolved in chlorobenzene p.a., benzensulfonic acid (1.5 eq) was added as a solid. The solution was heated at 70 °C under a $N_2$ stream. The conversion step was monitored by means of an UV-Vis technique carried out in solution. Therefore, samples were taken from

the reaction mixture at different times (10 minutes, 1h; 5h and 24h) (**Figure 5.2**) and consecutively analysed.

After 10 minutes the colour of the reaction mixture was already deep blue, such dark colour indicates a good conversion ratio.

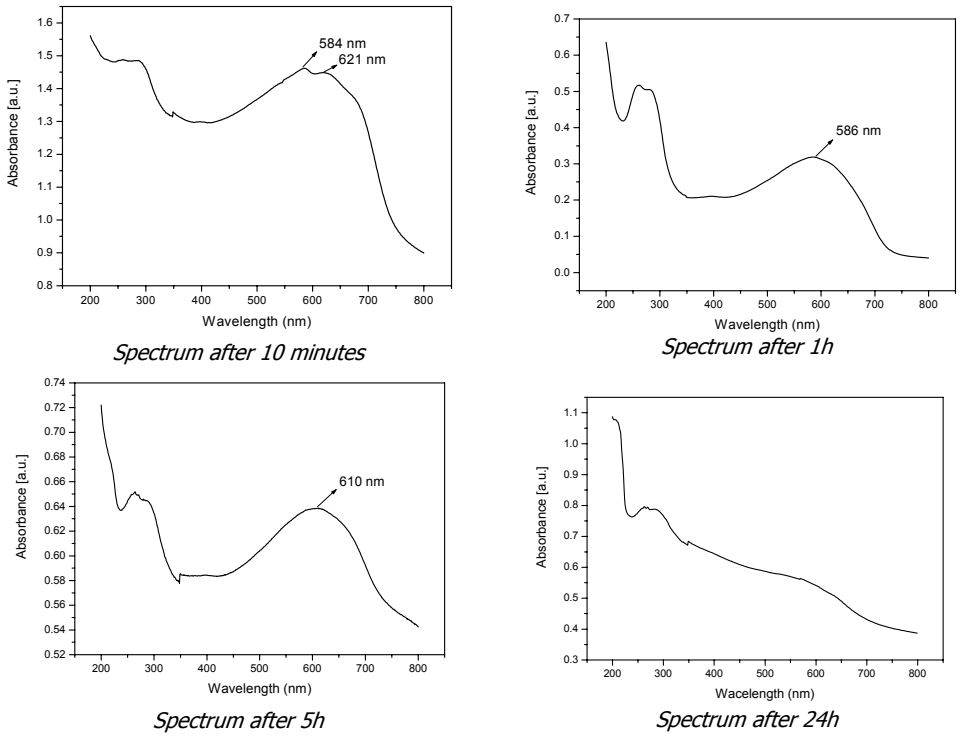


***Figure 5.2*** *UV-Vis in thin film at R.T. at different reaction times*

After 24 hours the reaction mixture showed a red-burgundy colour with black solid particles in suspension. These black particles were not soluble in organic solvents. The conjugated polymer obtained after conversion with acid shows similar values for $\lambda_{max}$ (610 nm) as compared to polymers converted at reflux in o-dichlorobenzene ($\lambda_{max}$ of 621 nm chapter three). Thus, it seems that the conjugated polymer is obtained high effective conjugation length and thus low defect content in the polymer backbone. However for a long reaction time (24 hours) degradation of the conjugated system occurs.

Since the elimination proceeded quite fast we wanted to evaluate also the effect of the temperature. An experiment using the same concentration of acid but without any heat treatment of the reaction mixture was carried out. The conversion was followed by means of UV-Vis spectroscopy in solution for 24 hours (**Figure 5.3**).

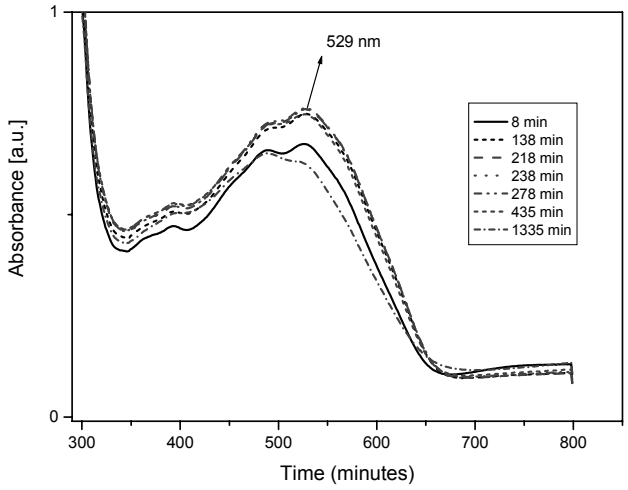


***Figure 5.3*** *Uv-Vis in solution of the acid induced conversion at R.T. with 1.5 eq of acid*

It can be noticed that the conversion process is not completed if one uses the $\lambda_{max}$ values obtained in the former experiment and reported in **Figure 5.2**. Indeed, it can be seen that the formation of the conjugated system is formed quite fast. Already after eight minutes a $\lambda_{max}$ value of about 525 nm is obtained. It evolves in time until a $\lambda_{max}$ value of 529 nm (lower than 610 nm **Figure 5.2**) and then decreases again (absorption at 1335 minutes **Figure 5.3**), pointing to side reactions that deteriorate the conjugated system. We can conclude then, that at R.T. the elimination also seems to proceed at high pass, but occurs to a minor extent probably due to the introduction of defects into the polymer backbone. This points to a secondary reaction which may be less effective at higher temperatures.

The second parameter we wanted to evaluate was the effect of acid concentration. Consequently, an experiment with lower concentration of the

acid (0.3eq) was performed and monitored by UV-Vis spectroscopy in solution (**Figure 5.4**).

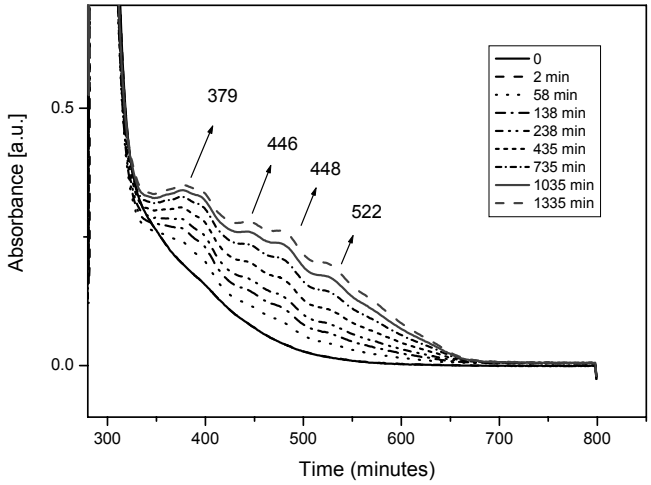


***Figure 5.4*** *Uv-Vis in solution of the acid induced conversion at R.T. with 0.3 eq of acid*

Only a partial conversion was induced as it is pointed out in the UV-Vis spectrum. The absorption maxima observed were compared with the absorption maxima of hexyl PTV oligomers reported in literature showing a good agreement. Even after more then 20 h no full developed conjugated system is obtained. This observation is not consistent with an acid catalyzed reaction, rather it indicates that the acid is consumed and thus an acid induced elimination reaction is at hand.

In order to have a better insight of the elimination process also a different acid was tested. To a solution of precursor polymer in chlorobenzene, trifluoroacetic acid (1.5 eq.) was added, which is a weaker acid (pka = 0.5) compared to the benzenesulfonic acid (depending on the source pka = -3 till -6). The reaction was monitored at R.T. in solution by means of UV-Vis technique. The experimental evidence proved that the conversion process was fast even at room temperature (**Figure 5.5**), but slower then in case of the use of benzene sulphonic acid. Indeed, a similar $\lambda_{max}$ value of 525 nm is

only achieved after 16 minutes instead of 8 minutes. On the other hand the system evolves to a higher $\lambda_{max}$ value of 566 nm instead of 529 nm.

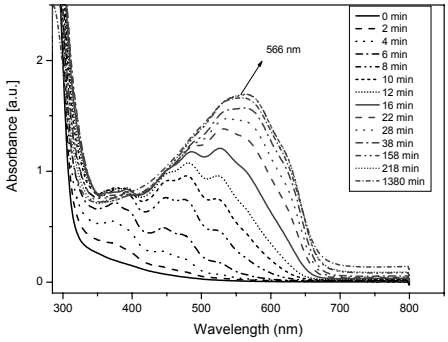


***Figure 5.5*** *Uv-Vis in solution at R.T. for conversion with $CF_3COOH$*

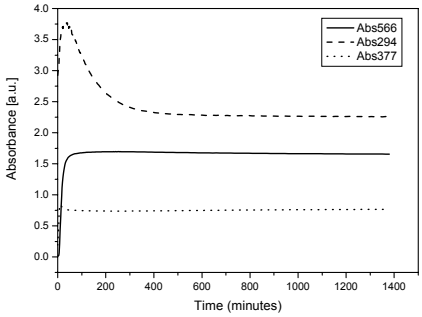


***Figure 5.6*** *Profile of the conversion process*

Furthermore, after 24 hours no sign of degradation is present since a plateau in the absorbance profile *versus* time is present (**Figure 5.6**). Seemingly, the degradation reaction observed in the case of the use of benzene sulphonic acid is not active to the same extent when a weaker acid is used.

In order to summarise the evidence so far obtained we can conclude that three striking observations were made. The first one relates to the effect of the temperature. It seems that at R.T. some defects are introduced leading to a minor extent of the elimination. Secondly, we can say that using a minor concentration of acid leads also to limited elimination. Consequently, the acid is consumed during the reaction and thus the elimination is acid induced rather than acid catalysed. Finally, depending on the strength of the acid used, consecutive degradation of the conjugated system obtained can occur or be avoided.

## *5.4 Proposed mechanism for the acid induced elimination of the dithiocarbamate precursor polymer*

As stated before, the conjugation seems to be achieved by an acid induced elimination of the remaining dithiocarbamate group that acts as a leaving group, at temperature as low as 70 °C. The conjugated polymer, obtained in this way, showed a low structural defect level, comparable with the conjugated polymers obtained after conversion by heat treatment.

The reaction mechanism (**Figure 5.7**) we propose is consistent with the experimental observation that the acid is consumed. Actually the acid used is converted to the weaker conjugated acid of the amine (pKa (DMSO) = about 20). This can lead to the possibility to control the extent of the elimination by adapting the amount of acid used. Furthermore, it may be expected that the kinetics of the reaction is function of the strength of the acid, as the protonation of the dithiocarbamate group takes part in the rate limiting step. Thus weaker acids lead to a slower process. Furthermore, it is assumed that the reaction proceeds *via* an intermediate carbenium ion. This is consistent with the fact that the electron rich thiophene ring can contribute efficiently to its stabilisation. This also implies that the kinetics are expected to be sensitive to the capability of the aromatic structure to stabilize the carbenium ion intermediate.

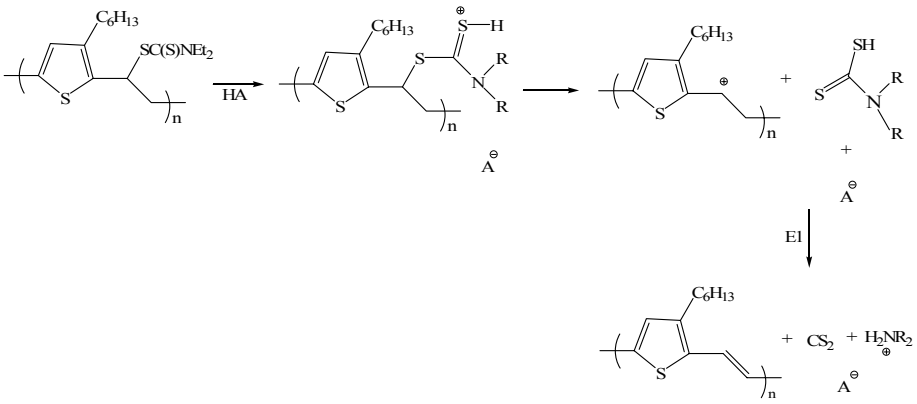


***Figure 5.7*** *Proposed mechanism of the acid induced elimination of the dithiocarbamate group.*

The second hypothesis of a "E1"-type of elimination reaction opens the possibility of the occurrence of a competing nucleophilic substitution *via* an $S_N1$ mechanism. Basic Organic Chemistry Textbooks teach that the competition between the substitution reaction $S_N1$, and the elimination reaction E1, can be controlled by increasing the temperature (favours the elimination reaction) or, by adding strong nucleophiles (favours the substitution reaction). This may explain why using a reaction temperature of 70 °C gives rise to a higher $\lambda_{max}$ value of the conjugated system so obtained than performing the reaction at R.T. This implies that in the latter case the limitation on the $\lambda_{max}$ value may be related to the introduction of $sp^3$-defects as a consequence of a competing $S_N1$ reaction (**Figure 5.8**).

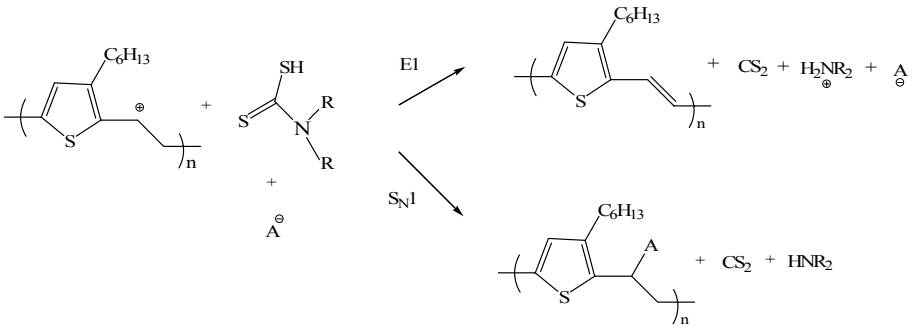


***Figure 5.8*** *Proposed mechanism for the competition between elimination and nucleophilic substitution reactions*

Furthermore, by controlling this competition, we might be allowed to perform modifications of the precursor polymer obtained *via* the dithiocarbamate precursor route. Such modifications could be used to introduce in an easy and controllable way all kind of functional groups onto the backbone of the precursor polymer. Beside a wide variation of modifications, this may lead to the formation of, for example, (macro)-initiators. This could allow for consecutive other polymerisation reactions applied to the initial modified precursor polymer. In this way, grafted-copolymers could be synthesised. Moreover, this could lead to a two-step modification of the polymers.

### 5.4.1 Competition between elimination and nucleophilic substitution mechanism.

In order to confirm said hypothesis some specific experiments were carried out. Firstly, to a mixture of the precursor polymer and trifluoroacetic acid a nucleophile reagent (*i.e.* octanethiol 1 eq.) was added. Indeed, it was observed that the elimination was partially inhibited as shown by the reduced formation of the conjugated system even after a reaction time of 24 hours. It is assumed that the addition of octane thiol favours the nucleophilic substitution (**Figure 5.9**).

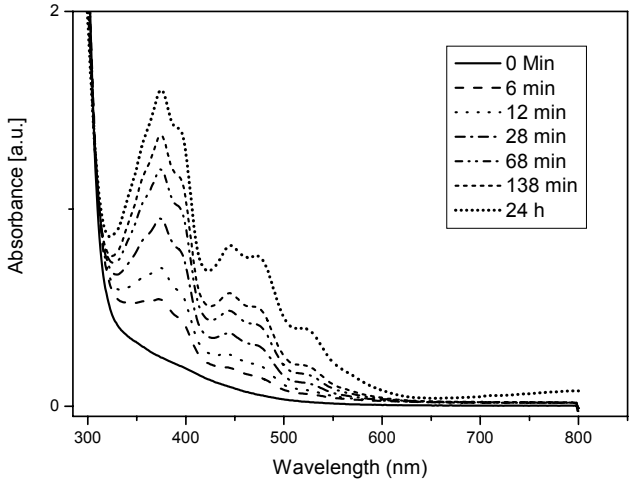


***Figure 5.9*** *Uv-Vis in solution of the acid induced conversion at R.T. with the addition of a thiol.*

Use of a larger excess of octane thiol (5 eq) drastically inhibited the formation of the conjugated system (**Figure 5.10**).

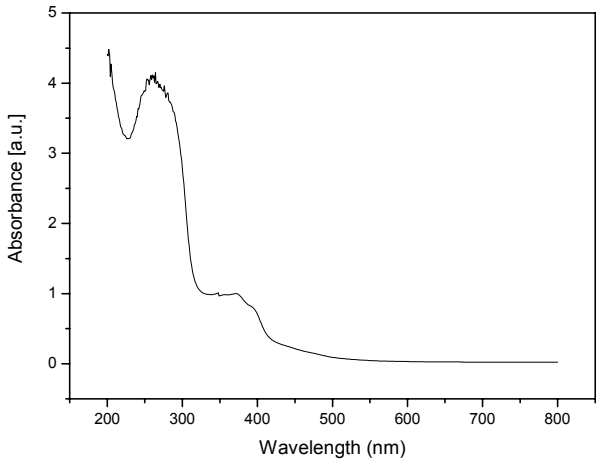


***Figure 5.10*** *Uv-Vis in solution of the acid induced conversion at R.T. with the addition of an excess of octanethiol.*

The assumption that a substitution on the polymer backbone occurred, was further confirmed by carrying out a follow-up experiment. An oxidation in the presence of hydrogen peroxide ($H_2O_2$) and tellurium dioxide ($TeO_2$) according to the scheme in **Figure 5.11** was performed.

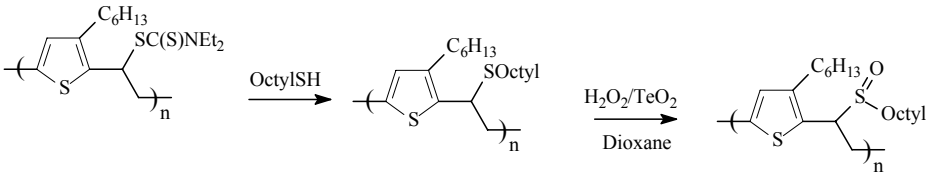


***Figure 5.11*** *Substitution of precursor polymer with octanethiol followed by on oxidation reaction in $H_2O_2/TeO_2$*

The formation of the oxidised product was evaluated by infrared (FT-I.R.) measurements (**Figure 5.12**).

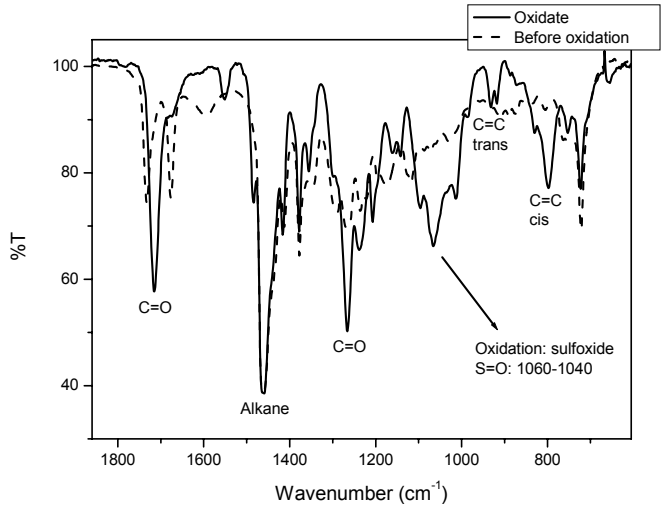


***Figure 5.12*** *FT-I.R. of the oxidised polymer*

Indeed, a clear peak related to the presence of a sulfoxide was visible in the FT-I.R. spectrum. This experiment does not only proves that the nucleophilic substitution took place but, even more important, that it is possible to do a post functionalisation of the dithiocarbamate precursor polymer.

## 5.5 Acid induced elimination: a specific behaviour of the dithiocarbamate moiety

The last step in exploring this new method for the elimination of the dithiocarbamate group, was to establish its unique character. With this scope in mind a reaction using a different precursor polymer was performed.
In this experiment, a xanthate precursor polymer was converted in the presence of benzenesulfonic acid (**Figure 5.13**) and the reaction was monitored by means of UV-Vis spectroscopy in solution.

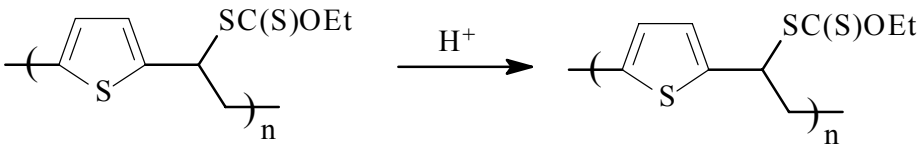


***Figure 5.13*** *Acid induced elimination of the xanthate precursor polymer*

As it is shown by the spectrum reported in **Figure 5.14**, no sign of formation of the conjugated system and thus elimination was observed.

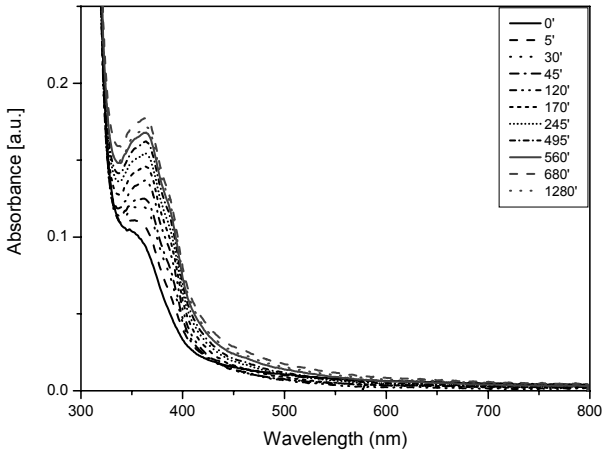


***Figure 5.14*** *Uv-Vis in solution at R.T.*

For a comparison, the spectrum of the thermal eliminated xanthate precursor polymer is reported (**Figure 5.15**).

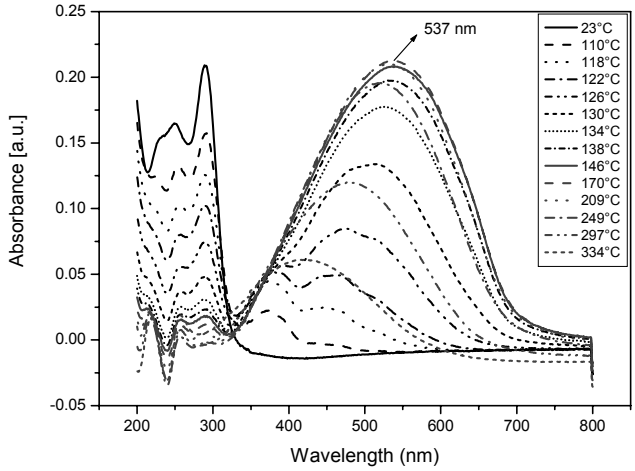


***Figure 5.15*** *Uv-Vis of the xanthate polymer in thin film at different temperatures*

The formation of the conjugated system was followed by means of an *in situ* UV-Vis technique with a ramping temperature of 2 °C/min from R.T. up to 350 °C. A $\lambda_{max}$ of 537 nm was found.

It can be concluded that this innovative way of performing a conversion of precursor polymer towards the conjugated form is typical for the dithiocarbamate precursor polymer. Indeed, others precursor polymers, (*i.e.* xanthate) did not show any conversion in the same conditions used for the dithiocarbamate precursor polymers.

## *5.6 Conclusions*

The acid induced elimination of dithiocarbamate precursor polymers show some distinctive characteristics leading to major advantages in comparison with a thermal elimination.

This innovative method allows lowering the temperature and the time of the conversion process and thus, it may be possible to avoid defects in the

polymer backbone introduced by high heating temperatures and long reaction times.

Another very promising feature of this method is that by changing the strength and the amount of the acid it may be possible to limit the extent of the elimination process. So, it is possible to tune the entire conversion process.

Moreover, by tuning the competition between the substitution reaction and the elimination reaction it may be possible to introduce new substituents on the polymer backbone. More specifically an easy post-functionalisation of the polymers could be possible. In this way different functionalities can be introduced such as chromophores, bio-active molecules, and any molecules that would behave as a nucleophile.

Possibly, the polymer may be used then as a macro-initiator and, grafted polymers can be easily accessible.

## *5.7 Experimental part*

**Materials**. Unless otherwise stated, all reagents and chemicals were obtained from commercial sources (Acros and Aldrich) and used without further purification.

**Characterisation**. FT-IR spectra were collected with a Perkin Elmer Spectrum One FT-IR spectrometer. UV-Vis spectroscopy was performed on a VARIAN CARY 500 UV-Vis-NIR spectrophotometer. Samples for temperature dependent thin film FT-IR and UV-Vis Characterisation were prepared by spin-coating the precursor polymer from a $CHCl_3$ solution (10 mg/mL) onto NaCl disks at 500 rpm or quartz disks at 700 rpm. The disks were heated in a Harrick high temperature cell (heating rate: 2 °C/min), which was positioned in the beam of either the FT-IR or the UV-Vis spectrometer to allow in-situ measurements. Spectra were continuously acquired under a continuous flow of $N_2$.

## 5.8 References


1. A. A. Entezami, M. Bagheri, *Iranian Polymer Journal*, 11, (1), **2002**, 3
2. H .H . Hoerhold, and M .Helbig, *Makromol, Chem . Macromol. Symp*., 12, **1987**, 229
3. H .H . Hoerhold, J. Gmeiner, M. Schwoerer, *Polym. Adv. Tecnol.*, 10, **1999**, 251
4. J. D. Capistran, D .R .Gagnon, S. Antoun, R. W. Lenz and P. E. Karasz, *Polym . Prepr.*, 25, (2), **1984**, 282
5. K. Y. Jen, T. R. Jaw and R. L. Elsenbaumer, *J Chem. Soc., Chem. Common.*, 14, **1987**, 1113
6. K. Y. Jen, M. R. Maxfield, L. W. Shacklette and R. L. Elsenbaumer, *J Chem Soc., Chem. Commun.*, 4, **1987**, 309
7. H. K. Shim, R. W. Lenz and J. Jin, *Makromol. Chem.*, 190, (2), **1989**, 389
8. H. Q. Xie, C. M. Liu, J. S. Guo, *Eur. Polym. J.*, 32, (9), **1996**, 1131
9. E. Kesters, M. M. de Kok, R. A. A. Carleer, J. H. P. B. Czech, P. J. Adriaensens, J. M. Gelan, D. J. Vanderzande, *Polymer*, 47, **2002**, 5749
10. F. Babudri, S. R. Cicco, G. M. Rarinola and F. Naso, *Macromol. Rapid Commun.*, 17, **1996**, 905
11. H. Saito, S. Ukai, S. R. Iwatsuki, T. Itoh, and M. Kubo, *Macromolecules*, 28, **1995**, 8363
12. K. Y. Jen, H. Eckhardt, T. A. Jow, L. W. Shacklette, R. L. Elsenbaumer, *J. Chem. Soc. Chem. Commun.*, 215, **1988**
13. S. H. Jin, Y. K. Sun, B. H. Sohn and W. Kim, *Eur. Palym. J.*, 36, **2000**, 957

14. L. H. Wangm, E.-T. Kang, W. Eluang, *Polymer*, 42, **2001**, 3949

15. M. Xue, D. Huang, and Y. Liu, *Synth. Met.*, 110, **2000**, 203

16. F. Cacialli, R. Daik, W. J.Feast, R. H. Friend and C. Lartigau, *Optical Materials*, 12, **1995**, 315

17. A. Marletta, D. Goncalves, O. N. Oliveira Jr., R. M. Faria, F. E. G. Guimaraes, *Adv. Mat.*, 12, **2000**, 69

18. C. A. M. Borges, A. Marletta, R. M. Faria, F. E. G. Guimaraes, *Mat. Res. Soc. Symp. Proc.* Vol. 707, **2002**

19. S. Y. Paik, S. H. Kwon, O. J. Kwon, J. S. Yoo, M. K. Han, *Synt. Met.*, 129, **2002**, 101

20. V. H. Tran, V. Massardier, T. P. Nguyen, J. Davenas, *Polymer*, 37, (11), **1996**, 2061

21. a) R. A. Wessling, R. G. Zimmerman, *US Patent 37116677*, **1972**, Dow Chemical Co.,b) R. A. Wessling, R. G. Zimmerman, *US. Patent 3401152*, **1968**, Dow Chemical Co.

22. T. A. Skotheim, Electroresponsive, *Molecular and Polymeric Systems*, New York, 197, **1991**

23. D. Gagnon, D. Capistran, F. Karasz, R. Lenz, *Polymer,* 28, **1987**, 267

24. A. F. Diaz, B. Hall, *J. Res. Dev.,* 27, **1983**, 342

25. L. M. Leung and G. L. Chik, *Polymer*, 34, **1993**, 24

26. R. A. Wessling, *J. Polym. Sci., Polym. Symp.*, 72, **1986**, 55

27. A. Pron, D. Billaud, A. Kulszewicz, C. Budrowski, J. Przyluski and J. Suwalski, *Mater. Res. Bull.*, 16, (10), **1981**, 1229

28. R. W. Lenz, C. C. Han, J. Stenger-Smith and F. E. Karasz, *J. Polym. Sci. Polym. Symp.,* 26, **1988**, 3241

29. V. H. Tran, V. Massardier, A. Guyot, *Polymer,* 34, **1993**, 3179

30. D. Gagnon, D. Capistran, F. Karasz, R. Lenz, *Polym. Bull.,* 12, **1984**, 293

31. J. R. Schaefgen, *J. Polym. Sci.*, 15, **1955**, 230

32. P. L. Burn, D. D. C. Bardley, R. H. Friend, A. B. Holmes, R. W. Jackson and A. Kraft, *J. Chem. Soc. Perkin Trans.*, 1, **1992**, 3225

33. H. D. Becker, L. Hansen, K. Anderson, *J. Org. Chem.*, 46, **1981**, 19

34. R. Ichikawa, Y. Ikenoue, F. Wudl, *US Patent 5510456*, **1996**

35. D. Vanderzande, L. Lutsen, A. Henckens, K. Colladet, *EP Patent 1548044*, **2005**

# Chapter Six

# General conclusions and perspectives

## *6.1 Introduction*

The work described in this dissertation was focused on the study of the Dithiocarbamate precursor route. A lot of progress was made since its discovery in our laboratory[1] but it is of course far from finished.
The dithiocarbamate route described in this work can be an interesting and new tool in the search for new materials. This route offers a whole range of possibilities: new materials can be made and additionally, materials that are already known can be made in an improved way. This was already demonstrated for PTV which had better characteristics compared to the PTV obtained via the xanthate route. Since it is a new precursor route a lot of work can be devoted to have a better insight into the mechanisms of this polymerisation process.

## *6.2 The Dithiocarbamate route: general observation*

Our goal was to find the optimal conditions for the polymerisation of dithiocarbamate monomers. Then, an extensive study on the influence of different reaction conditions on the course of the polymerisation was done. Different base were tested, such as LDA, LHMDS and phosphazene base $P_2$-t-Bu. LHMDS proved to be a better base in most cases. The drawbacks caused by the presence of side reactions promoted by LDA were avoided with the use of LHMDS. Moreover, the bimodal distribution of the $M_w$ observed when LDA was used was partially suppressed. The bimodal distribution was mostly attributed to the occurrence of two types of mechanisms taking place

simultaneously: an anionic polymerisation and a radical mechanism[2,3]. The anionic polymerisation was assumed to be responsible of the formation of the lower molecular weight fraction while the radical polymerisation mechanism was considered responsible of the formation of the higher molecular weight fraction. It seems that, in the presence of LHMDS the competition between these two mechanisms is partially suppressed and just some tailing in the $M_w$ distribution can be observed (chapter two). In some cases, like for the dodecyl PTV (chapter 3), the bimodal behaviour became again pronounced. The reason might be found in the purity of the monomer[4,5]. It is known that a radical polymerisation mechanism is not affected by the presence of impurities while, in the anionic polymerisation their presence plays an important role. Anionic processes are extremely sensitive to impurities, and, therefore, their performance requires special purification of the reagents. The mechanism of the polymerisation reaction should be also further investigated by the use of model compounds in order to allow *in situ* measurements.

## *6.3 Synthesis of low band gap polymers which are soluble in the conjugated state*

Soluble conjugated polymers were obtained by making PTV derivatives with long side chains (R) on the thiophene core (**Figure 6.1**).

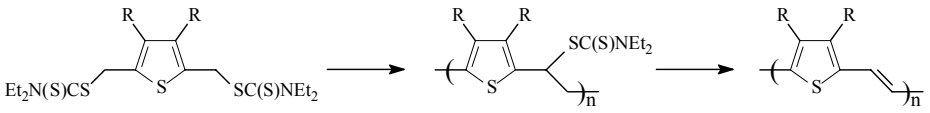


***Figure 6.1*** *Synthesis of soluble PTV via the dithiocarbamate route (R = alkyl, alkoxy, PEO)*

This has the advantage that, the elimination of the dithiocarbamate groups can be done in solution since the conjugated polymer can be processed. The different R-groups we attempt to implant were not only alkyl chains but also alkoxy or oligo ethylene oxide (PEO) chains. By introducing these hydrophilic

side chains, a polar polymer, which is soluble in polar solvents, may be obtained. This can be of interest for several applications since environment-friendly solvents (alcohols, water) could then be used for processing.
The synthesis of the alkyl derivatives was successfully achieved while the synthesis of the more polar derivatives failed.
The presence of oxygen directly attached to the thiophene core (chapter four) lowered the reactivity of the monomer as a result, after the polymerisation reaction, only the unreacted monomers were found in the reaction mixture. The reason of this lowered reactivity might be found not only in the increased electron richness of the monomer (it might lead to the necessity of stronger base) but also in the enhanced steric hindrance that lowers the accessibility to the monomer.
In order to increase the reactivity of the monomer, a mono substituted PTV derivative was synthesised. Moreover, a spacer was introduced between the oxygen atom and the thiophene ring. In this case the reactivity was restored indeed, all the monomer was consumed during the polymerisation reaction. However, an anionic polymerisation seemed to be promoted since just oligomers were obtained. Further investigations are necessary to clarify the polymerisation mechanism. In the future especially the mechanism of the dithiocarbamate precursor route will be studied. The influence of additives such as a radical inhibitor (2,2,6,6-tetramethylpiperinoxyl (TEMPO)) or of a chain transfer reagent on the reaction and its products will be tested. This way of investigating a polymerisation mechanism was also applied in the mechanistic study of the sulphinyl and the Gilch route[6-8].

## *6.4 Performance of materials in electronic devices*

Since low band gap materials already proved to be quite successful for the use in FETs and solar cells, especially these devices will be interesting to do tests with. But not only tests towards the applicability of newly synthesised materials are needed; also further experiments on the materials that were already made are planned.

The performance of the solar cells made showed to be promising (chapter 2 and chapter 3). Furthermore, an optimisation of the devices is necessary in order to increase the $V_{oc}$ values and consecutively the efficiency. Analysing the performance of a certain material in a device, not only will valorise the material itself but also the synthetical route by which the compound was made. All this requires an interdisciplinary approach. An intense cooperation between chemists, physicists and engineers is then indispensable to obtain the best results.

## *6.5 Conversion of the precursor polymer via an acid induced elimination*

A new technique for the conversion of the precursor polymer into the conjugated poly(arylenevinylene) followed by the introduction of specific functionalities on the polymer backbone was found. The process it relates to an acid induced elimination of the dithiocarbamate precursor polymer.

The technique used allows conversion at lower temperature compared to the thermal elimination and, the reduced temperature used, led to polymers with less structural defects in the structure.

Another important advantage, in the use of this method relates to the possibility of post-functionalise these polymers. In this way different kinds of functionalities may be introduced into the polymer backbone (**Figure 6.2**)

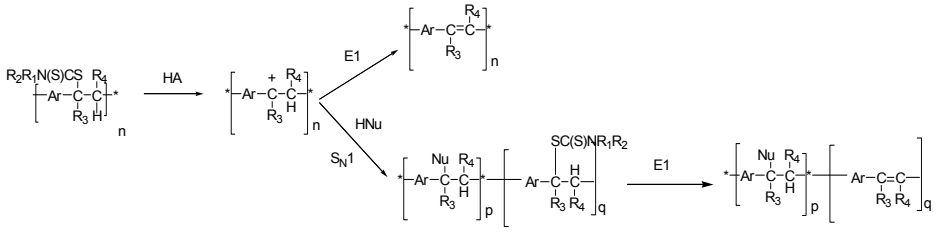


***Figure 6.2*** *Mechanism of acid induced conversion and post functionalisation of the polymer*

As we applied for a patent regarding this method, additional investigations should be planned.

Anyhow, this mechanism seems to be a peculiarity of the dithiocarbamate precursor polymers since, others precursors showed no reactivity in similar conditions towards the formation of the double bond (chapter five).

Further investigations on the mechanism will also include the synthesis of model compounds. As first attempt, a mono-substituted compound was synthesised (**Figure 6.3**) in order to obtain a more insight in the processes that occurred.

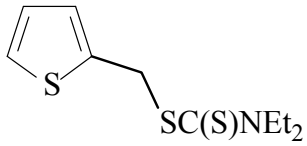


***Figure 6.3*** *Structure of the model compound*

The synthesised model compound, unfortunately, did not show any kind of reactivity. From TLC it was clear that nothing happened since only one spot, relative to the starting material, was observed.

Additional investigations will require the synthesis of other model compounds of general formula as represented in **Figure 6.4**.

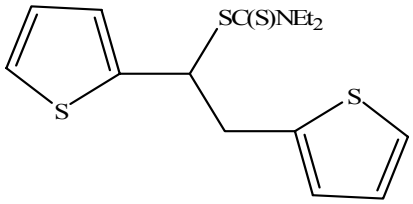


***Figure 6.4*** *Structure of the model compound*

## 6.6 References


1. D. Vanderzande, L. Lutsen, A. Henckens, K. Colladet, *EP Patent 1548044*, **2005**
2. L. Hontis, V. Vrindts, D. Vanderzande, and L. Lutsen, Macromolecules, 36, **2003**, 3035
3. L. Hontis, V. Vrindts, L. Lutsen, D. Vanderzande, and J. Gelan, Polymer, 42, (13), **2001**, 5793
4. L. M. Alassia, G. L. Frontini, J. R. Vega, G. R. Meira, *J. Pol. Sci. Part C: Polymer Letters*, 26, (4), **1988**, 201
5. T. A. Orofino and F. Wenger, *The Journal of Chemical Physics*, 35, (2), **1961**, 532
6. A. Issaris, D. Vanderzande, J. Gelan, *Polymer,* 38, (10), **1997**, 2571
7. L. Hontis, M. Van Der Borght, D. Vanderzande, J. Gelan, *Polymer,* 40, **1999**, 6615
8. L. Hontis, Ph. D. Dissertation, Limburgs Universitair Centrum, Diepenbeek, Belgium, **2002**

# List of abbreviations

| | |
|---|---|
| ACN | acetonitrile |
| $Ac_2O$ | acetic anhydride |
| AFM | atomic force microscopy |
| Ag wire | Silver wire electrode |
| Ag/AgCl | Silver/Silver Chloride electrode |
| Al | Aluminium |
| AM | Air mass |
| Bp | boiling point |
| BuLi | butyl lithium |
| c | speed of light ($3\ 10^8\ ms^{-1}$) |
| CB | conduction band |
| $CHCl_3$ | chloroform |
| $CH_2Cl_2$ | dichloromethane |
| CI | chemical ionisation |
| $CS_2$ | carbon disulfide |
| CV | cyclic voltammetry |
| cw | continuous wave |
| DBS | dodecylbenzenesulfonate |
| DIP-MS | direct insert probe mass spectrometry |
| DMF | N,N-dimethylformamide |
| DP | degree of polymerisation |
| DSC | differential scanning calorimetry |

| | |
|---|---|
| DTC | dithiocarbamate |
| E | Energy (in J) |
| E1 | Elimination |
| EA | electron affinity |
| EI | electron impact |
| EL | electroluminescence |
| EtOAc | ethyl acetate |
| $Et_2O$ | diethyl ether |
| $E_g$ | band gap |
| eV | electronvolt |
| Fc | ferrocene |
| FF | field factor |
| FET | field effect transistor |
| FT-IR | Fourier transform infrared |
| GC/MS | gas chromatography/mass spectrometry |
| GPC | gel permeation chromatography |
| h | Planck constant ($6.626\ 10^{-34}$ Js) |
| HCl | hydrogen chloride |
| HOMO | highest occupied molecular orbital |
| $H_2O_2$ | hydrogen peroxide |
| IP | ionisation potential |
| ITO | indium tin oxide |
| $J_{sc}$ | short circuit current |
| LBG | low band gap |

| | |
|---|---|
| LDA | lithium diisopropyl amide |
| LED | light emitting diodes |
| LHMDS | lithium hexamethyl disilazide |
| Li-EPR | light Electron Paramagnetic Resonance |
| LiF | lithium fluoride |
| LUMO | lowest unoccupied molecular orbital |
| KOH | potassium hydroxide |
| MeOH | methanol |
| $M_n$ | number-average molecular weight |
| $M_w$ | weight-average molecular weight |
| NaH | Sodium Hydride |
| NBS | N-bromosuccinimide |
| n-doping | reduction |
| NHE | Normal Hydrogen Electrode |
| $NiCl_2$(dppp) | dichloro[1,3-bis(diphenylphosphino)propane]nickel(II) |
| NMR | nuclear magnetic resonance |
| OFET | organic field-effect transistor |
| PA | poly(acetylene) |
| PCBM | [6,6]-phenyl-$C_{61}$-butyric acid methyl ester |
| PCE | power conversion efficiency |
| PD | polydispersity (Mw/Mn) |
| p-doping | oxidation |
| PEDOT/PSS or BAYTRON P | poly(3,4-ethylene dioxythiophene) poly(styrene) sulphonate |
| PITN | poly(isothianaphthene) |

| | |
|---|---|
| PL | photoluminescence |
| PLED | polymer light-emitting diode |
| PPP | poly(p-phenylene) |
| PPV | poly(p-phenylene vinylene) |
| PPy | poly(pyrrole) |
| PS | poly(styrene) |
| P3HT | poly(3-hexylthiophene) |
| PT | poly(thiophene) |
| Pt | platinum |
| p-TsOH | para-toluenesulphonic acid |
| PTV | poly(2,5-thienylene vinylene) |
| p-QM | para-quinodimethane |
| ROH | alcohol |
| R.T. | room temperature |
| SCE | Saturated Calomel Electrode |
| SEC | size exclusion chromatography |
| $S_N1$ | substitution |
| $SOCl_2$ | thionyl chloride |
| $TBAPF_6$ | Tetra Butyl Ammonium hexaFluoro Phosphate |
| $TeO_2$ | Telluriumoxide |
| TFT | thin film transistor |
| TEMPO | tetramethylpiperinoxyl |
| TGA | thermogravimetric analysis |
| THF | tetrahydrofuran |
| THT | tetrahydrothiophene |

| | |
|---|---|
| TLC | thin-layer chromatography |
| $T_1$ | spin-lattice relaxation time |
| $T_2$ | spin-spin relaxation time |
| TTC | trithiocarbonate |
| UV-Vis | ultraviolet visible |
| VB | valence band |
| $V_{oc}$ | open circuit voltage |
| XRD | X-ray diffraction |
| XTC | xanthate |
| $\nu$ | frequency |
| $\lambda$max | maximum absorption wavelength |

# List of publications

The synthesis of regio-regular poly(3-alkyl-2,5-thienylene vinylene) derivatives using lithium bis(trimethylsilyl)amide (LHMDS) in the dithiocarbamate precursor route - F. Banishoeib, P. Adriaensens, S. Berson, S. Guillerez, O. Douheret, J. Manca, S. Fourier, T.J. Cleij, L. Lutsen and D. Vanderzande, Solar Energy Materials and Solar Cells, Volume 91, Issue 11, 6 July 2007,1026-1034

The synthesis of poly(thienylene vinylene) derivatives via the dithiocarbamate route: low band gap p-type conjugated polymers for photovoltaics - F. Banishoeib, S. Fourier, T.J. Cleij, L. Lutsen and D. Vanderzande, Eur. Phys. J. Appl. Phys. 37, 237-240 (2007)

Synthesis of Poly(2,5-Thienylene Vinylene) (PTV) and its derivatives: Low Band Gap materials for photovoltaics - F. Banishoeib, A. Henckens, S. Fourier, G. Vanhooyland, M. Breselge, J.Manca, T.J.Cleij, L. Lutsen, D. Vanderzande, Thin Solid Film, 2007, in press

Low bandgap Poly(Thienylene Vinylene) for Organic Solar Cells: Photonics and Photovoltaic Performance – L. H. Nguyen, S. Günes, H. Neugebauer, N. S. Sariciftci, F. Banishoeib, A. Henckens, T. Cleij, L. Lutsen and D. Vanderzande, Organic Optoelectronics and Photonics II, Vol. 6192, 2006

Precursor RoutePoly(Thienylene Vinylene) for Organic Solar Cells: Photophysics and Photovoltaic Performance – L. H. Nguyen, S. Günes, H. Neugebauer, N. S. Sariciftci, F. Banishoeib, A. Henckens, T. Cleij, L. Lutsen and D. Vanderzande, Solar Energy Materials and Solar Cells, 90, 2006, 2815-2828

Method for the conversion of precursor poly(arylenevinylene) and for the post-functionalization of the same - L. Lutsen, D. Vanderzande, F. Banishoeib, *Patent application*

Acid induced elimination of Dithiocarbamate precursor PTV's – F. Banishoeib, L. Lutsen, D. Vanderzande, in preparation

Alkyl Derivatives of Poly(Thienylene Vinylene) in Organic Solar Cells – C. Girotto, T. Aernouts, J. Poortmans, F. Banishoeib, L. Lutsen, D. Vanderzande, in preparation

# Summary

Poly(arylenevinylene)s are considered to be promising candidates for electrical and/or optical materials. Such applications require the use of conjugated polymers with a sufficiently high quality, purity, and molecular weight ($M_W$ >30000). This dissertation deals with the study of the Dithiocarbamate precursor route as a possible synthetic route for the synthesis of low band gap (LBG) materials. Those materials show interesting properties which make them extremely attractive for application in plastic electronics. The processability becomes then a very important issue. This can be obtained either by introducing long side chains or by the use of a precursor route. In this dissertation both approaches are investigated. We aim at the development of an efficient synthetic route in order to obtain well defined materials. In collaboration with other research groups, the polymer produced were characterised and tested.

In **chapter one** an historical background of conjugated polymers as well as their semi-conducting properties are discussed. The relationship between the chemical structure and the electronic properties (*i.e.* Energy band gap) are also discussed. Furthermore, an overview on the working principles of plastic solar cells is given since, the materials were synthesised to serve these applications.

We have focused our attention on the development and the optimisation of the Dithiocarbamate precursor route towards poly(thienylenevinylene) PTV derivatives. In this approach, a non conjugated precursor polymer is obtained which is consecutively converted in its conjugated form. In **chapter two**, plain PTVs synthesised *via* this approach are described. Three different monomers were synthesised: the dithiocarbamate monomer; the xanthate and, the trithiocarbonate one. Their synthesis was optimised and several polymerisation conditions were studied. The dithiocarbamate precursor route showed to be the only promising perspective for the synthesis of electron rich conjugated system. Furthermore, two different bases were tested in the

polymerisation reaction, LDA and LHMDS. The latter led to significant improvement compared to the former, such as higher reaction temperature compared to -78 °C necessary with LDA, absence of side reactions and reduction of the competition between radical and anionic polymerisation mechanisms. The polymers obtained were fully characterised showing higher $M_w$ values, significantly improved $\lambda_{max}$ values and very high thermal stability as compared to previous reports. Moreover, solar cells were produced showing promising performance.

In **chapter three** both, the introduction of a long alkyl chain, and the precursor approach were tested. Alkyl derivatives of PTV were synthesised in good yields. The monomers were polymerised *via* the Dithiocarbamate precursor route using LHMDS as a base since LDA did not lead to polymers due to the presence of side reactions. Studies, in order to investigate the regio-regularity, were also carried out. Preliminary results showed that *via* the Dithiocarbamate precursor route it is possible to obtain regio-regular materials. Charge transfer measurements were also performed showing effective charge transfer in blends of the polymers with PCBM by Li-EPR measurements. Primary solar cell measurements gave promising results.

In **chapter four** two strategies were analysed in order to increase the polarity of PTVs and to fine-tune the solubility properties of these polymers in environmentally friendly solvents. In the first strategy, disubstituted PTVs were synthesised. Two kind of side chains were tested such as an alkoxy and an oligo(ethylene glycol) side chains. Unfortunately, the dithiocarbamate route did not lead to polymers. The monomers showed limited reactivity towards this route. Two bases were tested in order to get some polymers but the results were not satisfactory. In a second approach, a mono-substituted PTV was made in which the oligo(ethylene glycol) side chain is not directly attached to the thiophene ring, but a spacer is introduced between the thiophene core and the oxygen atom of the side chain. This approach led to a complete consumption of the monomer during the polymerisation reaction. However, it seems that the anionic polymerisation mechanism is favoured, leading only to oligomers with very short repeating units.

In **chapter five** a total new method for the conversion of the dithiocarbamate precursor polymers is presented. The first trials on the conversion were successful. Conjugated polymers with enhanced properties ($\lambda_{max}$ values) were obtained in a shorter time and at lower reaction temperatures compared to the conventional heat treatment. The mechanism involved allows an easy post functionalisation of the materials and it seems to be an exclusive behaviour of the dithiocarbamate precursor polymers. This new method opens the way for new challenges.

Finally a general conclusion and some perspectives and suggestions for further work are presented in **chapter six**. The Dithiocarbamate precursor route still remains, despite some unsuccessful results, the best approach to synthesise PTVs. Further research, on the polymerisation mechanism, in our laboratory, will disclose further possibilities and limitations of this route.

# Acknowledgements

*I would like to express my gratitude to all those who gave me the possibility to complete this thesis. I want to thank the Department of Organic and Polymer Chemistry (SBG|OS) of the University of Hasselt for giving me the opportunity to do a Ph.D in the first instance, and to do the necessary research work. I have furthermore to thank who encouraged me to go ahead with my thesis. I am indebted to my supervisor, prof. Dirk Vanderzande, and to my copromotor, dr. Laurence Lutsen,and to all my colleagues.*

*Furthermore, I thank the University of Antwerp, IMO division, IMEC (Leuven) and LIOS (Austria) for the stimulating suggestions and characterisation of the materials.*

*I learnt a lot thanks to all of you, my thesis would not be the same without your support. Especially, I want to thank all the people who helped and supported me over these four years in Belgium.*

*Il mio speciale ringraziamento va soprattutto alla mia famiglia, a mia nonna (che sicuramente veglia su di me), alla mia mamma, alle piccole Desirèe e Asia, a Nemica, a Vladimiro e, a tutti gli amici che mi hanno assistita, consolata e, stretta nel loro affetto durante questi travagliati quattro anni. Per ultimo, ma non per importanza, grazie Tesoro, che più di tutti mi sei stato vicino con amore e pazienza.*

*Grazie a tutti*